The Role of Airway Mucus as a Barrier to Nanoparticles: Implications for Pulmonary Drug Delivery

Dissertation
Zur Erlangung des Grades
Des Doktors der Naturwissenschaften
Der Naturwissenschaftlich-Technischen Fakultät
der Universität des Saarlandes

von

Xabier Murgia

Saarbrücken

2018

Die vorliegende Arbeit wurde von Januar 2014 bis April 2017 unter der Leitung Herrn Prof. Dr. Claus-Michael Lehr am Institut für Pharmazeutische Technologie der Universität des Saarlandes und am Helmholtz-Institut für Pharmazeutische Forschung Saarland angefertigt.

Tag des Kolloquiums: **15. Juli 2019**

Dekan: **Prof. Dr. Guido Kickelbick**

Berichterstatter: **Prof. Dr. Claus-Michael Lehr**

Prof. Dr. Thorsten Lehr

Prof. Dr. Jesús Pérez-Gil

Akad. Mitglied: **Dr. Agnes-Valencia Weiß**

Vorsitz: **Prof. Dr. Christian Wagner**

Table of Contents

I Summary

A layer of mucus covers the surface of the pulmonary airways. Mucus is a hydrogel mainly composed of water, mucins (glycoproteins), DNA, proteins, lipids, and cell debris, which conditions the inhaled air and protects us from airborne threats. The natural protective role of mucus is nowadays acknowledged as a major barrier to be overcome in non-invasive drug delivery. The heterogeneity of mucus components offers a wide range of potential chemical interaction sites for macromolecules, while the mesh-like architecture given to mucus by the intermolecular cross-linking of mucin molecules results in a dense network that physically, and in a size-dependent manner, hinders the diffusion of macromolecules and nanoparticles through mucus.
In this thesis, native airway mucus samples of porcine and human origin have been exhaustively characterized utilizing techniques that allow its investigation while preserving its original viscoelastic properties. The rheological properties and the penetration of differently sized nanoparticles either mechanically mixed with mucus or deposited as an aerosol onto mucus layers have been investigated. Additionally, a significant research effort has been spent in the development of *in vitro* models aimed at mimicking the bronchial region under diverse physiological conditions, including bacterial infection. These models have been proved suitable for investigating the translocation of nanoparticle-based drug delivery systems through the airways as well as for testing the efficacy of antibiotics in the context of cystic fibrosis.

II Zusammenfassung

Eine dünne Schleimschicht (Mukus) schützt und bedeckt die Epithelien der wichtigsten nicht-invasiven Applikationsrouten für Arzneistoffe, zu denen der Magen-Darm-Trakt, die Atemwege, die Augen und der weibliche Vaginaltrakt zählen. An diesen Orten stellt Mukus eine schwer zu überwindende Barriere für den Transport von nanopartikulären Arzneistoffformulierungen dar. Mukus ist ein komplexes Netzwerk miteinander verflochtener makromolekularer Strukturen, die ein Filternetz mit einer messbaren Porengröße bilden. Der somit entstehende physikalische Größenfilter ist wichtig für die Abwehr inhalierter Partikel. Zusätzlich wird dieser Effekt durch die hohe Anzahl funktioneller Gruppen, die mit dem Fremdmaterial chemische Interaktionen eingehen können, verstärkt. In den Atemwegen beispielsweise, wird von den Epithelzellen ein kontinuierlicher Mukusfilm sekretiert, der einer koordinierten Zilienbewegung in Richtung der oberen Atemwege folgt und auf diese Weise einen erfolgreichen Abwehrmechanismus gegenüber inhalierten Partikeln darstellt.

In dieser Arbeit wird die Interaktion von Nanopartikeln mit nativem Lungen und Schweine Mukus im Detail betrachtet. Die verwendeten Techniken erlauben eine umfassende Analyse, ohne dabei die ursprünglichen viskoelastischen Eigenschaften der Probe zu beeinflussen. Im Vordergrund stehen hierbei die rheologischen Eigenschaften von Mukus nach mechanischer- oder Aerosolapplikation von Nanopartikeln verschiedener Größe. Zusätzlich wurden zwei in-vitro Modelle der bronchialen Atemwege entwickelt, um damit die Lunge im pathologischen Zustand zu simulieren. Diese haben sich als geeignet erwiesen, sowohl die Penetration von nanopartikulären Formulierungen als auch die Wirksamkeit von Antibiotika - besonders im Kontext der Mukoviszidose (zystische Fibrose) - zu testen.

III Abbreviations

API	Active Pharmaceutical Ingredient
AT I	Alveolar Type I Cell
AT I	Alveolar Type II Cell
CF	Cystic Fibrosis
CFTR	Cystic Fibrosis Transmembrane Conductance Regulator
CRM	Confocal Raman Microscopy
CryoSEM	Cryogenic Scanning Electron Microscopy
COPD	Chronic Obstructive Pulmonary Disease
DNA	Deoxyribonucleic Acid
DPI	Dry Powder Inhaler
DPPC	Dipalmitoyl Phosphatidylcholine
FPF	Fine Particle Fraction
FRAP	Fluorescence Recovery After Photobleaching
G’	Elastic modulus
G’’	Viscous modulus
GSD	Geometric Standard Deviation
MIC	Minimum Inhibitory Concentration
MMAD	Mass Median Aerodynamic Diameter
MPT	Multiple Particle Tracking
MSD	Mean Squared Displacement
MUC	Mucin
MUC5AC	Mucin 5AC
MUC5B	Mucin 5B
NAC	N-acetyl cysteine
NP	Nanoparticle

PEG	Polyethylene Glycol
pMDI	pressurized Metered Dose Inhaler
PTS	Proline-Threonine-Serine
TEER	Trans-Epithelial Electrical Resistance

1. Introduction

Parts of this section have been addressed in depth in the following peer-reviewed publications:

Review articles:

Murgia X, de Souza Carvalho C, Lehr C-M. *Overcoming the pulmonary barrier: new insights to improve the efficiency of inhaled therapeutics*. Eur J Nanomedicine 2014;6:157–69

Murgia X, Loretz B, Hartwig O, Hittinger M, Lehr C-M. *The role of mucus on drug transport and its potential to affect therapeutic outcomes*. Adv Drug Deliv Rev 2018;124:82-97

Book Chapters:

Murgia X, Barthold S, Kunschke N, Loretz B, Carvalho C, Lehr C-M. *Chapter 8: Overview of Inhaled Nanopharmaceuticals*. In book: ISAM Textbook of Aerosol Medicine. Publisher: International Society for Aerosols in Medicine; Editors: Barbara Rothen- Rutishauser and Rajiv Dhand (**2014**)

Schneider-Daum N, Hittinger M, **Murgia X**, Lehr C-M. *Chapter 3: Cellular and non- cellular barriers to particle transport across the air-liquid interface of the lungs*. In book: Bio-Nano-Responses. Publisher: Springer; Editors: Peter Gehr and Reinhard Zellner (**under review**)

1.1 Lung physiology

The main function of the lungs is to accomplish gas exchange. During tidal breathing, a stream of inhaled air is conducted through the airways to the deep lung, where oxygen diffuses from the alveolar space to the pulmonary capillaries[1]. Oxygen-rich capillary blood is then collected by the pulmonary vein, delivered to the left ventricle of the heart, and distributed throughout the whole body by the systemic circulation. This mechanism ensures oxygen supply to all tissues, enabling cellular respiration. Conversely, carbon dioxide, a metabolic product of aerobic respiration, is excreted from the cells to the venous circulation and transported to the lung vasculature, where it diffuses from the blood vessels to the alveolar space following a concentration gradient. Intrapulmonary carbon dioxide is then eliminated by exhalation, completing the respiratory cycle.

To fulfil the general aim of gas exchange, the lungs have well-differentiated areas with specialized functions. The *trachea*, *bronchi*, and *bronchioles* conform the ***conducting airways***[2]. The main function of the airways is to condition the inhaled air. After the primary bifurcation of the trachea, at the carina, the airways systematically branch over approximately 20 generations, progressively reducing the caliber of the airways, yet increasing the total airway cross-section[1].

The airway epithelium is usually defined as a pseudostratified columnar epithelium, which is primarily composed of *ciliated*, *goblet*, and *basal* cells (**Figure 1**)[3]. The latter type is located at the basal membrane and technically does not contribute to the luminal side of the epithelium, but plays a role as progenitor of ciliated cells[4]. The apical cell membranes of epithelial cells are exposed to the airway lumen and are firmly joined by inter-cellular tight junctions, dividing cell membranes into functionally differentiated apical and basolateral domains[2]. Goblet cells are secretory cells which together with submucosal glands secrete a mucus layer that covers and protects the airway epithelium[5,6]. Club cells, formerly known as Clara cells, gradually replace goblet cells in performing the secretory role at the bronchiolar level. Club cells secrete a mixture of compounds similar to the pulmonary surfactant, maintaining the patency of the bronchioles[7]. Ciliated cells, which in average display 250 cilia in their apical domain[8], are in charge of continuously propelling the mucus layer out of the lungs[9]. All these cellular and non-cellular elements work in a coordinated manner creating a sophisticated defense mechanism termed *mucociliary clearance*.

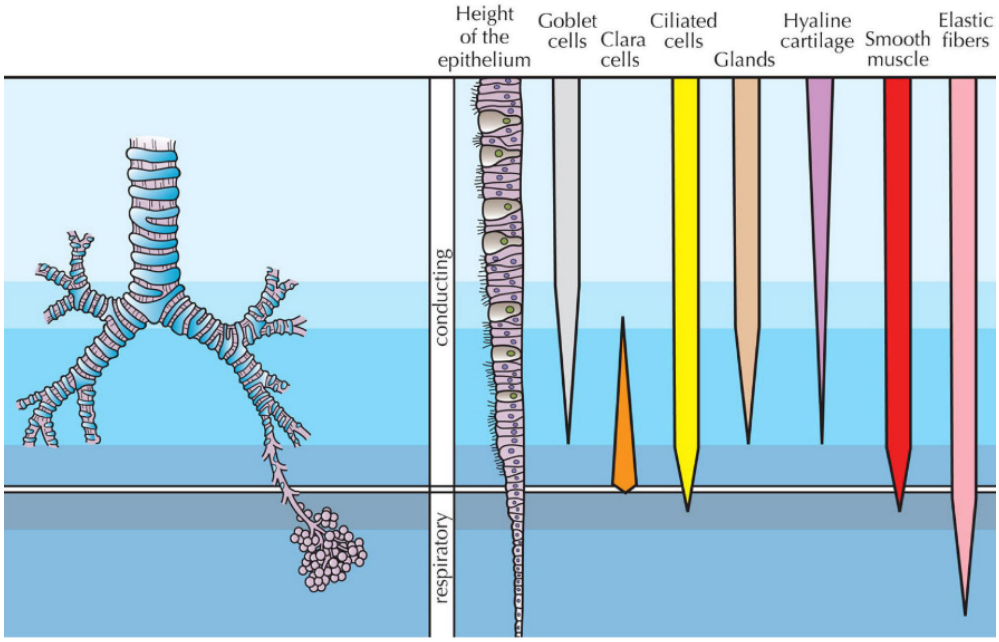

Figure 1. Schematic depiction of the respiratory system, from reference 10. Starting from the trachea, the *conducting* airways branch over more than 20 generations until the *respiratory* or *alveolar* region is reached. The main function of the conducting airways is to filter and moisturize the inhaled air. In the alveolar region, where the gas exchange occurs, the epithelium is organized as tiny air sacs, or *alveoli*, to increase the surface area for gas exchange. In advancing from the airways towards the alveolar region, the height of the epithelium decreases significantly. The cellular components of the mucociliary clearance mechanism (Goblet cells, Ciliated cells and submucosal glands) and the cartilage support predominate in the first airway generations. Clara cells gradually take over the secretory role of goblet cells at the bronchiolar level.

In advancing from the airways towards the deep lung, the composition of both the epithelium and the pulmonary lining fluid changes significantly. The main function at the deep lung, also known as the ***alveolar region***, is gas exchange[1]. The alveolar epithelium is organized as millions of extremely thin polyhedral air sacs, the *alveoli*, which serve to increase the surface area available for gas exchange[11]. In their luminal side, the alveoli are lined by a non-ciliated, squamous epithelium composed of alveolar type (AT) I and AT II cells[12]. Both AT I and AT II form tight junctions, creating a compact epithelial barrier at the air-liquid interface[13,14]. AT I cells cover approximately 90% of the alveolar surface and are extremely thin (0.2 µm in the cell periphery and 2–3 µm in the perinuclear region) to facilitate the diffusion of oxygen and carbon dioxide (**Figure 2**)[8,15]. In the opposite side of the basal membrane, a layer of endothelial cells mirrors the alveolar epithelium, completing the full picture of the so-called air-blood barrier. AT II cells, on the contrary, are cuboidal in shape and their main function is to synthesize and secrete the pulmonary surfactant, a substance composed of lipids and proteins that modulates the surface tension within the alveoli throughout the respiratory cycle[16,17]. The surface tension reducing function of surfactant is especially relevant at end-expiration, when the *radii* of the *alveoli* are very small, and the surface

tension reaches its maximum level. In this context, the presence of pulmonary surfactant counteracts the otherwise high surface tension at the alveolar air-liquid interface, avoiding alveolar collapse and facilitating alveolar re-expansion[16].

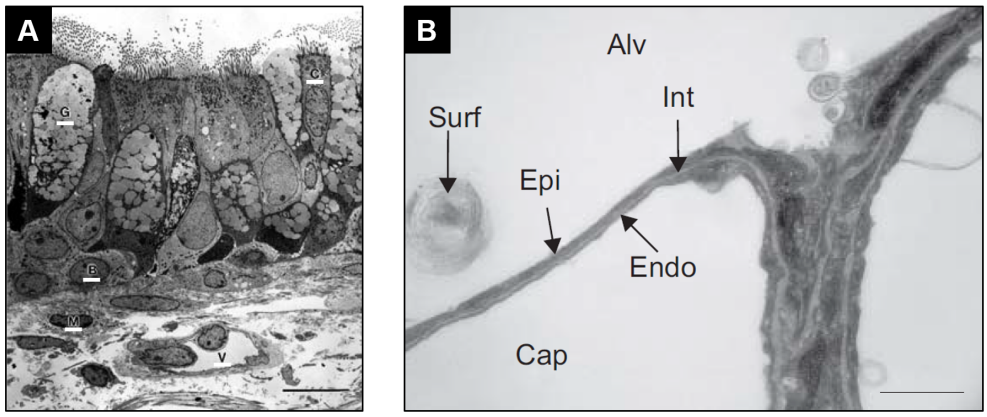

Figure 2. Transmission electron microscopy (TEM) images of the airway epithelium (A) and the alveolar epithelium (B), from references 18 and 19, respectively. The airway epithelium is a pseudostratified columnar epithelium. Ciliated cells (C), Mucus-secreting goblet cells (G) basal cells (B), mast cells (M) and a bronchial vessel (V) are in the TEM image. The scale bar in A represents 10 µm. Conversely, the alveolar epithelium is extremely thin (scale bar in B represents 1 µm). The sum of the alveolar epithelium (Epi), interstitium and endothelium (Endo), which sets the boundary between the alveoli (Alv) and the capillaries (Cap), the so-called air-blood barrier, accounts for less than 500 nm. A micelle of exogenous pulmonary surfactant (Surf), which had been previously delivered to the study subjects, is visible on the left-hand side of B.

The clearance of the deep lung is entrusted to alveolar macrophages, a monocyte-derived phagocytic cell type that engulfs foreign as well as exhaust endogenous material[20]. Alveolar macrophages preferentially phagocyte particles in the 1-5 µm size-range, but can also engulf and uptake particles in the submicron size-range[21–23]. Specific macrophages are located in the interstitial space, while other macrophages patrol the alveolar space[1]. Alveolar macrophages also play a relevant role in the immune and inflammatory response of the lungs by secreting inflammatory mediators and through their interaction with antigen presenting cells[24,25].

1.2 Drug delivery to the lungs

An average human inhale over 10,000 Liters of air every day, which ilustrates the high level of exposure of the respiratory epithelium with the surrounding medium. Therefore, the lungs represent an appealing entry route for non-invasive drug delivery, which expands over an approximate surface of around 100 m^2 [26,27]. Such a high surface area is intended to maximize gas exchange and is achieved by the optimized structure of more than 300 million *alveoli*[11]. In addition, the concentration of drug metabolizing enzymes is lower in the lungs compared, for instance, to oral and intravenous delivery[26]. The pulmonary route is ideal to treat lung diseases like chronic obstructive pulmonary disease (COPD), asthma, or respiratory infections, among others, because the dose of the active pharmaceutical ingredient (API) can be modulated and topically delivered to the site of action (air-to-lung delivery), reducing the overall systemic exposure as well as the potential side effects[28]. Nevertheless, the use of the pulmonary route is not limited to the treatment of lung diseases and may also be used for systemic delivery of APIs, taking advantage of the high surface area, the thin alveolar epithelium, and the high vascularization of the lungs[26]. Two examples of lung-to-blood delivery are inhaled insulin and inhaled dihydroergotamine, intended for the management of diabetes and migraine, respectively[29,30].

The use of nanoparticle (NP)-based drug delivery systems, or ***nanopharmaceuticals***, may not only improve current drug formulations, but may as well enable innovative therapies in the context of pulmonary drug delivery[31]. **Figure 3** gives an overview of the different possible structures of nanopharmaceuticals. The primary aim of formulating drugs as *nanopharmaceuticals* is to increase the therapeutic efficacy of active pharmaceutical ingredients (API), which may initially be attenuated by intrinsic physicochemical properties of the API, such as poor water solubility, reduced *in vivo* pharmacokinetics, and high toxicity[32,33]. Further appealing features of nanopharmaceuticals are the opportunity to deliver drugs to defined targets (e.g. tumors)[34], and the possibility to tune their size[35], shape[36], and release kinetics[37], which enables an overall improvement of drug bioavailability. Additionally, NPs can be coated with versatile polymers[38,39] or decorated with targeting molecules such as antibodies or cell penetrating peptides[40,41], which might enhance tissue penetration or even facilitate subcellular trafficking. Nanocarriers further protect their cargo from degradation, a feature that is particularly interesting in the case of nucleic acid delivery.

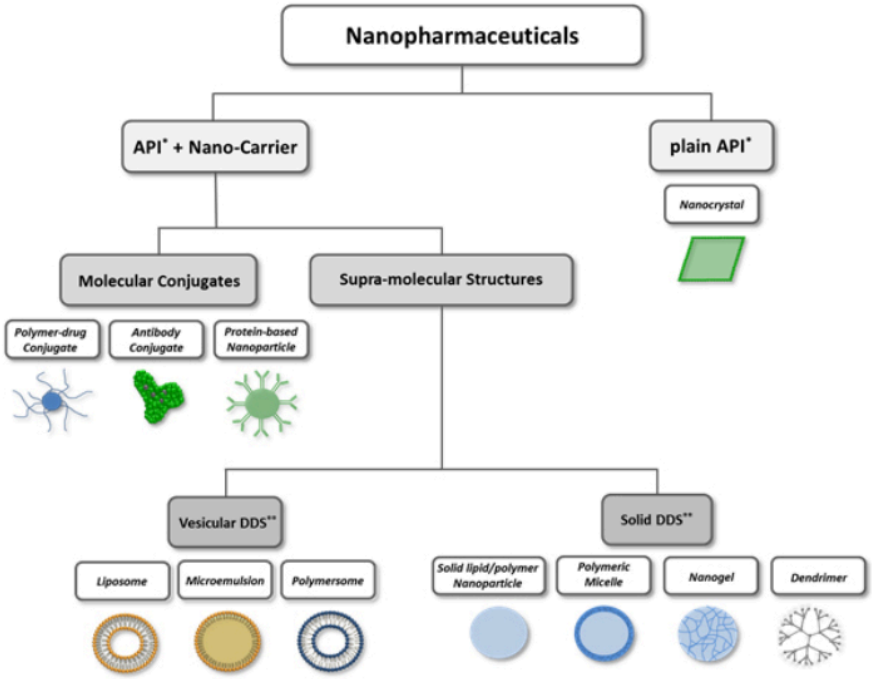

Figure 3: Overview of nanopharmaceuticals, from reference 42. API: Active Pharmaceutical Ingredient, DDS: Drug Delivery System.

Modern aerosol medicine dates back to the 1950s and was associated to the development of the first nebulizers[43]. Aerosol generating devices have significantly evolved since then and are capital to produce respirable aerosols with an appropriate particle size[28]. Pressurized metered dose inhalers (pMDI) are the most common type of device. pMDIs deliver metered dose of API upon actuation, which is propelled by a pressurized gas contained within the device. Dry powder inhalers (DPIs) are designed to release a dose of dried API when the patient's inspiratory effort reaches a threshold flow (usually around 30 L/min)[44]. DPIs and pMDIs provide a single dose of API in just one actuation and require a good inhalation technique from the patient's side. Nebulizers can deliver larger volumes of API converting a solution or a suspension into micron-sized droplets[28]. The choice of the device will mainly depend on the formulation, the required dose, and patient's characteristics and disease state.

The efficacy of an inhaled drug therapy is proportional to lung deposition[45], which is in turn significantly influenced by the aerosol characteristics and in particular by the particle size distribution of aerosol droplets. The ideal particle size for optimal lung deposition remains a disputed topic among aerosol researchers. Nevertheless, it is widely accepted that particles with an aerodynamic size above 6 µm impact on mouth and throat, particles between 2-6 µm deposit in the airways, and particles with an aerodynamic diameter below 2 µm deposit mainly in the deep

lung (**Figure 4A**)[46]. The characteristics of a therapeutic aerosol are usually defined by i) the Mass Median Aerodynamic Diameter (MMAD), which defines the particle diameter at which 50% of the aerosol mass is above and 50% is below (**Figure 4B**) ii) the Geometric Standard Deviation (GSD), which indicates the spread of particle size of an aerosol (GSD < 1.2 homodisperse aerosol; GSD > 1.2 heterodisperse aerosol) and iii) the Fine Particle Fraction (FPF), which describes the percentage of particles in mass with an diameter below 4.7 μm[47].

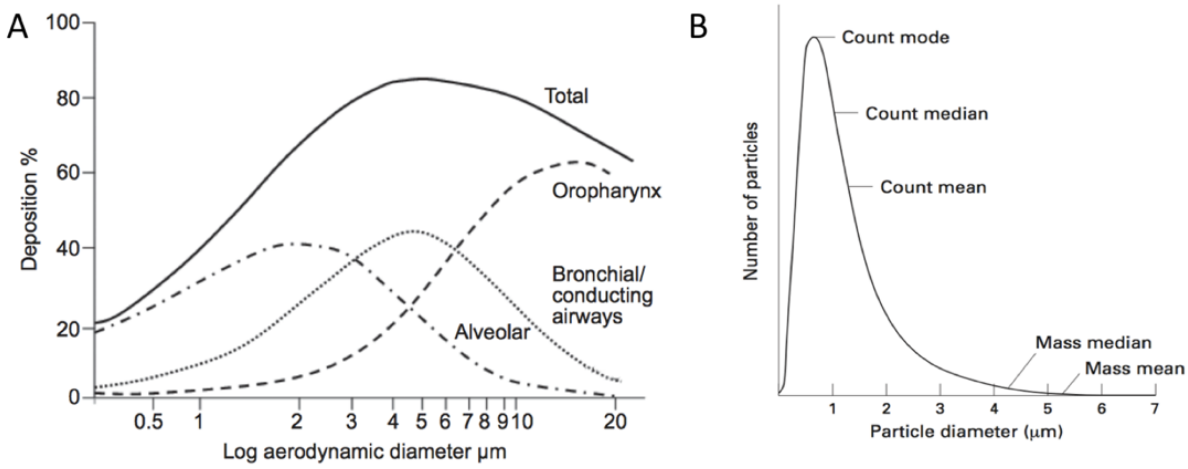

Figure 4. (A) Relationship between aerodynamic diameter and lung deposition, from reference 48. (B) Log normal particle size distribution of an aerosol produced by a nebulizer, from reference 49.

Significant advances in device development and aerosol medicine over the last decades have increased the relatively low lung deposition fractions of 10-15% of the nominal dose reported in the past to remarkable 50% deposition fractions obtained with currently available modern devices[28]. The optimization of aerosol lung deposition has shifted the focus of aerosol medicine towards addressing the fate of inhaled particles once they have landed in the lungs. It is particularly interesting to characterize how the physical-chemical characteristics of drugs and/or formulations influence the interaction with the biological barriers of the lungs, including non-cellular (mucus and surfactant) and cellular barriers (airway and alveolar epithelia as well as macrophages). The present thesis, analyzes in detail the role of airway mucus as a barrier to NPs.

1.3 Pulmonary mucus in health and disease

A protective layer of mucus covers the pulmonary airways. The main function of mucus is to entrap potential harmful particles contained in the inhaled air, including pathogens, pollutants, allergens, and other particulates[50]. Pulmonary mucus is in turn constantly cleared out of the lung by the coordinated beating of the cilia located in the apical side of epithelial cells[51].

Mucus is a hydrogel composed mainly of water (95%), mucin glycoproteins, lipids, DNA, non-mucin proteins, and cell debris[52,53]. The main organic component of mucus are mucins (MUC), a class of glycoproteins composed of a polypeptide backbone, encompassing a high number of tandem repeats of the amino acids proline-threonine-serine (PTS Sequences)[52,54], to which oligosaccharides are covalently bound through O-glycosylation[55]. The sugar portion of mucins may account up to 80% the total weight of mucin macromolecules[56]. Sialic acid (pKa 2.0-2.5) as well as sulfated monosaccharides (pKa of sulfate 2.0-2.6) predominate as terminal residues of the oligosaccharide side chains[57]. Therefore, at neutral pH these groups are deprotonated, conferring mucus a net negative charge (**Figure 5**).

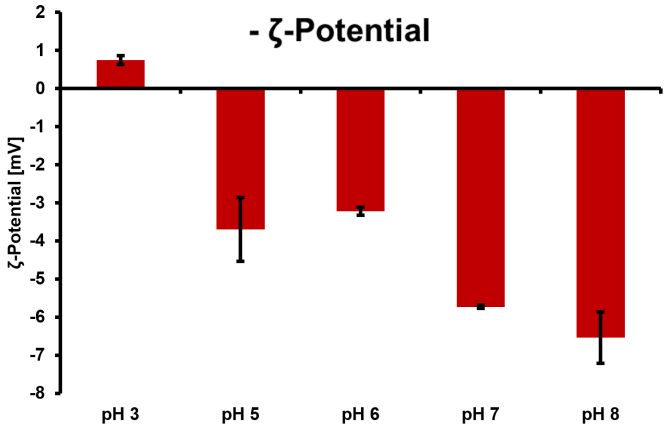

Figure 5. ζ-potential as a function of pH of commercially available mucin glycoproteins. Acetate buffer was used to achieve mucin solutions with pH values of 3, 5, and 6, and PBS and phosphate buffer to achieve pH of 7 and 8, respectively. The size and ζ-potential of all mucin suspensions were measured by means of dynamic light scattering.

MUC5A and MUC5B are the most relevant gel-forming mucins of the airways[58], which display a polypeptide backbone of over 5,000 amino acids and expand over 350 and 550 nm in length, respectively[59]. The edges of the polypeptide backbone of mucins have cysteine-rich domains[60], enabling the formation of intermolecular disulfide bonds[61]. Structured inter-mucin interactions create a covalently-linked, three-dimensional biopolymer network, which is primarily responsible for the viscoelastic properties of mucus (**Figure 6**).

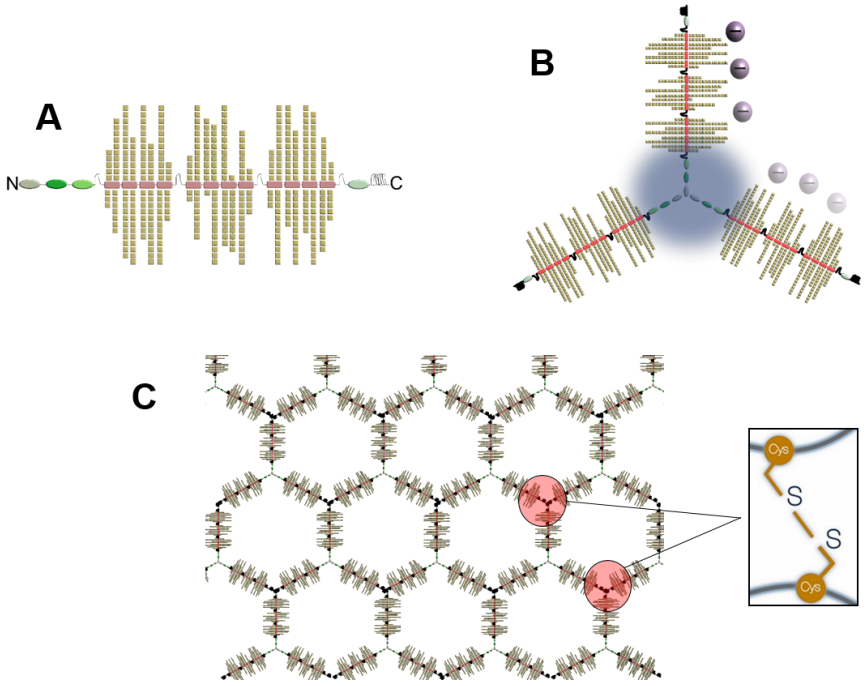

Figure 6. (A) The primary structure of mucins consists of a protein backbone (from N-terminal to C-terminal) with a high number of tandem repeats of the amino acids (pink boxes). Side-oligosaccharide chains are attached to PTS domains through O-glycosylation (yellow squares): sialic acid and sulfated N-acetylgalactosamine and galactose are the predominant outermost sugar residues. Cysteine-rich regions in the flanks of the mucin monomers serve to establish disulfide bonds with other mucin molecules. (B) Mucins can form dimers and trimers that further polymerize by establishing intermolecular disulfide bonds with neighboring mucins forming a dense network. Due to the prevalence of sialic acid and sulfated sugars, mucins are negatively charged. In addition, the naked protein regions (blue shadowed area) provide a site for hydrophobic interactions. (C) Disulfide bonds between mucin glycoproteins form a covalently-linked, three-dimensional biopolymer network. Adapted from reference 50.

There are two main mechanisms by which mucus can filter inhaled particles (**Figure 7**). On the one hand, mucus gels are riddled with submicron pores (20–500 nm)[62–64] and therefore, particles of a bigger size than the pores are physically hindered[65]. On the other hand, mucus hydrogels display a wide array of free functional groups that can eventually adsorb macromolecules and NPs[66,67], even when their size is lower than the mesh spacing of the mucin network[68]. As mentioned before, mucus has a net negative charge at physiological pH and can therefore adsorb cationic particles by electrostatic interactions[33,67–69]. Moreover, the non-glycosylated globular regions of mucins provide sites for hydrophobic interactions[50].

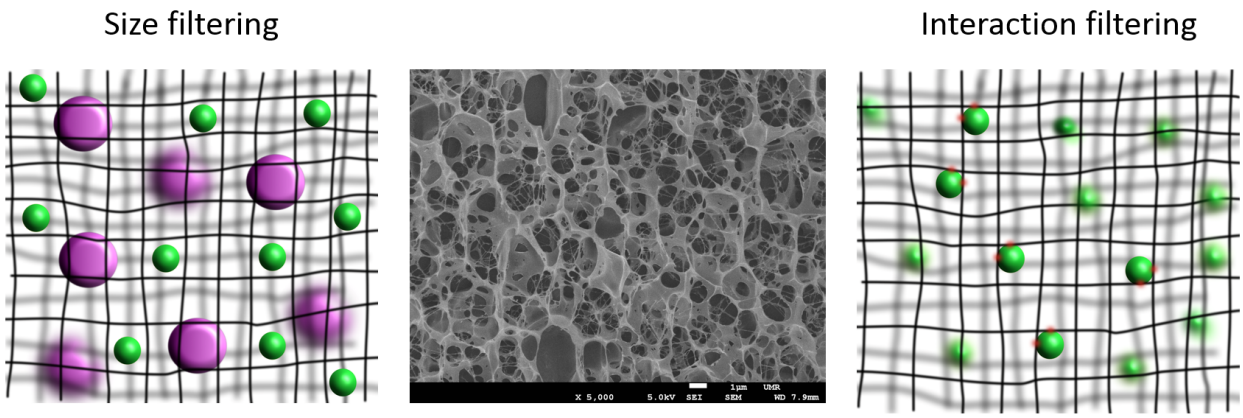

Figure 7. Schematic representation of the filtering properties of the mucus barrier. The size filtering mechanism of mucus is depicted on the left side: purple particles have a bigger size than the mesh spacing between mucus fibers and are therefore trapped within the network. On the other hand, green particles, with a smaller size than the mesh spacing could theoretically diffuse through the pores. However, the interaction filtering mechanism of mucus, depicted on the right side, allows adsorbing particles with a smaller size than the mesh spacing through different interactions. A cryogenic scanning electron microscope micrograph of human native tracheal mucus is shown in the middle. Adapted from reference 50.

Airway mucus is constantly shed from the airways featuring an efficient clearance mechanism termed mucociliary clearance (**Figure 8**)[51]. The coordinated ciliary beating of epithelial cells enables the unidirectional mucus transport out of the lungs. In healthy, non-smoking human volunteers the mucociliary clearance rate showed a high inter-subject variability ranging from 3.6 to 11.4 mm/min[70,71], which correlates good with experimental studies reporting mean clearance rates of 2 mm/min and 16 mm/min in chicken and in pig trachea, respectively[72,73]. According to these clearance rates, the residence time of inhaled particles trapped by mucus would be limited to a few hours, setting a limited time-window for drug delivery. Nevertheless, this estimation might not be entirely accurate since inhaled aerosol particles remain in the lungs up to several weeks. Möller *et al.* studied the dynamics of mucocilairy clearance in healthy, non-smoker humans[74]. The volunteers inhaled an aerosol dose of iron oxide particles (aerodynamic diameter of 4.2 µm) with the shallow bolus technique, which guarantees a high airway deposition. The authors found out that 25% of the particles were cleared form the airways after approximately 3 h, 50% after 24 h, while the remaining fraction was slowly cleared over a period expanding up to several weeks[74].

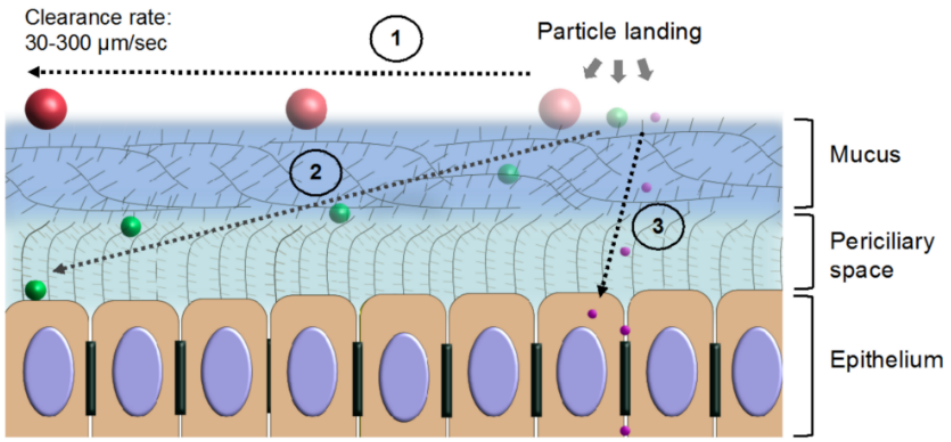

Figure 8. In the airways, mucus clearance sets a limited time-window for drug delivery. Mucus is continuously propelled out of the lungs by the coordinated movement of the cilia on top of the epithelial cells. When inhaled drug particles land onto mucus, their fate will depend on their physical-chemical properties: large (>500 nm) and/or mucoadhesive particles will most probably show reduced diffusion and will be rapidly removed from the lungs by mucociliary clearance (1). Particles with a size compatible with the mesh spacing of the mucus network (below 200 nm) and with an appropriate surface chemistry (non-interacting) may diffuse through mucus and eventually reach the cell surface (2). Small, uncharged drug molecules can rapidly penetrate mucus and be absorbed by the epithelium (3). From reference 50.

In disease states such as COPD, asthma, or cystic fibrosis (CF), the mucociliary clearance mechanism may be severely compromised, primarily due to changes on mucus composition, which significantly affect mucus viscoelasticity[75–77]. CF is a paradigmatic example of an impaired mucociliary clearance mechanism. It is a congenital autosomal recessive disease caused by a mutation of the cystic fibrosis transmembrane conductance regulator (CFTR)[78]. The main function of CFTR is the transport of ions, contributing to epithelial as well as to airway fluid homeostasis. Therefore, non-functional CFTR causes an imbalance of mucus hydration, which leads to highly viscous mucus[79] as well as to a reduction and eventually a full depletion of the periciliary fluid[80]. Such a tenacious mucus cannot be cleared out by the mucociliary escalator, providing opportunity for bacterial colonization and proliferation. Mucus thickening in the course of CF is further increased by additional pathophysiological events such as mucin hypersecretion[77], DNA and actin accumulation from apoptotic neutrophils[81], the establishment of additional intra-mucin disulfide bonds promoted by oxidant stress[82], and the development of bacterial biofilms (**Figure 9**)[83].

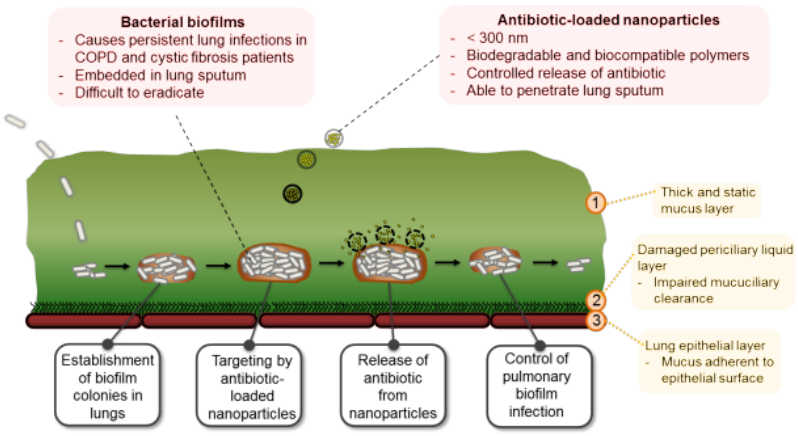

Figure 9. Airway colonization of *Pseudomonas aeruginosa* and development of drug-resistant biofilms. Mucus penetrating nanoparticles, may provide a controlled and sustained antibiotic release in the vicinity of bacterial biofilms.

CF airways are prone to infection with pathogens such as *Staphylococcus aureus*, *Haemophilus influenza*, *Pseudomonas aeruginosa*, *Burkholderia cepacia* complex, and *Stenotrophomonas maltophilia*[84]. Among these, the Gram-negative, rod-shaped *Pseudomonas aeruginos*a is the major biofilm-building pathogen in CF lungs[85], which in turn also worsens the prognosis for morbidity and mortality in the context of CF[78]. Upon airway colonization, *Pseudomonas aeruginosa* has a great capacity to adapt to the airway environment. For instance, it can counteract the loss of motility with the development of biofilms, defined by HØiby *et al.* as a structured consortium of bacteria, embedded in a self-produced polymer matrix consisting of polysaccharide (e.g. alginate), protein and DNA[86].

CF patients receive antibiotic therapy from the early childhood[87]. Antibiotic therapy works best at early stages of *Pseudomonas aeruginosa* infection. Nevertheless, after *Pseudomonas aeruginosa* chronic colonization, a full eradication is difficult to achieve due to the assorted *armamentarium* displayed by the bacteria to evade antibiotic treatment (**Figure 10**)[88].

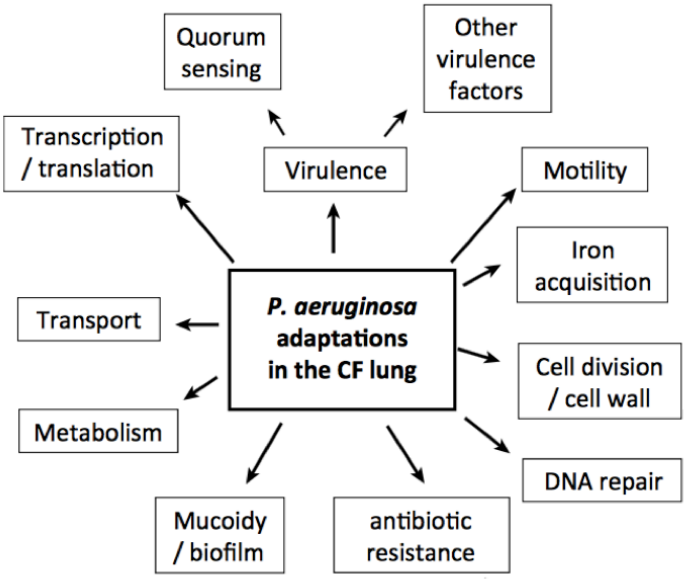

Figure 10. Pathoadaptive mutations in Pseudomonas aeruginosa. Adapted from reference 88.

Although intravenous antibiotic therapy is feasible and sometimes necessary, topical, non-invasive delivery of antibiotics by aerosolization reduces the systemic toxicity and thereby provides higher tolerance. Five antibiotics are currently prescribed or undergoing clinical trials for the management of lung infections in the context of CF: colistin, tobramycin, aztreonam, levofloxacin, and ciprofloxacin[89,90]. Interestingly, colistin and tobramycin are polycationic antibiotics, which may reduce their diffusion through airway mucus[66,91].

1.4 Strategies to deliver nanomedicines to and through mucus

A layer of mucus covers and protects the epithelia of the most relevant non-invasive drug delivery routes, including the whole gastro-intestinal drug, the airways, the eyes and the vaginal tract[50]. This protective mechanism is nowadays acknowledged as a significant barrier to drug delivery, in particular to NP-based drug delivery systems[92,93].

Early studies on the mucus barrier focused mainly on the permeation of relatively small drug molecules through intestinal mucus. These studies consisted mainly on testing the permeation through mucous gels of different arrays of molecules of well-known molecular weight, solubility, and charge[94–98]. These studies suggested that mucus can reduce the diffusion of most (macro)molecules due to unspecific interactions, but particularly hinders the diffusion of lipophilic as well as positively charged molecules.

For NP-based drug delivery systems, not just the chemical filtering but also the size-filtering mechanism applies[63,99]. The pore-size of respiratory mucus has been estimated from electron microscopy as well as from particle tracking studies. These studies revealed that mucus has a highly inhomogeneous structure with a broad pore-size distribution spanning from few nanometers to micrometer size-range pores[62,99,100]. Nevertheless, the number of pores in the micrometer size-range must be relatively low, since 500 nm stealth particles (i.e. coated with polyethylene glycol) are almost exclusively immobilized by native airway mucus[63]. Irrespective of their size, NPs displaying cationic surface charge or an exposed hydrophobic core are avidly adsorbed by mucus components[33,67,68,99].

The physico-chemical characterization of mucus has enabled the development of different mucosal drug delivery strategies, including muco-adhesion and muco-penetration (**Figure 11**). ***Muco-adhesion*** intentionally seeks the interaction between mucus and drug delivery systems. This strategy aims at increasing the residence time of the API in the epithelial surface, providing a sustained release[101]. Muco-adhesion can be achieved, among others, by coating drug delivery systems with cationic polymers (e.g. chitosan)[102,103], by employing thiolated polymers, which form disulfide bonds with cysteine residues of mucins[104,105], or by formulating drug delivery systems with polymers such as poly(acrylic) acid (PAA), which will further promote physical entanglement between the polymer chains and mucins[106]. Muco-adhesive systems may be beneficial for oral, occular, or vaginal delivery. In the context of pulmonary drug delivery, however, the efficiency of muco-adhesive drug delivery systems may be limited due to the relatively fast clearance rates. Moreover, such muco-adhesive NPs may simultaneously interact with several mucin fibers, which

has been associate to an increased mucus elasticity and altered microstructure[68,107,108]. These changes may significantly impact the clearance rate and the protective barrier properties of mucus.

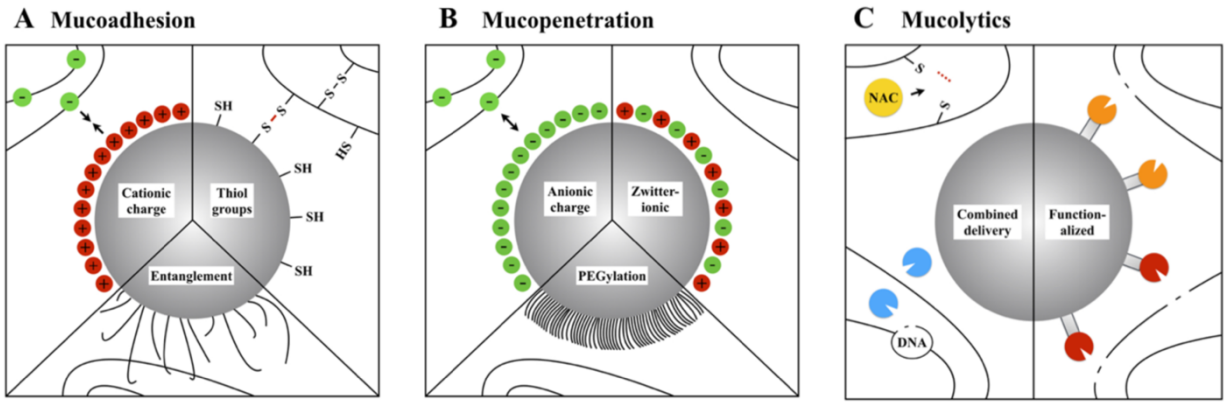

Figure 11. Several strategies have been used to modify the surface of nanocarriers for an improved drug delivery to mucosal tissues. Mucoadhesive drug delivery systems provide an increased interaction with the mucus layer (A). Positively charged particles (e.g. chitosan) bind to negatively charged mucins based on electrostatic interactions (left side). Particles that incorporate reactive thiol groups (-SH) on their surface attach to mucus by forming disulfide bonds (right side). Carrier systems decorated with polymers like PAA lead to physical chain entanglements with mucus fibers and increase steric hindrance (bottom). Mucus-penetrating systems tend to reduce mucus interaction (B). Highly negatively charged particles avoid mucus interaction due to electrostatic repulsion (left side). Zwitterionic particles are modified with interspersed positive and negative surface charges, producing a net neutral charge that facilitates the diffusion through mucus (right side). PEGylated particles possess densely packed polymer chains that form a hydrophilic layer for effective mucus penetration (bottom). The application of mucolytic agents enables the diffusion of drug delivery systems through mucus by altering its structure and decreasing the overall viscosity (C). Encapsulated therapeutic compounds are delivered in combination with mucolytic agents such as NAC (yellow) that reduces disulfide bonds (S-S) between cross-linked mucins or DNase (blue) that degrade DNA present in mucus (left side). Particles that are functionalized with enzymes like papain (orange) and bromelain (red) disrupt the mucus gel structure in order to enhance muco-penetration of delivery systems (right side). Adapted from reference 50.

For airway targeting with NPs (e.g. transfection in CF or antibiotic therapy in lung infections), where a deeper level of mucus penetration is often required, ***muco-penetration*** represents a more appropriate strategy[93,109]. Muco-penetrating NPs must be compatible with the mucus' pore-size (<300 nm) and must display a *muco-inhert* surface chemistry. In this regard, coating NPs with polyethylene glycol (PEG) is a widespread strategy that renders NPs hydrophilic, shielding them from mucus adsorption[38,110]. Liposomes, polymeric NPs, and dendrimers coated with a dense layer of PEG generally show a higher diffusion through native mucus compared to their uncoated versions[63,111–115]. In the same spirit as PEGylation, *zwiterionic* NPs display interspersed positive and negative charges on their surface, yielding a net neutral charge, which in turn reduces the adsorption of endogenous molecules, thus improving their diffusion through mucus[116]. A potential advantage of zwiterionic NPs over PEGylated ones relates to their cellular uptake. Zwiterionic NPs

have shown good NP-cell interaction, and may be advantageous for intracellular targeting[117]. Conversely, in the case of PEGylation, the same mechanism that improves muco-penetration impedes, to a certain extent, the establishment of NP-cell contacts as well as their cellular uptake[110].

The use of mucolytic agents has also been proposed as an alternative strategy to increase the diffusion of NPs through mucus layers[118,119]. Mucolytics are routinely prescribed in the context of CF to manage the tenacious airway secretions of CF patients. They cleave specific chemical bonds occurring in mucus gels, thereby reducing their overall viscoelasticity [120]. N-acetyl cysteine (NAC) cleaves the disulfide bonds established between mucin macromolecules[121], whereas recombinant DNase is used to degrade the extracellular DNA accumulated in the airways of CF patients[82]. For instance, the application of an intranasal dose of NAC before the administration of highly compacted DNA NPs was associated with a marked increase of gene expression in mice compared to the application of NPs alone[122]. Thus, the co-delivery of mucolytics and NPs may provide deeper mucus penetration in pathophysiological scenarios in which the overall mucus' viscoelasticity is increased. An alternative strategy of mucolysis, consist of decorating the surface of NPs with mucolytic molecules, such as DNase, or the proteolytic enzymes bromelain and papain[123–125].

1.5 Models and tools to investigate nanoparticle-mucus interactions

One of the major drawbacks regarding the study of drug-mucus interactions is the limited accessibility to good quality human mucus samples. In addition, one must bear in mind that common scientific technical procedures such as fixation, washing, drying, and other routine sample manipulations significantly alter the original structure of mucus hydrogels, which may introduce a bias in the experimental read-outs.

Expectorated sputum of CF patients can be collected in tubes for further experimentation[91,126,127]. Such samples, however, are usually contaminated with saliva and show a marked inter-subject variability as a function of the patient's disease state[62]. Small volumes of native tracheal mucus can be collected from the endotracheal tube of patients undergoing elective surgery[128]. Alternatively, native mucus samples from animal origin can be obtained from abattoirs by directly scratching the mucus from the surface of excised mucosal tissues[99,129]. To counteract the limited availability of native mucus samples, some researchers have developed synthetic mucus surrogates[129–131]. Although some of these synthetic mixtures could somehow mimic the mechanical properties of native mucus[129,131], other surrogates lack inter-mucin cross-linking and do not elicit a three-dimensional network, which may overestimate the diffusion of NPs[132–134].

Drug-mucus interactions have been traditionally addressed by investigating the transport rate over time of drugs in diffusion cells[135,136]. Such systems comprise a donor compartment, where a certain concentration of the drug molecule of interest can be added, a central compartment with a semipermeable membrane, where mucus is placed and held by the membrane, and an acceptor compartment, which allows repeated sampling and detection of the drug molecule of interest. Using the donor-to-acceptor strategy several methods have been developed by different research groups including side-by-side systems[94], Franz diffusion cells[137], Ussing chambers[138], and Transwell®-based permeation assays[139], among others. These systems have been used for many decades and are still used in drug permeation studies. When using this approach, a diligent experimental design should include a set of control experiments aimed at determining the capacity of the semipermeable membrane to retain drug molecules, in particular, if NP-based drug delivery systems are tested. The diffusion of nanocarriers through such systems might require longer experimental times, which might lead to a partial dissolution of the mucus layer into both the donor and acceptor compartments[62].

Fluorescence Recovery after Photobleaching (FRAP) has been used to estimate the diffusion through mucus of macromolecules, including proteins and DNA, viruses, and NPs[99,119,140,141]. In this technique, fluorescent molecules are dispersed within mucus and transferred to a laser-

equipped fluorescence microscope. Thereafter, the region of interest is localized, and a short series of pre-bleaching images are recorded at relatively low laser power to define the baseline (100%) intensity. The next step consists of bleaching a defined area by increasing the laser power until the fluorescence of the fluorophores is ablated or at least significantly attenuated (at least a 50% reduction of the baseline fluorescence intensity). The post-bleaching point is set as 0% fluorescence intensity. In the last part of the experiments, the laser power is reduced to pre-bleaching values, and a time-series of photomicrographs is captured to investigate the percentage intensity recovery of fluorescence over time (from 0% to 100%). If the molecules can diffuse through mucus, then, new, fresh-fluorescent molecules will replace the bleached ones, and the fluorescent intensity will increase over time until the recovery curve saturates at a certain level **(Figure 12**).

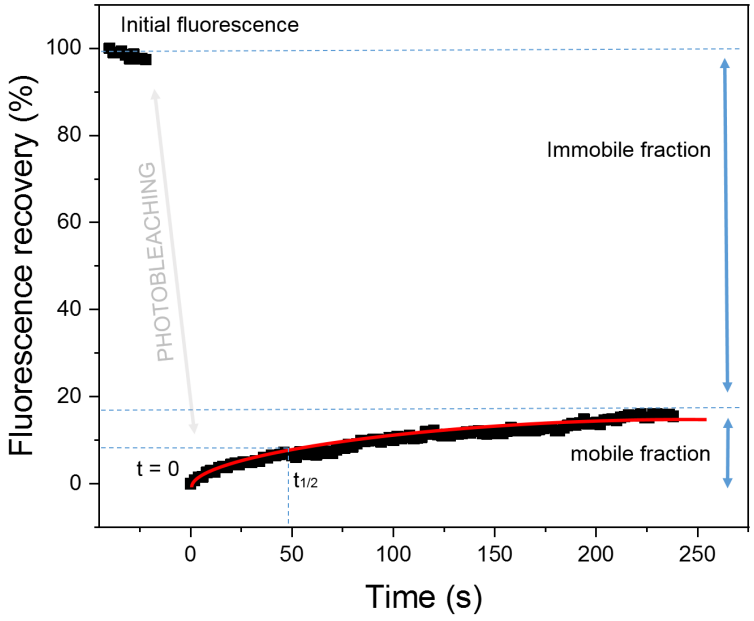

Figure 12. Representative Fluorescence Recovery after Photobleaching (FRAP) experiment of 100 nm carboxyl-coated polystyrene nanoparticles (NPs) dispersed in human tracheal mucus. In FRAP experiments, a short series of pre-bleaching images are recorded at relatively low laser power to define initial fluorescence intensity (100%). The next step consists of bleaching a defined area by increasing the laser power until the fluorescence is significantly reduced. The post-bleaching point is set as 0% fluorescence (t=0). The laser power re-set to pre-bleaching values, and a time-series of photomicrographs is captured to investigate the percentage intensity recovery of fluorescence over time. The percentage of recovered fluorescence resembles the mobile NP fraction, whereas the non-recovered intensity represents the immobile fraction. Mathematical modelling of the recovery curve allows (red fitting line) the calculation of $t_{1/2}$, which may be further used to calculate the diffusion coefficient of the mobile particle ensemble.

Conversely, if particles cannot diffuse through mucus at all, the fluorescence intensity will remain steady after photobleaching (close to 0%). The fluorescence intensity percentage value at which

the recovery curve saturates is often referred to as the mobile particle fraction, whereas the remaining percentage represents the immobile fraction. Applying mathematical fits to the recovery curves the diffusion coefficient can be estimated[142,143]. By using FRAP, however, the obtained diffusion coefficient corresponds to that of the particle ensemble, because FRAP does not consider the particles individually.

Multiple particle tracking (MPT) is a powerful technique that allows the simultaneous analysis of the diffusion of about 100-300 NPs in a single experiment[144]. Interestingly, MPT considers each particle trajectory individually, providing a high statistical power to each experiment (**Figure 13**). In this technique, NPs are mechanically dispersed in mucus, and their trajectories are followed by means of video-microscopy over a short period (usually 1-10 seconds). MPT experiments are commonly performed with high magnification, high numerical aperture objectives and the image series are captured at a relatively high frame rate (minimally, 20 frames per second). By computing the X and Y position of each particle at each frame of the sequence, the trajectories of the particles can be reconstructed, and the mean squared displacement (MSD) can be calculated.

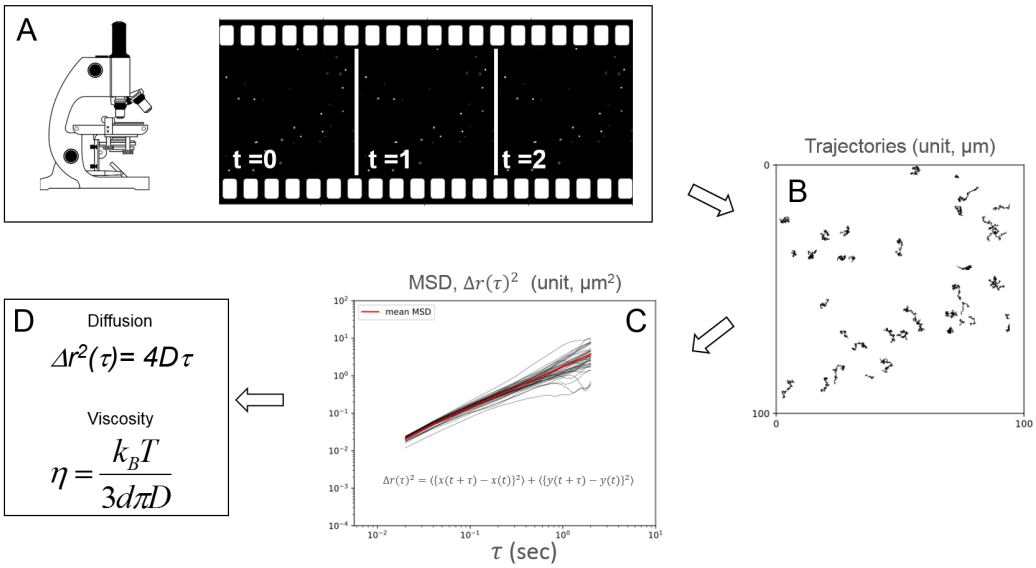

Figure 13. Schematic process of Multiple Particle Tracking (MPT) analysis. Tracer nanoparticles are mechanically dispersed in mucus and video-microscopy is performed over a short period (usually 1-10 seconds) at a frame rate not lower than 30 fps (A). By computing the X and Y position of each particle at each frame of the video-sequence, the trajectory of each particle in the microscopic field can be reconstructed (B), and the Mean Squared Displacement (MSD or $\Delta r(\tau)^2$) as a function of the time scale (τ) can be calculated (C). The MSD can be used to determine particle diffusion as well as the viscosity (η) of the surrounding medium. Diffusion, D; Boltzmann constant, K_B; Temperature, T; particle Diameter, d.

The MSD can be further used to obtain the diffusion coefficient of the NPs. The MSD values can also be used to determine further rheological parameters of the surrounding medium such as viscosity and elasticity[145].

Mucus-secreting, cell-based *in vitro* models provide an excellent tool to investigate NP translocation through the bronchial epithelium[56,146]. Such models, would theoretically allow as well to address the uptake of NPs in the presence as well as in the absence of mucus, a condition that is difficult to resemble in animal models. Human-derived primary cells from patients and healthy volunteers can be regarded as preferential sources to study drug permeation through the lung epithelium[14,147]. Cultured primary bronchial cells form a close-fitting barrier expressing tight junctions[148]. Moreover, primary cells can secrete mucus and even display ciliary motion *in vitro*[149]. However, the availability of human primary cells is limited and their culture is associated to a relatively high cost.

As an alternative to primary cells, immortalized cell-lines represent a readily accessible, cost-effective solution. In this regard, several cell lines have been used in the literature to mimic the bronchial epithelium including A549, NCI-H441, BEAS-2B, 16HBE140-, CFBE410- and Calu-3[3,8,69,146,150,151]. Although all these cell lines show some interesting features in the context of pharmaceutical research, they also a have a number of limitations. A549 and BEAS-2B monolayers fail to establish tight junctions with neighboring cells[56], which limits their use as models for the permeation of small drugs. Conversely, H441, 16HBE140-, CFBE410- and Calu-3 express tight junction if they are cultured under submerged culture conditions in so called Transwell® supports[67,150,152,153]. However, their barrier properties, as determined by trans-epithelial electrical resistance measurements (TEER), drop dramatically if they are cultured at the air-liquid interface[154,155], i.e. cells receive nutrients from the basolateral compartment, while their apical compartment is directly exposed to air. Excluding Calu-3, a major limitation of all these bronchial-like cell-lines is that they lack the capacity to synthesize and secrete mucins[69]. Calu-3 cells grown at the air-liquid interface differentiate into a pseudostratified columnar monolayer, display functional tight junction proteins, and secrete mucins, which further accumulate over time on top of the cell monolayer[153,154]. Thus, Calu-3 cell line meets most of the requirements for drug permeation studies and is widely used in this regard. A drawback of Calu-3 cells cultured at the air-liquid interface is the relatively large culture time required to secrete a confluent mucus layer, which can take up to 3 weeks[69,153,154].

2. Aims of this thesis

1. To **characterize** the barrier properties of **native airway mucus** and its implications for the therapeutic delivery of NPs, with special emphasis on:
    a. Addressing the size-dependent diffusion of NPs after being mechanically dispersed within mucus.
    b. Correlating the corresponding diffusivity data for differently-sized NPs with the penetration of such NPs delivered as aerosols onto mucus.
    c. Analyzing mucus' structure by means of label-free methods, which avoid chemical fixation

2. To develop a **cell-based model of the airways**, minimally comprising epithelial cells and mucus. Such model should allow:
    a. Depositing aerosolized NPs at an air-liquid interface.
    b. Studying the role of mucus as non-cellular element of the bronchial barrier.
    c. Investigating the transport, diffusion, and efficacy of small drugs, macromolecules and NPs through the airway model.

3. Major outcomes of the thesis

3.1 Characterization of Native Airway Mucus: implications for NP-based drug delivery to the airways

This chapter refers to the following publications:

Murgia X*, Pawelzyk P*, Schaefer UF, Wagner C, Willenbacher N, Lehr C-M. *Size-limited penetration of nanoparticles into porcine respiratory mucus after aerosol deposition*. Biomacromolecules 2016;17:1536–42.

Vukosavljevic B*, **Murgia X***, Schwarzkopf K, Schaefer UF, Lehr C-M, Windbergs M. Tracing molecular and structural changes upon mucolysis with N-acetyl cysteine in human airway mucus. Int J Pharm 2017;553:373–6.

*Equal contribution

Nanomedicine holds a great potential as an alternative method for the development of new therapeutic delivery approaches in the context of aerosol medicine, including gene-therapy, anti-cancer treatments, and antibiotic delivery[123,156,157]. d'Angelo *et al.* systematically summarized a broad range of NP-based drug delivery systems intended for pulmonary drug delivery[31]. Those therapeutic NPs targeting the airway epithelium may require different mucus penetration levels. For instance, intracellular nucleic acid delivery requires full penetration of the mucus layer, whereas the delivery of encapsulated antibiotics may just need certain mucus penetration to reach the bacterial biofilms developed within the airways of CF patients. Therefore, it is essential to characterize and understand the interaction between native airway mucus and therapeutic NPs.

In this thesis, state-of-art techniques such as FRAP and MPT analysis were applied to address the size-dependent mobility of NPs through native airway mucus[63,119]. In the first place, 100 nm, 200 nm, and 500 nm carboxyl-terminated, polystyrene NPs were mechanically dispersed in porcine mucus and observed under the microscope. With regard to MPT data, it was found that 43%, 51% and 6% of 100 nm, 200 nm and 500 nm particles, respectively, were diffusive in native porcine tracheal mucus (**Figure 14 A**). FRAP data correlated well with MPT observations, showing a mobile NP fraction of 24%, 54% and 14% for 100 nm, 200 nm, and 500 nm particles respectively (**Figure 15 B**).

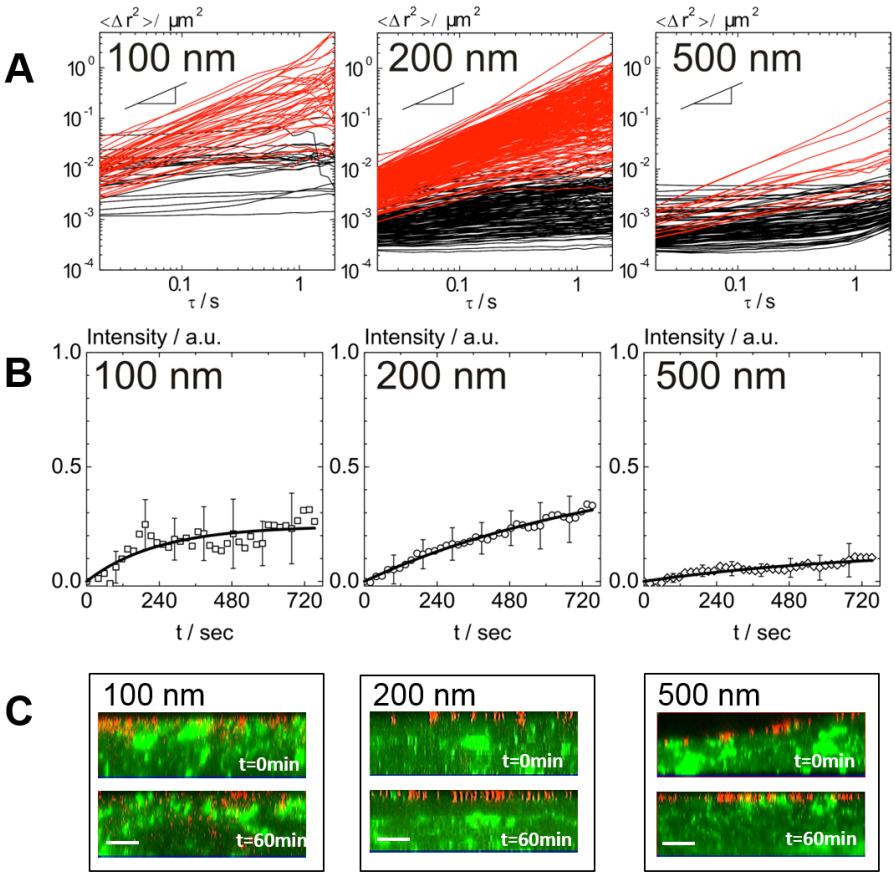

Figure 14. (A) Mean squared displacement (Δr^2) of carboxylated nanoparticles in pulmonary pig mucus as a function of time scale (τ). The red lines represent the MSDs with a slope α >0.5, classified as diffusive, and the black lines the MSDs with α <0.5, classified as immobile. The gradient triangle in each Figure illustrates a slope of 1. (B) Fluorescence intensity recovery over time t determined from Fluorescence Recovery After Photobleaching experiments using 100 nm (squares), 200 nm (circles) and 500 nm (diamonds) particles and the corresponding exponential fits. (C) Confocal laser scanning microscopy study on the penetration of aerosolized 100 nm, 200 nm and 500 nm red-fluorescent carboxylated nanoparticles through native porcine pulmonary mucus (stained green with wheat germ agglutinin). Representative cross-sections of 25-40 µm of the Z-stacks captured at t=0min, directly after aerosol delivery of nanoparticles, and at t=60 min, one hour after aerosol delivery. Adapted from reference 99.

These data, and that of others[63], clearly show that particles with a size of 500 nm and above are not optimal for drugs requiring a full translocation of the mucus layer. The limited diffusion through airway mucus of particles above this cutoff size is directly related to the pore-size of mucus, since stealth, PEGylated particles are also immobilized by the mucin network[63].

In FRAP and MPT techniques, particles are mechanically dispersed in mucus with a pipette, forcing their penetration into mucus' pores. The way in which particles and mucus interact with this mixing method, however, differs significantly compared to depositing particles in the form of

an aerosol onto a mucus layer, which represents a more realistic scenario in the context of aerosol medicine and pulmonary drug delivery. Therefore, an alternative experiment was designed in which NPs were deposited as aerosols onto fluorescently-labelled mucus layers. A clinically-approved vibrating-mesh nebulizer was used to generate the aerosols[158]. Immediately after aerosol deposition, cross-sections (X-Z) of the mucus layer were captured (t=0 min) by confocal laser scanning microscopy. The procedure was repeated again one hour later, at t=60 min. As expected, most NPs were concentrated at the air-mucus interface at t=0, irrespective of their size. Surprisingly, only 100 nm penetrated the mucus layer after one hour (**Figure 14 C**). Five-hundred and 200 nm NPs could not penetrate the mucus layer within the set experimental time, most probably, by the lack of sufficiently large pores.

A limitation of this study was the use of porcine tracheal mucus as a surrogate of the human material. Porcine tracheal mucus was directly scratched from the windpipes of slaughtered pigs, which often introduces blood as well as airway epithelial cell contamination. Additionally, airway mucus samples derived from slaughtered pigs may contain traces of edema fluid, derived from an increase of the alveolar permeability during sacrifice (source: personal interview with the veterinary Dr. Bianca Schwarz). Therefore, to confirm the previously describe observations, MPT, FRAP, and aerosol deposition experiments where replicated in native human tracheal mucus.

A technique to obtain human airway mucus was adopted from Rubin *et al.*[128]. According to this method, the distal parts of the endotracheal tubes of patients undergoing elective surgery with general anesthesia were collected immediately after surgery and placed into centrifuge tubes. Mucus was then extracted by centrifuging the endotracheal tube at 190 g for 30 s (**Figure 15**). Mucus samples were obtained after obtaining informed consent from all patients and in compliance with a protocol approved by the *Ärztekammer des Saarlandes* (file number 19/15).

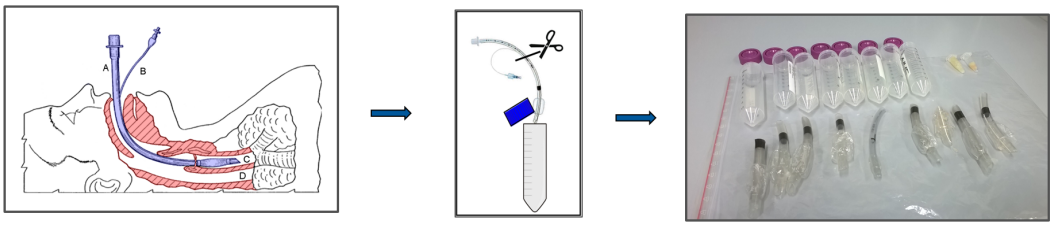

Figure 15. Undiluted human tracheal mucus samples were obtained from patients undergoing elective surgery, non-related to pulmonary diseases (left). The distal portion of the tracheal tubes was collected in centrifuge tubes (center). Airway mucus was extracted by brief centrifugation of the samples (right).

The rheological profiling of human mucus showed a markedly more tenacious material compared to porcine mucus. The yield point (cross-link between the elastic modulus, G', and the viscous modulus, G'') of the human material could not be detected within the 1-10% strain range, whereas it was as low as 0.8% for porcine mucus (**Figure 16 A**). In addition, the elastic modulus of human tracheal mucus was noticeably higher compared to porcine mucus, indicative of a more cross-linked hydrogel (**Figure 16 B**).

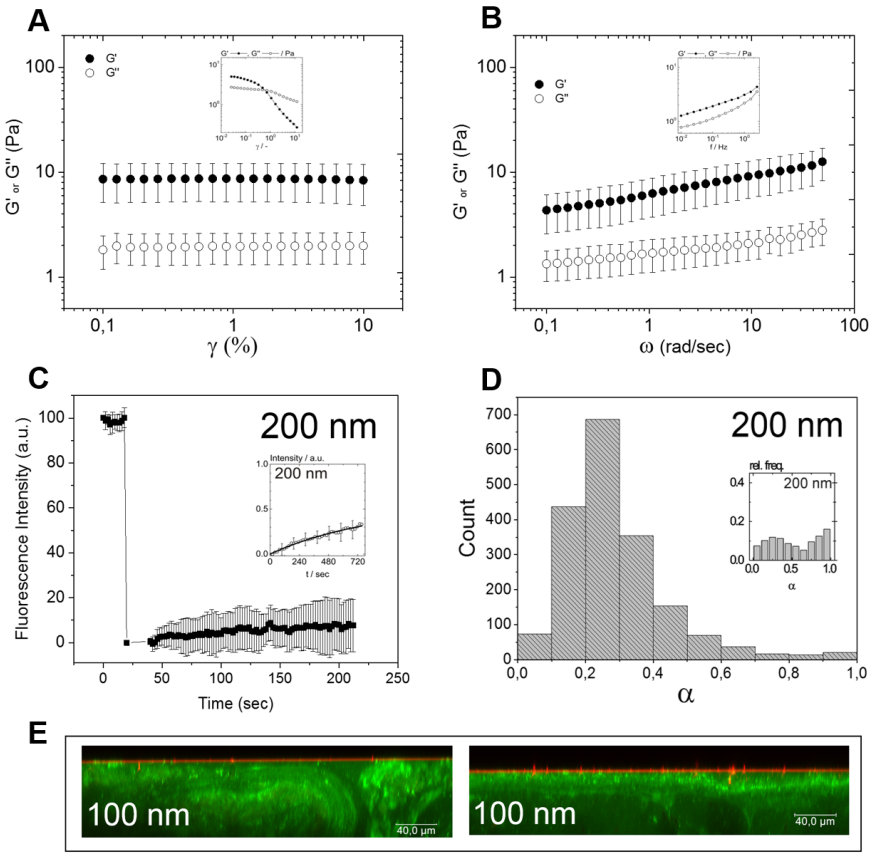

Figure 16. Interaction of nanoparticles with undiluted human tracheal mucus. (A) Strain (γ)-dependent viscous (G'') and elastic (G') moduli from 0.1 to 10% strain at a frequency of 6.28 rad/s (1 Hz). (B) Frequency-dependent viscous (G'') and elastic (G') moduli from 0.1 to 50 rad/s at 1% strain. The mean ± standard error for n=5 are shown. (C) Fluorescence intensity recovery over time determined from Fluorescence Recovery After Photobleaching experiments 200 nm carboxylated particle. The mean ± standard error for n=12, from 3 independent mucus samples are shown. (D) The histogram depicts the slope of the mean squared displacement at a time scale of 2 sec averaged from the relative frequencies of n = 9, from 3 independent mucus samples. (E) Confocal laser scanning microscopy study on the penetration of aerosolized 100 nm red-fluorescent carboxyl-coated nanoparticles through native porcine pulmonary mucus (stained green with wheat germ agglutinin). Two representative cross-sections of the Z-stacks captured at t=60 min, one hour after aerosol delivery. The insets in A, B, C and D correspond to the same measurements performed with porcine tracheal mucus.

The mobile fraction of 200 nm NPs, which was estimated to be 54% ± 5 in FRAP experiments with porcine mucus, was dramatically reduced in human mucus to just 7.64% ± 12 (**Figure 16 C**). Similarly, the distribution of the slopes of MSD, as determined by MPT, showed just 8.9% of diffusive 200 nm NPs in human mucus, compared to 51% in porcine mucus (**Figure 16 D**). Lastly, opposite to what it was observed with the porcine mucus, 100 nm particles could not penetrate human mucus and were almost exclusively concentrated at the air mucus interface 60 min after their delivery **(Figure 16 E**).

The ultrastructure of human tracheal mucus was further investigated by cryogenic scanning electron microscopy (CryoSEM). At the first sight, CryoSEM images revealed areas of high cross-linking density (**Figure 17 A and B**), as well as areas with bigger voids (**Figure 17 C**). The pore-size at prominently cross-linked areas appears to be of just few nm, which would perfectly explain the low fraction of mobile NPs detected by FRAP and MPT experiments. A closer look to the larger voids evidenced the existence of highly cross-linked structures as well (**Figure 17 D and E**), ratifying the strict steric barrier of human tracheal mucus.

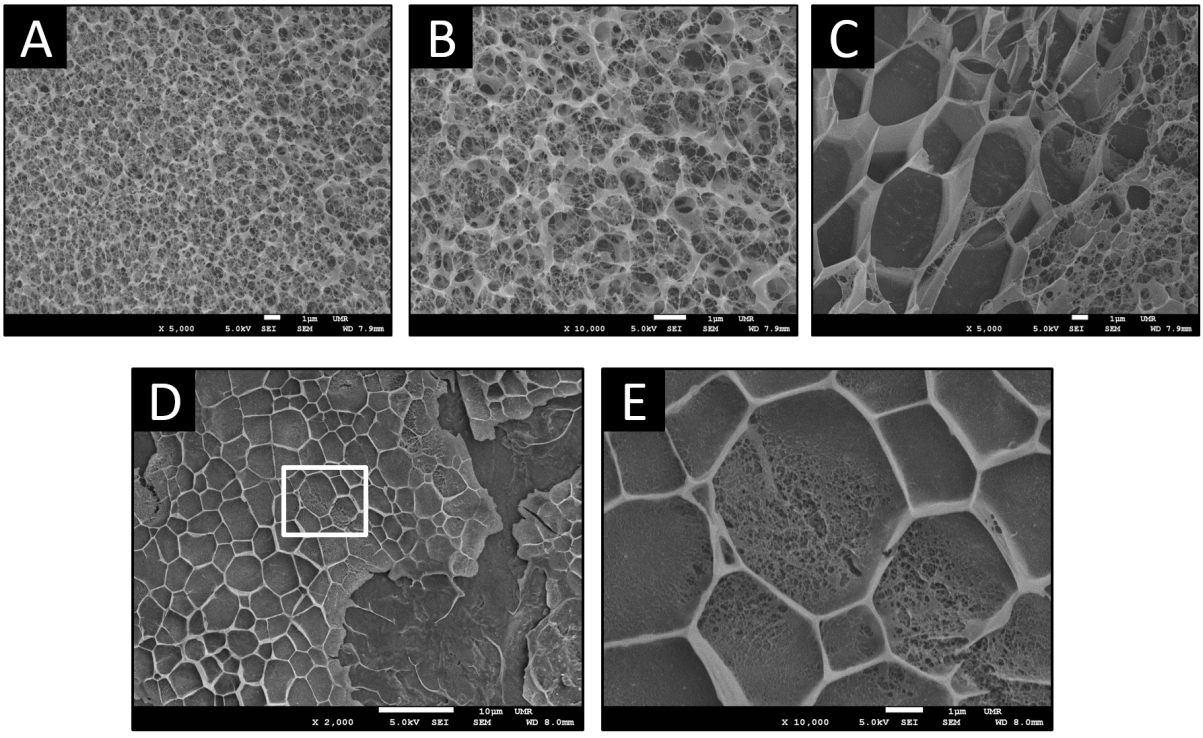

Figure 17. Ultra-structure of human tracheal mucus investigated by means of cryogenic scanning electron microscopy. At the first sight, undiluted airway mucus showed a great inhomogeneity with areas of a high cross-linking density and areas with bigger voids (A-C). A closer look to the larger voids, revealed fine structures of a high cross-linking density (D-E).

As a complementary investigation to the CryoSEM study, a confocal Raman microscopy (CRM) analysis of airway mucus was performed with the aim of obtaining a chemically selective spatial distribution of mucus components. The investigation of native airway mucus samples by CRM allowed the differentiation of two distinctive spectra. One spectrum showed marked similarities with the spectrum of dipalmitoyl phosphatidylcholine (DPPC), a phospholipid exclusively found in pulmonary surfactant[16], and was therefore defined as the "surfactant-like" spectrum. Both surfactant-like and DPPC spectra show a peak for choline head group at 717 cm^{-1}, three distinct peaks at 1066 cm^{-1}, 1102 cm^{-1} and 1128 cm^{-1} representing the carbon backbone vibrations, and a peak for aliphatic ester at 1740 cm^{-1} (**Figure 18 A**). The second type of spectra consist of glycoproteins and lipids and was assigned to the mucus matrix.

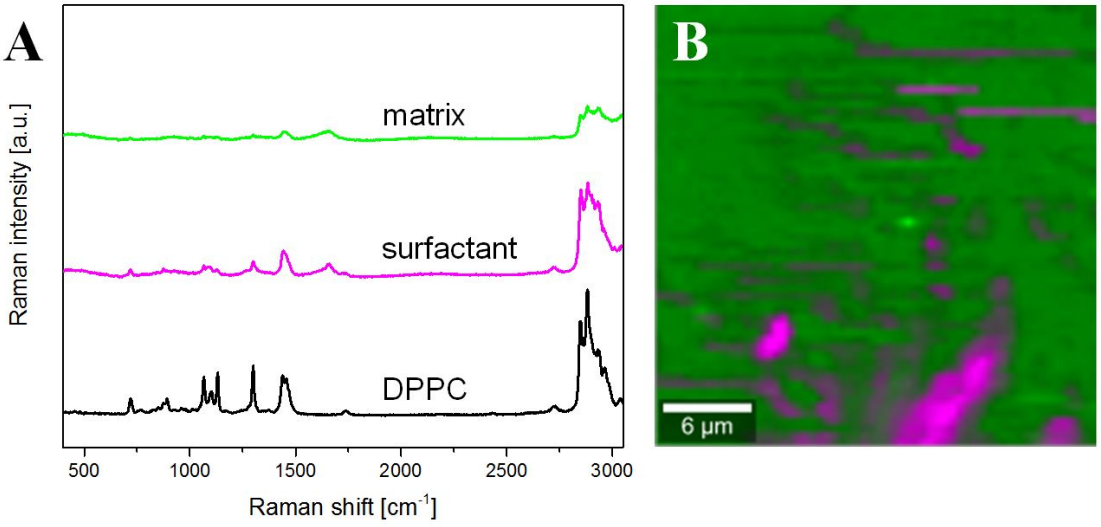

Figure 18. Confocal Raman microscopy analysis of undiluted human tracheal mucus. (A) Representative Raman spectra assigned to the mucus matrix, to pulmonary surfactant and to dipalmitoyl phosphatidylcholine (DPPC). (B) False color Raman image of a XY-scan representing the spatial distribution of the spectra (mucus matrix in green, and the pulmonary surfactant in pink). From reference 121.

Unfortunately, the network structure of mucus samples could not be resolved applying CRM to undiluted native mucus samples (**Figure 18 B**). Therefore, a further CRM analysis was performed on freeze-dried human mucus samples[159]. Conventional scanning electron microscopy revealed a preserved network structure for mucus after freeze-drying, although the magnitude of the pores was significantly increased by the water sublimation process (pore size range 1-10 µm, **Figure 19 A**). For this particular sample preparation, a spectrum containing characteristic peaks

corresponding to disulfide bonds (S-S, peak at 492 cm^{-1}) and to choline head groups (peak at 717 cm^{-1}) were successfully identified (**Figure 19 B)**.

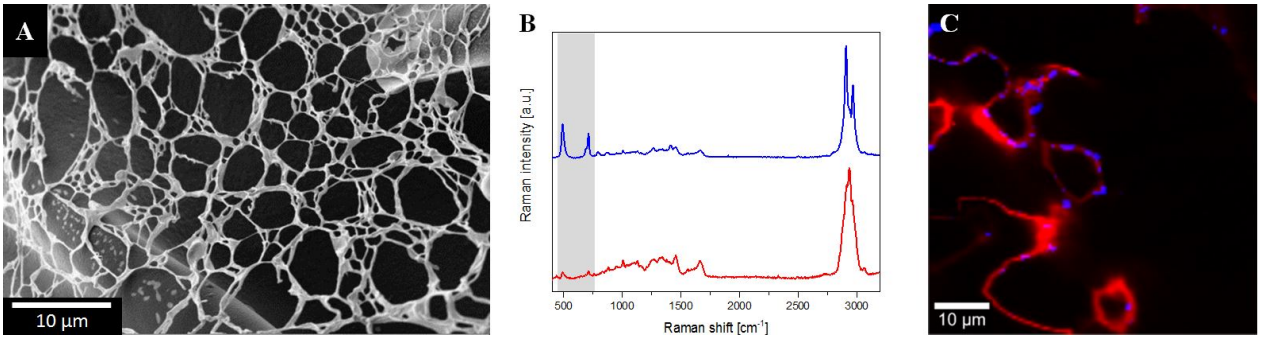

Figure 19. Confocal Raman microscopy analysis of freeze-dried human tracheal mucus. (A) Scanning electron microscopy image. (B) Representative Raman spectra corresponding to the mucus matrix (red) and disulfide bonds (blue). The spectral region of interest, corresponding to disulfide bonds (492 cm^{-1}) and choline head groups (717 cm^{-1}), is highlighted by a grey shadow. (C) false color Raman image of the spatial distribution of the different Raman spectra (the same color code has been applied in B and C). From reference 121.

The incubation of mucus with NAC (10% w/w) before freeze-drying partially collapsed the network structure (**Figure 20 A**). After mucolysis, a single type of Raman spectra could be detected, which revealed the presence of free thiol (-SH) groups at 2560-2590 cm^{-1}, but without evident peaks for disulfide bonds or choline head groups.

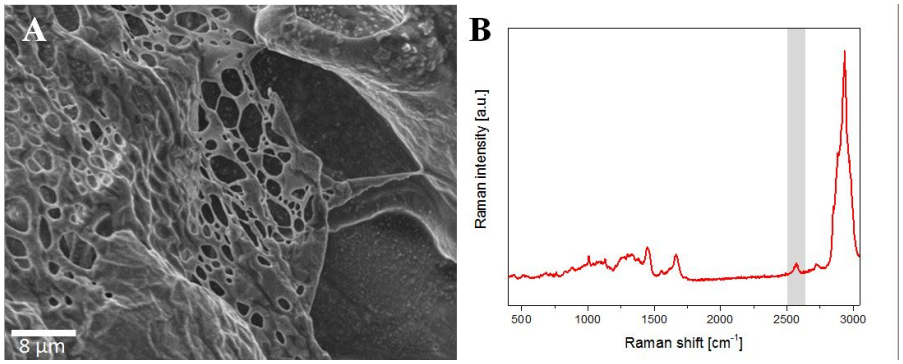

Figure 20. Confocal Raman microscopy analysis of freeze-dried human tracheal mucus, which had been incubated with 10% w/w of N-acetyl cysteine (NAC, 100 mg/ml) before freeze-drying. (A) Scanning electron microscopy image. (B) Representative Raman spectrum. The peak corresponding to free thiol groups (2560-2590 cm^{-1}) is highlighted by a grey shadow. From reference 121.

In summary, the characterization of native mucus performed here leads to the following conclusions:

- Rheological profiling of porcine tracheal mucus as well as FRAP and MPT experiments performed with polystyrene tracer NPs of 100 nm, 200 nm, and 500 nm particles determine a heterogeneous structure of mucus with pores at a length scale between 100 nm and 1000 nm. The elastic regions of this gel exhibit different crosslink densities with the mesh size potentially below 100 nm in some areas, but also containing larger interconnected pores with diameters above 200 nm but below 500 nm.
- Particle deposition in the form of aerosols onto porcine mucus layers showed that just 100 nm, but not 200 nm or larger particles, could penetrate mucus. The lack of penetration of 200 nm particles, which showed a relatively high mobile fraction when mechanically dispersed within mucus, may be best explained by the absence of sufficiently large pores at the air-mucus interface.
- The comparison between human and porcine tracheal mucus gels showed marked differences between both materials. Rheological investigations characterized human mucus as a stronger and more cross-linked gel compared to porcine mucus. The differences between both materials can be best explained by differences in the collection method. Indeed, collection of human mucus requires minimal sample manipulation. FRAP, MPT, and CryoSEM investigations revealed a higher crosslink density for human mucus, which significantly reduced particle mobility within the hydrogel.
- This study clearly illustrates the relevance of experimenting with high quality mucus samples, which may further produce meaningful and translatable results.
- CRM allowed us to successfully resolve the pulmonary surfactant from the mucus matrix in the native mucus hydrogel. The analysis of freeze-dried mucus revealed the presence of disulfide bonds, which are responsible for the structural stabilization of the mucus mesh. On the contrary, disulfide bonds were not detectable after mucolysis with NAC.

- The present CRM study describes, for the first time to our knowledge, the label-free investigation of human airway mucus. This investigation brings Raman microscopy in focus as an upcoming tool for elucidation of the effects induced by drugs and other substances on mucous hydrogels.

3.2 Modelling the Pulmonary Airways in Health and Disease

This chapter refers to the following publications:

Murgia X, Yasar H, Carvalho-Wodarz C, et al. *Modelling the bronchial barrier in pulmonary drug delivery: A human bronchial epithelial cell line supplemented with human tracheal mucus*. Eur J Pharm Biopharm 2017;118:79–88.

Müller L, **Murgia X***, Siebenbürger L, et al. *Human airway mucus alters susceptibility of Pseudomonas aeruginosa biofilms to tobramycin, but not colistin*. J Antimicrob Chemother [Internet] 2018;73:2762–9.

*Equal contribution

Cell-based *in vitro* models play a relevant role at the early stages of drug development. They allow, among others, performing time-resolved permeation studies of small drug molecules[160,161], testing the cellular toxicity of novel therapeutic compounds[33,162], and investigating drug uptake mechanisms and molecular pathways of APIs[151,152].

The natural protective role of mucus is nowadays acknowledged as a major barrier to be overcome in non-invasive drug delivery[50]. Therefore, cell-based *in vitro* models mimicking the pulmonary airways must include the mucus feature, in particular if the transport and uptake of NP-based drug delivery systems is to be investigated with such models.

The starting point for this investigation was the optimal characteristics in the context of pharmaceutical research described by Ehrhardt *et al.* for the CFBE41o- cell line[155]. CFBE41o- cells express tight-junction proteins and display high trans-epithelial electrical resistance (TEER)[163,164]. Nevertheless, unlike the Calu-3 cell line[153], CFBE41o- cell monolayers lack the ability to synthesize and secrete mucus. To address this limitation, the possibility of incorporating a mucus layer of exogenous origin onto confluent CFBE41o- monolayers was explored in the present thesis.

Mucus samples were obtained from patients undergoing elective surgery. Unfortunately, such samples are unsterile and highly elastic. The high elasticity of such mucus samples represents a significant difficulty in terms of sample manipulation, precluding the possibility of pipetting precise

mucus volumes as well as the efficient distribution of mucus over cell monolayers without inducing undesired cell damage. To overcome this limitation, thin mucus layers with approximately the same shape and dimension as Transwell® (1.12 cm^2) membranes were freeze-dried over Teflon surfaces. The produced freeze-dried mucus disks were further incorporated onto CFBE41o- cell monolayers grown on Transwell® membranes and re-hydrated with cell culture medium.

The mechanical properties of native undiluted mucus were compared to those of mucus samples that had been freeze-dried and re-hydrated. Bulk rheology studies showed an equivalent rheological profile for native tracheal mucus compared to the freeze-dried and re-suspended material. The elastic modulus (G') exceeded the viscous modulus (G'') in the case of undiluted mucus as well as in the case of freeze-dried and re-suspended mucus samples. This held true for both the strain and the frequency sweeps (**Figure 18**). This rheological signature, typical for cross-linked gels, confirmed a preserved network structure following freeze-drying and re-hydration of human tracheal mucus.

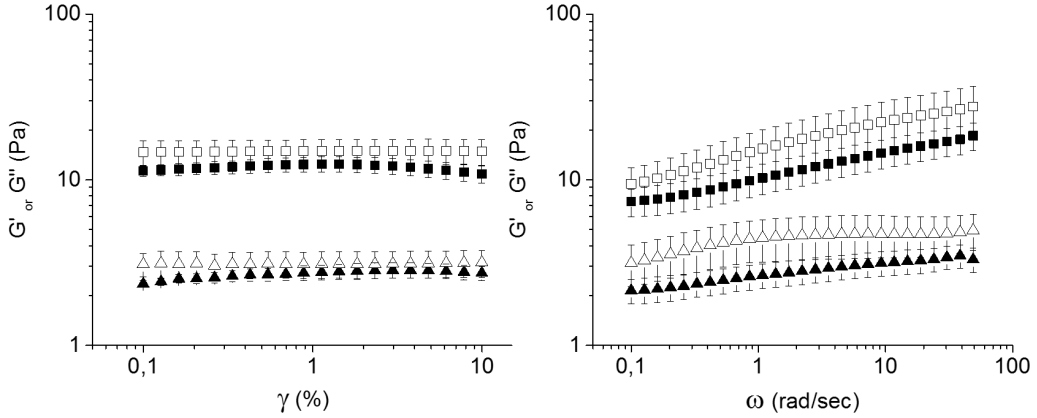

Figure 21. Bulk rheology of native human tracheal mucus (solid symbols) compared to native airway mucus which was freeze-dried and re-suspended (open symbols). (A) Strain (γ)-dependent viscous (G'', triangles) and elastic (G', squares) moduli from 0.1 to 10% strain at a frequency of 6.28 rad/s (1 Hz). (B) Frequency-dependent viscous (G'', triangles) and elastic (G', squares) moduli from 0.1 to 50 rad/s at 1% strain. The mean ± standard error for n=5 are shown. From reference 67.

It was hypothesized that human-derived mucus would be compatible with CFBE41o- cells, which are also from human origin. To address this hypothesis, the viability of CFBE41o- cells after a 24h incubation with freeze-dried and re-suspended mucus was investigated with two independent assays, namely live/dead staining and MTT assay. Both techniques confirmed a full compatibility

between the exogenous mucus and CFBE41o- monolayers, exhibiting a 100 % cell viability 24h after mucus addition.

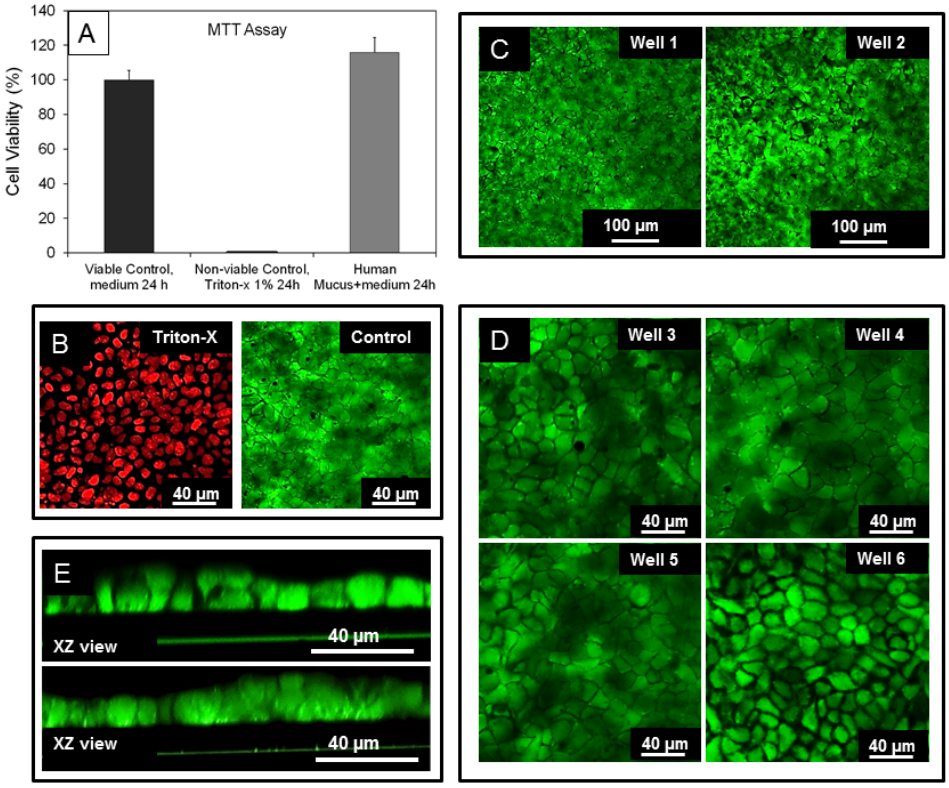

Figure 22. The viability of CFBE41o- cells upon contact with exogenous human mucus was assessed with the MTT assay and by live/dead staining with fluorescein diacetate (FDA) and propidium iodide (PI). (A) CFBE41o- cells exposed to mucus for 24 hours had a viability over 100 % (grey bar), slightly greater than that of control cells incubated with the appropriate medium (black bar); CFBE41o- cells incubated with the detergent Triton-X served as a negative control with 0% viability. (B) Representative fluorescence microphotographs of the negative (left) and positive (right) controls for the live/dead staining; cells with their nuclei stained in red represent non-viable cells, whereas cells with a green cytoplasm represent viable cells. (C) and (D) Representative fluorescence microphotographs of independent experiments at different magnifications, showing different Transwells® (wells 1-6) supporting CFBE41o- monolayers that had been incubated for 24 hours with human mucus in the apical compartment. (E) X-Z cross-sectional view of viable CFBE41o- monolayers that had been incubated for 24 hours with human mucus. From reference 67.

The presence of tight junctions between neighboring CFBE41o- cells following the 24h incubation with exogenous mucus was confirmed by the high TEER values recorded (**Figure 23**).

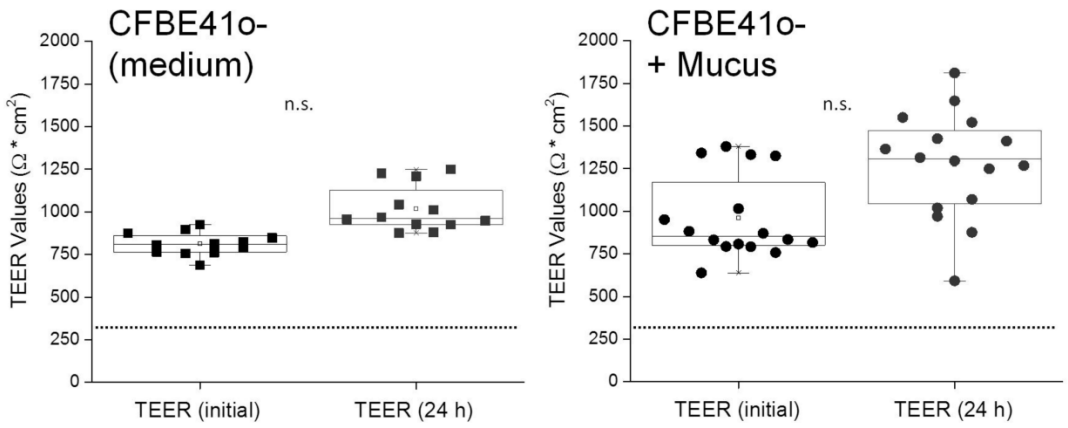

Figure 23. The barrier properties of the CFBE41o- monolayers grown for at least 10 days under submerged conditions were monitored for 24 h. The TEER values were measured before (initial) and 24 h after addition of mucus (CFBE41o- + Mucus, right). CFBE41o- cells not exposed to mucus but incubated under submerged conditions with regular medium served as controls (CFBE41o-, left). The horizontal line at 300 Ω*cm^2 indicates the threshold values deemed to indicate the presence of a tight barrier. The mean ± standard error of n=12 (CFBE41o-) and n=16 (CFBE41o- + mucus) from three independent experiments are shown. No significant (n.s.) differences were found. From reference 67.

As a proof of concept for the developed *in vitro* model, chitosan-coated PLGA NPs were incubated for 24 hours in "naked" CFBE41o- cell monolayers and in CFBE41o- cell monolayers supplemented with an additional mucus layer. The NPs had a mean size of 168 nm and a charge of +13 mV. By using cationic NPs, the interaction between mucus and NPs was intentionally pursued. If NPs were incubated with "naked" CFBE41o- cell monolayers, a significant uptake could be observed in the confocal images (**Figure 24 A**). Conversely, after 24h, NP uptake in CFBE41o- monolayers supplemented with a layer of mucus was significantly reduced, indicating that most of the NPs had been entrapped by the mucus layer (**figure 24 B**).

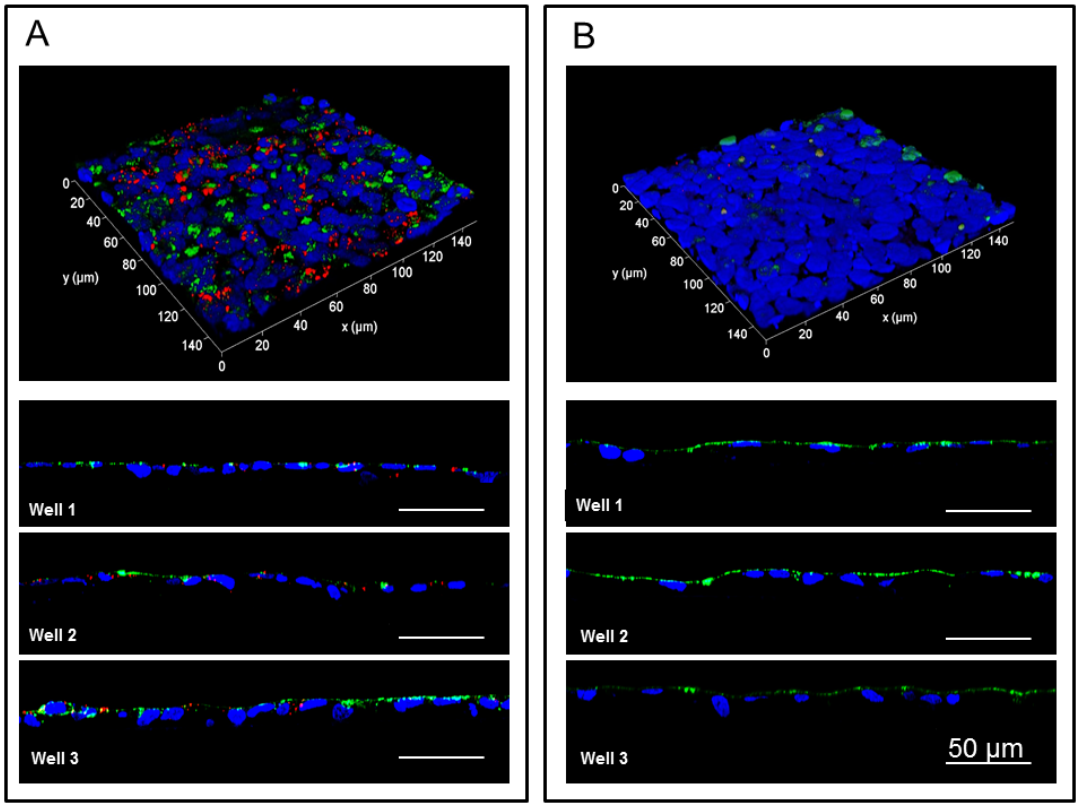

Figure 24. Confocal laser scanning microscopy images of the cellular uptake study performed with DiD-labeled chitosan-PLGA nanoparticles (NP) on CFBE41o- cells with and without mucus. (A) CFBE41o- monolayers were incubated with 400 µl of the NP suspension (40 µg/ml) for 24 h; after incubation, although the apical surface was thoroughly washed with PBS, a widespread presence of NPs either in close contact with or internalized by cells was noted, as evidenced by the 3D rendering (top) and the X-Z cross-sections (wells 1-3). (B) CFBE41o- monolayers supplemented with human tracheal mucus were incubated with 400 µl of the NP suspension (40 µg/ml) for 24 h. After incubation, the apical surface was thoroughly washed with PBS, resulting in the removal of both mucus and entrapped NPs. The absence of NPs in contact with cells in this case indicates that a vast majority of the NPs were trapped within the mucus and washed away. Nuclei were stained with DAPI (blue), the cell membrane was stained with wheat germ agglutinin (green), and the DiD-labelled chitosan-PLGA NPs were labelled with DiD (red). From reference 67.

Modelling lung infection in cell-based *in vitro* models is certainly challenging. Several research efforts have attempted to model the CF airway by co-culturing epithelial cells and *Pseudomonas aeruginosa* biofilms[165]. Unfortunately, due to bacterial overgrowth, such models show a limited time span, which in the best case does not surpass a few hours from the establishment of the co-culture[165,166].

As an alternative to epithelial cell-based models, a model consisting of growing the *Pseudomonas aeruginosa* strain PAO1 using human tracheal mucus was developed. This model simulates the initial stages of biofilm formation in CF and was aimed to be used for the efficacy testing of anti-infective drugs.

The efficacy of tobramycin and colistin, which are routinely prescribed for the management of CF infections[89], were tested in the developed biofilm model. Although they differ in their mechanism of action, both antibiotics are poly-cationic and therefore prone to interact with the negatively charge mucus. The minimum inhibitory concentrations (MIC) for tobramycin and colistin with planktonic PAO1 were 0.5 and 1 mg/L, respectively. For the treatment of 24h-old PAO1 biofilms, doses that were 100, 300, and 900 times higher than the MIC were selected. Full eradication of biofilms grown in PBS required a concentration 900 times higher than the MIC, irrespective of the antibiotic used. In biofilms grown in a mucus environment, a concentration-dependent decrease in viable bacterial load could still be seen for both antibiotics (**Figure 25**); however, tobramycin efficacy was significantly impaired in the presence of mucus, leading to a shift of the IC50 value from 100 mg/L without mucus to > 900 mg/L with mucus. Thus, killing of biofilm-grown bacteria was not achieved with tobramycin under normal culture conditions in the presence of mucus.

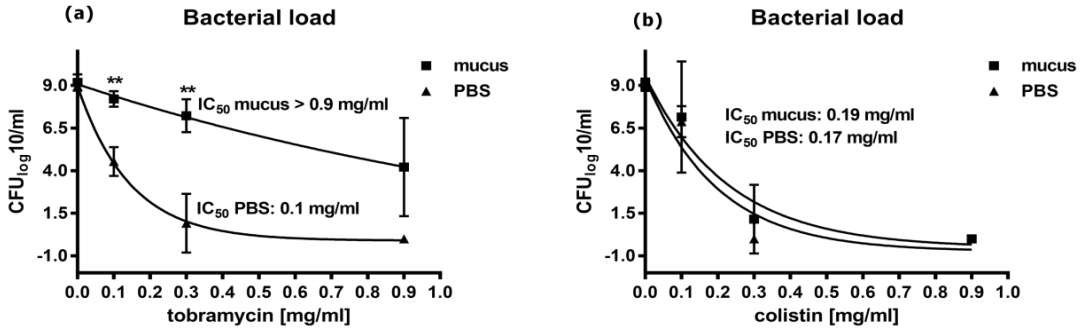

Figure 25. Biofilm susceptibility to antibiotic treatment. PAO1 biofilms grown in mucus or PBS for 24 h were treated with tobramycin (a) or colistin (b). After 24 h of incubation, efficacy was assessed by determination of cfu. The cfu counts are depicted logarithmically as regression curves showing the mean + standard deviation for n = 3 experiments, each with technical duplicates. A double asterisk indicates statistical significance at $P < 0.01$, according to the Mann–Whitney U-test, for comparison of mucus versus PBS at the individual concentrations. From reference [87].

The lack of efficacy of tobramycin in the presence of mucus is difficult to explain, and is best explained by a sum of events. The interaction between poly-cationic antibiotics and mucus components may have reduced the diffusion as well as the net bioavailability of the antibiotics[66,91,167]. However, adaptive resistance mechanisms such as an increase of efflux pump activity, alterations of permeation due to changes of lipopolysaccharides or porins, or the expression of biofilm-specific genes upon contact with mucus may also be in part responsible for the loss of efficacy of tobramycin[89,168]. A higher bacterial load was also noticed if PAO1 were cultured in mucus (**Figure 26**). In this regard, mucus' pores may act as PAO1-immobilizing scaffolds, while bacteria can degrade mucus components to promote a sustained growth.

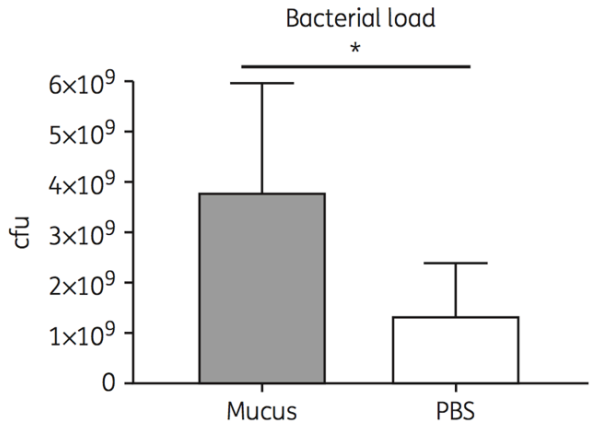

Figure 26. Bacterial load in 48h-old PAO1 biofilms grown either in human mucus or in PBS. Mean ± standard deviation for n = 3 samples, each with technical duplicates. *P < 0.05. **P < 0.01. From reference [87].

In summary, this thesis proposes two different *in vitro* models for diverse pharmaceutical applications. The first model comprises an epithelial cell monolayer (CFBE41o- cells) and a layer of native pulmonary mucus. The main features of this model are:

- The epithelial CFBE41o- cell monolayer is complemented with freeze-died re-hydrated human tracheal mucus, which is fully biocompatible and displays native viscoelastic properties.
- The re-hydrated mucus behaves as a semi-permeable layer, allowing the permeation of small molecules but severely hindering the passage of positively-charged 168 nm diameter polymeric NPs.
- The present model combines the excellent epithelial barrier properties of CFBE41o- cells with the option to implement an additional mucus barrier. Therefore, this model allows studying the net influence of the mucus barrier on drug transport.
- The relatively short culture time needed to achieve a tight epithelial monolayer allows having a cell line-based mucus-containing *in vitro* model of the airways ready for use within a timeframe of less than a week, in contrast to the relatively long culture times (3-4 weeks) required for the growth of Calu-3 cells displaying a confluent mucus layer.

The second model, consist of growing PAO1 embedded in freeze-dried and re-suspended native tracheal mucus. The main features of this model are:

- Growing PAO1 in combination with mucus provides a more realistic scenario of the CF airway. Biofilm formation in human mucus results in a more heterogeneous structure and a higher bacterial load.

- A significantly decreased efficacy of tobramycin against biofilms was observed in the presence of human mucus, suggesting that the mucus environment should be considered as a key factor in *in vivo* biofilm formation
- This model provides a complementary tool to the already available assays in the context of anti-infective drug development and may represents an excellent platform for testing novel compounds, including encapsulated antibiotics and quorum sensing inhibitors.

4. Original Publications

4.1 Size-Limited penetration of nanoparticles into porcine respiratory mucus after aerosol deposition

Xabier Murgia[a,1], Paul Pawelzyk[b,1], Ulrich F. Schaefer[c], Christian Wagner[d], Norbert Willenbacher[b], Claus-Michael Lehr[a,c]

[a]*Helmholtz Institute for Pharmaceutical Research Saarland (HIPS), Helmholtz Centre for Infection Research (HZI), Saarland University, 66123 Saarbruecken, Germany*

[b]*Institute for Mechanical Process Engineering and Mechanics, Karlsruhe Institute of Technology (KIT), 76131 Karlsruhe, Germany*

[c]*Biopharmaceutics and Pharmaceutical Technology, Department of Pharmacy, Saarland University, 66123 Saarbruecken, Germany*

[d]*Experimental Physics, Saarland University, 66123 Saarbruecken, Germany*

[1]*Equal contribution*

Accepted 9 March 2016

Biomacromolecules 2016, 17, 1536-1542

DOI: 10.1021/acs.biomac.6b00164

BioMACROMOLECULES

Article

pubs.acs.org/Biomac

Size-Limited Penetration of Nanoparticles into Porcine Respiratory Mucus after Aerosol Deposition

Xabier Murgia,[†,‡] Paul Pawelzyk,[†,§] Ulrich F. Schaefer,[∥] Christian Wagner,[⊥] Norbert Willenbacher,[§] and Claus-Michael Lehr*[,‡,∥]

[‡]Helmholtz Institute for Pharmaceutical Research Saarland (HIPS), Helmholtz Centre for Infection Research (HZI), [∥]Biopharmaceutics and Pharmaceutical Technology, Department of Pharmacy, and [⊥]Experimental Physics, Saarland University, 66123 Saarbruecken, Germany

[§]Institute for Mechanical Process Engineering and Mechanics, Karlsruhe Institute of Technology (KIT), 76131 Karlsruhe, Germany

Supporting Information

ABSTRACT: We investigated the rheological properties and the penetration of differently sized carboxylated nanoparticles in pig pulmonary mucus, on different distance and time scales. Nanoparticles were either mechanically mixed into the mucus samples or deposited as an aerosol, the latter resembling a more physiologically relevant delivery scenario. After mechanical dispersion, 500 nm particles were locally trapped; a fraction of carboxylated tracer particles of 100 or 200 nm in diameter could however freely diffuse in these networks over distances of approximately 20 μm. In contrast, after aerosol deposition on top of the mucus layer only particles with a size of 100 nm were able to penetrate into mucus, suggesting the presence of smaller pores at the air-mucus interface compared to within mucus. These findings are relevant to an understanding of the fate of potentially harmful aerosol particles, such as pathogens, pollutants, and other nanomaterials after incidental inhalation, as well as for the design of pulmonary drug delivery systems.

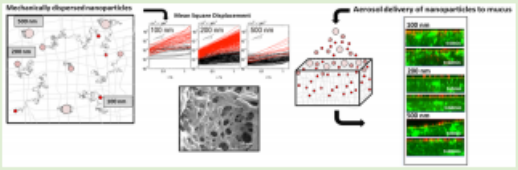

INTRODUCTION

Mucus is a complex hydrogel that provides tissue lubrication, first-line defense, and residual material clearance in the mucosal tissues of the human body, including the pulmonary airways, the gastrointestinal tract, the genitourinary tract, and the ocular surface.[1−3] In the lungs a mucus layer coats the conducting airways. Gel-forming mucins are continuously secreted into the airway lumen and incorporated into a high-viscosity, gel-like mucus layer,[4,5] which is continuously propelled toward the trachea and finally cleared from the lungs.[5] The highly dynamic nature of the mucociliary machinery therefore confers the ability to entrap and eliminate inhaled particles in a short time window ranging from minutes to a few hours, with clearance rates in the order of 100 μm/sec.[6] In the context of aerosol medicine and pulmonary drug delivery, the protective barrier properties of mucus against inhaled pathogens and pollutants may therefore impose a significant challenge, in particular, for nanoparticles intended for use as therapeutic drug carriers.[7]

Bulk rheological studies conducted within the linear viscoelastic region, where the structural properties of mucus are unaffected by the macroscopic shear deformation, show that pulmonary mucus behaves as an elastic solid on the macroscopic level.[3,8,9] Direct information on nanoparticle-mucus interactions can be obtained by tracking the Brownian motion of tracer particles, that is, using microrheological methods.[10−12] Mucus can adsorb particles due to electrostatic and hydrophobic attractive forces (interaction filtering).[13,14] Noninteracting nanoparticles with a smaller size than the pore size of the mucus can diffuse freely through the pores, in contrast to particles of bigger size that are confined by the surrounding mucin fibers (steric filtering).[12] Particle tracking investigations have revealed that the microscopic structure of mucus is highly heterogeneous, showing that within the same submicron particle size range freely diffusing particles coexist with particles which are immobilized by the mucus gel. These studies highlight that the overall particle mobility depends on mucus composition,[8,15] as well as particle diameter[3,16] and surface functionality.[3,10,17] In the case of human pulmonary mucus, most particles with a size of 500 nm are immobilized,[3,16] whereas, for smaller particles in the size range of 100−200 nm, the fraction of diffusing particles can be significantly increased if the surface of the particles is densely coated with polyethylene glycol (PEGylation).[3] The same studies however demonstrated that a fraction of carboxylated 100 and 200 nm particles still diffused within pulmonary mucus, indicating that interaction filtering is not the only mechanism.[3,16]

The starting point for the present study was the intriguing observation that magnetic nanoparticles did not penetrate a capillary filled with pulmonary mucus under application of a magnetic field, while the same particles penetrated a hydroxyl-ethyl-cellulose (HEC) hydrogel with apparently similar

Received: February 3, 2016
Revised: March 4, 2016
Published: March 9, 2016

DOI: 10.1021/acs.biomac.6b00164
Biomacromolecules 2016, 17, 1536−1542

viscoelastic properties under the same conditions rather easily.[18] Subsequent cryogenic-scanning electron microscope studies revealed a cage-like structure of the native mucus hydrogel, with both micron- as well as submicron-sized pores. This observation brought us to a new hypothesis: While the partly contradictive reported results regarding particle mobility and transport within and through mucus are clearly a reflection of particle size and surface properties,[3,19,20] differences in the time and distance scales employed within the conducted experiments may also play a role. The transport over longer distances, but at the same time rather free, Brownian-like mobility of some nanoparticles over shorter distances, can probably be best explained by the peculiar structure of the mucus gel network, which is also reflected in the different macro and microrheological properties of native mucus.[18]

In this study, we therefore investigated the linear viscoelastic properties of mucus and the mobility of particles over different distance and time scales, using carboxylated polystyrene particles of different sizes (100, 200, and 500 nm) as model systems. Multiple particle tracking (MPT), in which particle displacement is followed over short time-scales (usually up to 10 s), was used to study the diffusion on the microscale (0.1−1 μm). Fluorescence recovery after photobleaching (FRAP) experiments were used to elucidate particle mobility through mucus on time (760 s) and distance (bleached area of 35 μm) scales closer to therapeutic scenarios.[2,21] After deposition in the airways, for example, when inhaled as aerosols within droplets or carrier particles, with an adequate aerodynamic particle size in the micron range (a typical scenario in pulmonary drug delivery), administered nanoparticles have to travel 3−50 μm to traverse the mucus layer before reaching the epithelial cell surface.[6,22] The time scale for penetration is determined by the highly dynamic mucociliary machinery, that is, several minutes up to a few hours.[6] We therefore tried to correlate the corresponding diffusion data for differently sized particles with the penetration of nanoparticles within mucus or across the air-mucus interface, in an attempt to model a more realistic scenario for nanoparticle-based drug delivery to the airways. Most importantly, we found a striking difference between the mobility of particles within mucus after mechanical dispersion and the penetration of the same particles into mucus after deposition as an aerosol.

MATERIALS AND METHODS

Mucus Sample Collection. Native porcine pulmonary mucus was obtained from the tracheas of slaughtered pigs, sourced from a local slaughterhouse. Approximately 10 cm of windpipe was isolated in each case by cutting the trachea below the larynx and before the carina. Tracheas were stored on ice for further transport and mucus extraction. Prior to extraction procedures tracheas were cut in half longitudinally. The mucus was gently scratched from the luminal surface with a spatula (approximately 100−300 μL of mucus per sample). For MPT and shear rheology experiments, mucus samples were stored at 4 °C, and experiments were conducted within 12−36 h of mucus collection. Remaining mucus samples were stored at −20 °C until further analysis.

Shear Rheology. Experiments were conducted on a Thermo MARS II rheometer equipped with cone−plate geometry (diameter, 35 mm; cone angle, 1°) at room temperature. The edges of mucus samples were coated with a low viscosity paraffin oil to prevent sample evaporation. Strain amplitude sweeps were performed at a frequency of 1 Hz. Frequency dependency of the storage modulus G' and the loss modulus G'' was measured in the range between 0.01 and 10 Hz at strain amplitudes of $\gamma \leq 0.1$. The characterization of the bulk rheological properties of mucus was based on independent measurements of four different samples.

Multiple Particle Tracking (MPT). Carboxylated, green-fluorescent polystyrene microspheres with diameters of 100, 200, and 500 nm (Bangs Laboratories, U.S.A.) were used in MPT experiments. Particle diameters, polydispersity indices (PdI) and zeta potential (ζ) were measured prior to MPT studies, using a Malvern Zetasizer Nano ZSP or a Zetasizer Nano ZS (Malvern, U.K.; Table 1).

Table 1. Particle Characterization

nominal particle size	diameter[a] (d) nm	polydispersity index[b] (PdI)	surface charge density[c] charges/nm^2	ζ-potential[d] mV
100 nm	112 ± 1	0.02 ± 0.01	3.0	−49 ± 4
200 nm	221 ± 2	0.01 ± 0.01	1.9	−57 ± 4
500 nm	524 ± 10	0.07 ± 0.05	14.6	−34 ± 2

[a]Z-average diameter measured by dynamic light scattering. Standard deviation is based on six independent measurements. [b]PdI = $(\sigma/d)^2$ calculated from the Z-average diameter (d) and the standard deviation of the particle size distribution. [c]Provided by the manufacturer. [d]Measured in 10 mM NaCl at pH 7.4.

Approximately 20 μL of fresh mucus sample was then mixed with 0.5 μL of the particle dispersions. The 500 nm particles were used at the original particle concentration of 1% w/v. Dispersions of the smaller particles were diluted with PBS buffer to obtain particle concentrations of 0.05% w/v for 100 nm and 0.25% w/v for the 200 nm particles, thus keeping the number concentration of particles below 2−10^{10} particles/ml in all cases. The whole sample was then transferred to a custom-made chamber, sealed, and placed in the microscope.[23] Measurements were performed using an inverted fluorescence microscope (AxioObserver D, Zeiss, Germany) with a Fluar 100× objective and an oil-immersion lens with a numerical aperture of 1.3. The temperature was maintained at 37 °C using a temperature controlled chamber. Tracking videos of random fields of each mucus sample were recorded by an sCMOS camera Zyla X (Andor Technology), at a resolution of 0.062 μm per pixel and a frame rate of 50 frames per second. The field of view of the camera represents an area of 127 × 127 μm. Image analysis was conducted using Image Processing System software (Visiometrics iPS). The data were evaluated as described by Kowalczyk et al.[23]

Fluorescence Recovery after Photobleaching (FRAP). Previously frozen native pulmonary mucus samples were thawed at 4 °C the day prior to FRAP experiments. The following day, samples were allowed to reach room temperature and thereafter 60 μL of mucus was mixed with 1.5 μL of the particle dispersions. Mixtures of mucus and tracer particles were prepared as mentioned above for the MPT experiments, using the same carboxylated green-fluorescent polystyrene microspheres at the previously stated concentrations. These nanoparticle concentrations were all within the range where a linear relationship exists between concentration and fluorescence (Supporting Information, 1). The samples were then transferred into previously mounted adhesive gastight sealing chambers (Gene Frame, Thermo Scientific), and sealed with cover slides. The experiments were conducted using a LSM 710 Axio Observer confocal laser scanning microscope (Zeiss, Germany) with an Apochromat 40×/1.1 objective equipped with a 488 nm laser (LASOS RMC 7812 Z2). The temperature of samples was maintained at 37 °C using a temperature controlled chamber. Four circular regions of interest (radius = 17.5 μm in all cases) were selected within the analyzed field, of which three were used for bleaching experiments and one was retained as a control for photofading. A time-series analysis was programmed with the following settings: Prebleaching images were recorded at 2% laser transmission, immediately followed by bleaching with the laser transmission set at 100%. A postbleaching recovery step followed, for a duration of 760 s at a frame rate of 30 frames per minute with the laser transmission again set at 2%. The fluorescence intensity after bleaching was defined as zero, and the intensity at t = 0 was subtracted

DOI: 10.1021/acs.biomac.6b00164
Biomacromolecules 2016, 17, 1536−1542

from all values. Arbitrary values of intensity were then calculated, dividing each obtained value by the difference between the intensities prior to and directly after bleaching. The results were further corrected for the intensity of the control area. The presented data were extracted from four independent bleaching experiments per particle size.

Aerosol Delivery of Nanoparticles and Confocal Microscopy. Carboxylated red-fluorescent polystyrene nanoparticles of 100, 200, and 500 nm diameter (Invitrogen, stock 2%) were dispersed in PBS at 0.1%, 0.025% and 0.005% w/v, respectively. Frozen native pulmonary mucus samples were thawed at 4 °C the day prior to experiments. A 40 μL volume of mucus was then stained by gentle mixing with 1 μL of Alexa488 Wheat Germ Agglutinin (Vector Laboratories, CA, U.S.A.), and transferred to an imaging chamber to create a confluent mucus layer.

Nanoparticle suspensions were aerosolized using a micropump nebulizer (AerogenLab, Aerogen Ltd., Ireland, droplet size range 2.5–4 μm). The nebulizer was aligned 6 cm above the mucus-containing imaging chamber and 20 μL of nanoparticle suspension was aerosolized over the sample, allowing 2 min for particle deposition. The sample was then transferred to the confocal laser scanning microscope (LSM 710 Axio Observer Zeiss, Germany) with an Apochromat 40×/1.1 objective to study the time-dependent vertical penetration of the particles through mucus. The temperature was maintained at 37 °C using a humidified and temperature controlled chamber. The stained mucus was detected in the green channel (excitation 488 nm, detection 467–554 nm) and the fluorescent nanoparticles in the red channel (excitation 561 nm, detection 624–707 nm). Once the surface of the mucus sample was located, Z-stacks encompassing 30–50 μm of the mucus layer were imaged (t = 0 min). The procedure was repeated after 1 h (t = 60 min).

RESULTS AND DISCUSSION

2.1. Bulk Rheology. The frequency dependence of the viscoelastic properties of bulk mucus samples in the linear viscoelastic region is shown in Figure 1. The error of these

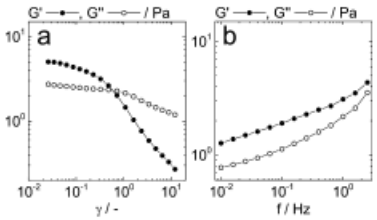

Figure 1. Representative amplitude sweep experiment at a frequency f = 1 Hz (a), and frequency sweep experiment at a strain γ = 0.1 (b).

measurements, calculated from four independent experiments, is below 10%. As expected, the storage modulus G' was found to be larger than the loss modulus G'' in the frequency range between 0.01 and 3 Hz, while the ratio of the loss modulus and the storage modulus ($\tan(\delta) = G''/G'$) ≈ 0.6 at a frequency of 0.159 Hz. Both moduli are only weakly frequency dependent in the investigated frequency range. These characteristics are typical of cross-linked gels or sample-spanning particle networks.[23] Tracheal mucus obtained from humans or other animal models exhibits similar bulk rheological properties.[3,9,24] The amplitude sweep performed at a frequency of 1 Hz shows that the mucus layer is a weak gel which starts to soften already at deformations around $\gamma \approx 0.05$. The sample yields at deformations of γ = 0.6, as indicated by the crossover of G' and G''.

2.2. Multiple Particle Tracking (MPT). Investigations into the pulmonary mucus pore size have shown significant variability in the pore dimensions of the mucin network, ranging from pores of a few nanometers to voids in the micrometer size range.[3,18,25] Pore size estimations, however, have often been derived from scanning electron microscopy, and might therefore be biased by the mandatory fixation and dehydration steps. MPT, on the other hand, provides information on the mucus architecture with minimal manipulation of the sample. The mean squared displacement (MSD) $\Delta r(\tau)^2$ in native pulmonary mucus for 100 nm, 200 and 500 nm carboxylated polystyrene particles shows a broad distribution irrespective of particle size, indicating that mucus samples are heterogeneous on this scale (Figure 2; Supporting Information, videos 1–3).

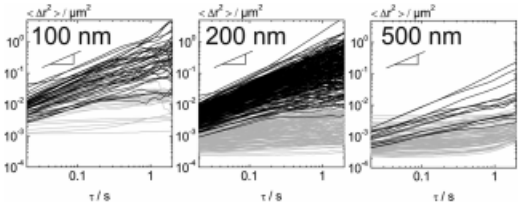

Figure 2. Mean squared displacement (MSD, $\langle \Delta r^2 \rangle$) of carboxylated nanoparticles in pulmonary pig mucus as a function of time τ. Black lines represent MSDs with a slope $\alpha > 0.5$, classified as diffusive, while gray lines denote MSDs with $\alpha < 0.5$, classified as immobile. The gradient triangle in each figure illustrates a slope of 1.

Therefore, instead of analyzing the average $\langle \Delta r(\tau)^2 \rangle$ for a collection of particles, we analyzed the slope $\alpha = d \log(\Delta r(\tau)^2)/d \log(\tau)$ of each individual MSD and classified each particle as either diffusive or immobile according to its α-value. This scaling exponent describes the diffusive properties of the particles; for Newtonian fluids α = 1, while α = 0 in purely elastic materials. We used a cutoff value of 0.5 to classify the particles as diffusive ($\alpha > 0.5$) or immobile ($\alpha < 0.5$). The classification as shown in Figure 2 is based on α-values obtained at τ = 0.1 s. However, classification according to the α = 0.5 criterion is essentially independent of τ. The slope of the MSDs of the diffusive (black lines) and the immobile particle fraction (gray lines) is either approximately zero or close to one, respectively.

MSDs increasing linearly with time (Figure 2, black lines) correspond to a constant diffusion coefficient as typical for Newtonian fluids. The corresponding particles move freely through the fluid within the pores of the mucin network, and their diffusion coefficient can be directly calculated according to

$$\Delta r^2(\tau) = 4D\tau \quad (1)$$

The viscosity of fluid surrounding these particles can be estimated from the diffusion coefficient D and the particle diameter d, using the Stokes–Einstein equation:

$$\eta = \frac{k_B T}{3d\pi D} \quad (2)$$

with k_B denoting the Boltzmann constant and T is the absolute temperature. This simple relationship is valid for particles diffusing in an infinitely viscous environment.

The broad variation of MSDs is an intrinsic characteristic of the heterogeneous mucus microstructure. Hence, rather than using the mean values of collective particles, we decided to focus on the 10th and 90th percentiles of the MSD fractions

DOI: 10.1021/acs.biomac.6b00164
Biomacromolecules 2016, 17, 1536–1542

classified by the slope criterion, as depicted in Figure 2, to proceed with calculation of the related physical parameters, namely, the diffusion coefficient D of the tracer particles, and the effective viscosity η in the viscous regions. These interpercentile ranges therefore represent the viscoelastic properties traced by 80% of the particles. Results based on these considerations and corresponding numerical values are summarized in Table 2.

Table 2. Range of Physical Properties in Relation to 100, 200, and 500 nm Particles within the Viscous Mucus Fractions

	viscous fraction	
particle size	diffusion coefficient D (10^{-13} m^2/s)	viscosity η (mPa s)
100 nm	0.46–22	2–90
200 nm	0.12–1.7	12–175
500 nm	[a]	
overall range	0.12–22	2–175

[a]Number of diffusive particles too small for a reasonable calculation of D or η. With $n = 3$ measurements, each performed on an independent mucus sample.

The distribution of the slopes of the individual particle MSDs at $\tau = 0.1$ s, calculated from three independent samples, is shown in Figure 3. The 100 and 200 nm particles exhibit a

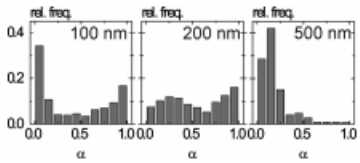

Figure 3. Histograms depict the slope $\alpha = d\log(\mathrm{MSD})/d\log(\tau)$ of the MSDs at a time scale $\tau = 0.1$ s, averaged from the relative frequencies of three measurements, each performed on an independent mucus sample.

broad distribution, whereas mainly immobile particles with $\alpha < 0.5$ were observed at a particle diameter of 500 nm. According to the selected classification criterion, 43, 51, and 6% of 100, 200, and 500 nm particles, respectively, were found to be diffusive, that is, moving in a viscous environment.

Our MPT data shows that mucus is an extremely heterogeneous, viscoelastic material consisting of viscous regions, termed pores, and highly elastic areas thought to consist of a dense polymeric network. The mesh size of this network seems to be smaller than 100 nm in some areas (since even 100 nm particles are trapped). On the other hand, essentially all 500 nm particles are found to be in an elastic environment, that is, they cannot enter the porous regions and as a result the pore size is estimated to be smaller than 500 nm. The limited diffusion of particles above this cutoff size within pulmonary mucus is directly linked to the pore size of the mucin network, and is independent from particle-mucin chemical interactions since even 500 nm particles coated with a dense layer of PEG, which significantly reduces the adsorption of biomolecules on particle surfaces, are immobilized within the mucin network.[3]

2.3. Fluorescence Recovery after Photobleaching (FRAP). In a subsequent step, FRAP experiments were performed to determine the transport of particle populations on longer time (720 s) and distance scales. We conducted these experiments with mucus stored at −20 °C after having found equivalent results in terms of mobility for 100 and 200 nm particles during pilot MPT experiments with fresh or slow-thawed porcine pulmonary mucus (Supporting Information, 4). FRAP experiments confirmed the low mobility of the 500 nm particles. The fluorescence recovery for 500 nm particles was very modest, barely reaching 10% recovery within the experimental time, indicating that these particles were mostly immobile (Figure 4).

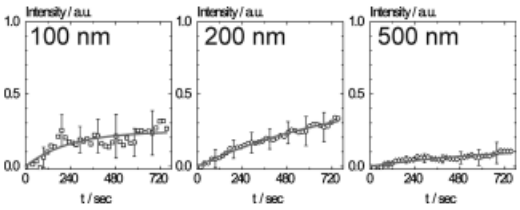

Figure 4. Fluorescence intensity recovery over time t determined from FRAP experiments using 100 (squares), 200 (circles), and 500 nm (diamonds) particles and the corresponding exponential fits (gray line). With $n = 12$, from four independent samples.

As expected, 100 and 200 nm particles showed a higher fluorescence recovery than 500 nm particles within the time frame of the experiment, which was approximately 760 s. Nevertheless, at this time the mobile particle fraction depicted by the mean fluorescence recovery was higher for the 200 nm (33%) than for the 100 nm (26%) particles.

In order to obtain further information regarding the diffusion of the nanoparticles in native pulmonary mucus, the following exponential function was fitted to the data of the arbitrary intensities I:

$$I(t) = A(1 - e^{-\tau t}) \tag{3}$$

The parameter A corresponds to the estimated fraction of mobile particles. The time constant τ is a characteristic of the intensity increase over time and can be used to calculate the halftime recovery $\tau_{1/2}$:

$$\tau_{1/2} = \ln(2)/\tau \tag{4}$$

The diffusion coefficient can then be obtained from the halftime recovery and the radius of the bleached area ($w = 17.5$ μm) following the approach of Axelrod et al.:[26]

$$D = 0.88w^2/4\tau_{1/2} \tag{5}$$

The diffusion coefficients for the differently sized particle samples yielded values in accordance with those obtained for the most diffusive particles during the MPT experiments (Table 3).

We observed a higher diffusion coefficient in pulmonary mucus for 100 nm particles in comparison to the larger ones, suggesting a critical mucus pore size between 100 and 200 nm. According to our data (Figure 4) and the applied model (Table 3), the mobile fraction of the 100 nm particles (24%) was also larger than that of the 500 nm particles (14%). Surprisingly, however, the model yielded a mobile fraction for the 200 nm particles (around 50%), which was even higher than for both the larger 500 nm and smaller 100 nm particles. By applying the model described by Axelrod et al. to the FRAP data, we were

DOI: 10.1021/acs.biomac.6b00164
Biomacromolecules 2016, 17, 1536−1542

Table 3. Physical Properties of Mucus, as Calculated from FRAP Data[a]

particle size	time constant τ (10^{-3} s^{-1})	diffusion coefficient (10^{-13} m^2/s)	half time ($\tau_{1/2}$) s	calcd mobile particle fraction (A) %
100 nm	4.27 ± 1.0	4.2 ± 0.1	160 ± 40	24 ± 2
200 nm	1.16 ± 0.1	1.1 ± 0.02	600 ± 80	54 ± 5
500 nm	1.37 ± 0.5	1.3 ± 0.05	500 ± 200	14 ± 4

[a] n = 12, from four independent samples.

able to calculate and compare the diffusion coefficients to those obtained in the MPT experiments. Nevertheless, as indicated by the wide diffusion ranges obtained by MPT, the transport of nanoparticles through mucus appears to be much more complex than simple diffusion and may be better explained by short as well as long transient binding of the particles with the mucin matrix.[27,28] The unexpectedly low mobile fraction of the 100 nm particles may be explained by the assumption that these particles may get trapped within pores not accessible for the larger particles. This effect is well-known and even applied as a principle in gel exclusion chromatography (GPC), where large molecules pass through the separation columns faster than small ones. Still, a considerable fraction of the 200 nm particles can somehow access the previously bleached area. This implies that the heterogeneity of the pore size distribution within pulmonary mucus also allows somewhat larger particles eventually to find their way through pores that are compatible with their size.

2.4. Aerosol Deposition at the Air–Mucus Interface. Finally, in order to mimic the penetration of inhaled nanoparticles into the mucus gel layer, we deposited aerosolized nanoparticles onto mucus by means of a vibrating-mesh nebulizer. The aim of these experiments was to correlate the findings in terms of size dependent particle mobility observed during MPT and FRAP experiments, where the particles had been mechanically dispersed within the mucus gel, with a situation that is closer to the physiological scenario of inhaling such particles. Red-fluorescent, carboxylated polystyrene particles of 100, 200, and 500 nm could be successfully aerosolized, deposited, and detected on the surface of a thin layer of native pig pulmonary mucus. As expected, at t = 0 min, most of the particles were concentrated at the air–mucus interface, irrespective of their size (Figure 5A).

A total of 1 h later (t = 60 min), 500 nm particles were still unable to penetrate into the mucus layer at all and remained at the air–mucus interface (Figure 5). Remarkably, however, 200 nm particles also remained at the air–mucus interface, in contrast to the behavior of such particles when they are mechanically dispersed in mucus. This suggests that their penetration across the air-mucus interface is impeded, possibly by the lack of sufficiently large pores. Only 100 nm particles showed certain penetration into mucus, correlating well with the previously illustrated mobility within mucus.

Taking together, the results of this study suggest that there is a critical pore size that limits the penetration of nanoparticles into the mucus gel layer after aerosol deposition, which must be somewhere between 100 and 200 nm. These critically small pores ("micro-pores") are presumably located close to the air-mucus interface but connect to areas with much larger pores ("macro-pores") in the inner parts of the mucus layer. The mechanically dispersed particles were more equally distributed within the mucus layer, where the macro-pores are also located. This results in a much larger fraction of particles not restricted by micropores, which can freely diffuse on the length scales

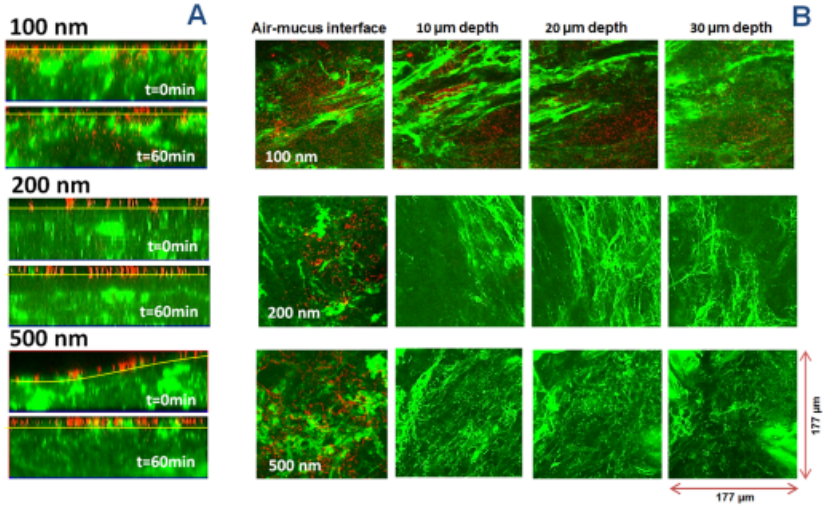

Figure 5. Confocal laser scanning microscopy study of the penetration of aerosolized 100, 200, and 500 nm red-fluorescent carboxylated nanoparticles through native porcine pulmonary mucus. Representative cross sections of 25–40 μm of the z-stacks captured at t = 0 min, directly after aerosol delivery of nanoparticles, and at t = 60 min, 1 h after aerosol delivery, are shown in A. Pulmonary mucus, in green, was stained with wheat germ agglutinin. Irrespective of their size, the particles were concentrated at the air–mucus interface (indicated by the yellow line) at t = 0 min. After 1 h, particle penetration through mucus was only apparent for 100 nm particles, whereas 200 and 500 nm particles remained at the air–mucus interface. Mucopenetration of 100 nm particles was accordingly observed in the micrographs at t = 60 min (177 μm × 177 μm) extracted from the z-stack at 10, 20, and 30 μm depths of the mucus layer (B); n = 3 measurements, each performed on an independent mucus sample.

DOI: 10.1021/acs.biomac.6b00164
Biomacromolecules 2016, 17, 1536–1542

observed by MPT and FRAP. Nonetheless, the limited penetration at the air-mucus interface could be due to a nanoparticle concentration-induced mucus fiber collapse, as reported by Lai et al.[1] In this study the authors reported that high concentrations of particles can make mucus fibers collapse into bundles. Once the mucin fibers collapse around particles, they can provide sufficient hydrophobic interactions to immobilize the particles. This scenario could apply after aerosol deposition of particles at the air-mucus interface.

CONCLUSION

Rheological measurements as well as FRAP and MPT experiments with polystyrene model particles of 100, 200, and 500 nm mechanically dispersed in vitro in native porcine pulmonary mucus suggest a heterogeneous mucus structure at a length scale between 100 and 1000 nm. The elastic regions of this gel exhibit different cross-linking densities with the mesh size potentially below 100 nm in some areas, but also contain larger interconnected pores with diameters in the range of 500 nm.

After aerosol deposition at the air−mucus interface, only particles of 100 nm, but not of 200 nm or larger, could penetrate into mucus. Such a penetration barrier can be best explained by a structure with micropores smaller than 200 nm and the absence of macro-pores close to the air-mucus interface. The even more strict size limit for particle penetration across the air-mucus interface compared to particle mobility within mucus provides another protective element of this important biological barrier to the exposure of inhaled nanoparticles that needs to be taken into account for the development of future inhalation nanomedicines.

ASSOCIATED CONTENT

Supporting Information

The Supporting Information is available free of charge on the ACS Publications website at DOI: 10.1021/acs.biomac.6b00164.

Calibration curves showing a strong linear correlation between the concentration and fluorescence intensity of the fluorescently labeled particles; Comparison of the MSD plots of 100, 200, and 500 nm carboxylated nanoparticles in fresh pulmonary pig mucus, versus pig mucus stored at −20 °C and thawed gradually (PDF).

Video-recording of 100 nm COOH-modified particles in native porcine pulmonary mucus (MPG).

Video-recording of 200 nm COOH-modified particles in native porcine pulmonary mucus (MPG).

Video-recording of 500 nm COOH-modified particles in native porcine pulmonary mucus (MPG).

AUTHOR INFORMATION

Corresponding Author

*E-mail: claus-michael.lehr@helmholtz-hzi.de. Tel.: +49 681 98806-1000.

Author Contributions

†These authors equally contributed to this work (X.M. and P.P.).

Notes

The authors declare no competing financial interest.

ACKNOWLEDGMENTS

This work was supported by the Marie Curie Initial Training Network PathChooser (PITNGA-2013−608373). The critical review of the manuscript performed by Dr. Sarah Gordon is gratefully acknowledged. The authors would like to thank Dr. Blatt and the team of the slaughterhouse in Zweibrücken for kindly providing airway samples.

REFERENCES

(1) Lai, S. K.; O'Hanlon, D. E.; Harrold, S.; Man, S. T.; Wang, Y. Y.; Cone, R.; Hanes, J. *Proc. Natl. Acad. Sci. U. S. A.* **2007**, *104*, 1482−1487.

(2) Nordgard, C. T.; Nonstad, U.; Olderoy, M. O.; Espevik, T.; Draget, K. I. *Biomacromolecules* **2014**, *15*, 2294−2300.

(3) Schuster, B. S.; Suk, J. S.; Woodworth, G. F.; Hanes, J. *Biomaterials* **2013**, *34*, 3439−3446.

(4) Knowles, M. R.; Boucher, R. C. *J. Clin. Invest.* **2002**, *109*, 571−577.

(5) Rubin, B. K. *Respir. Care* **2002**, *47*, 761−768.

(6) Lai, S. K.; Wang, Y. Y.; Hanes, J. *Adv. Drug Delivery Rev.* **2009**, *61*, 158−171.

(7) Ruge, C. A.; Kirch, J.; Lehr, C. M. *Lancet Respir. Med.* **2013**, *1*, 402−413.

(8) Hill, D. B.; Vasquez, P. A.; Mellnik, J.; McKinley, S. A.; Vose, A.; Mu, F.; Henderson, A. G.; Donaldson, S. H.; Alexis, N. E.; Boucher, R. C.; Forest, M. G. *PLoS One* **2014**, *9*, e87681.

(9) Khan, M. A.; Wolf, D. P.; Litt, M. *Biochim. Biophys. Acta, Gen. Subj.* **1976**, *444*, 369−373.

(10) Crater, J. S.; Carrier, R. L. *Macromol. Biosci.* **2010**, *10*, 1473−1483.

(11) Griessinger, J.; Dunnhaupt, S.; Cattoz, B.; Griffiths, P.; Oh, S.; Gomez, S. B.; Wilcox, M.; Pearson, J.; Gumbleton, M.; Bernkop-Schnurch, A. *Eur. J. Pharm. Biopharm.* **2015**, *96*, 464−476.

(12) Lai, S. K.; Wang, Y. Y.; Wirtz, D.; Hanes, J. *Adv. Drug Delivery Rev.* **2009**, *61*, 86−100.

(13) Lieleg, O.; Ribbeck, K. *Trends Cell Biol.* **2011**, *21*, 543−551.

(14) Sigurdsson, H. H.; Kirch, J.; Lehr, C. M. *Int. J. Pharm.* **2013**, *453*, 56−64.

(15) Macierzanka, A.; Mackie, A. R.; Bajka, B. H.; Rigby, N. M.; Nau, F.; Dupont, D. *PLoS One* **2014**, *9*, e95274.

(16) Dawson, M.; Wirtz, D.; Hanes, J. *J. Biol. Chem.* **2003**, *278*, 50393−50401.

(17) Yu, T.; Chan, K. W.; Anonuevo, A.; Song, X.; Schuster, B. S.; Chattopadhyay, S.; Xu, Q.; Oskolkov, N.; Patel, H.; Ensign, L. M.; van Zijl, P. C.; McMahon, M. T.; Hanes, J. *Nanomedicine* **2015**, *11*, 401−405.

(18) Kirch, J.; Schneider, A.; Abou, B.; Hopf, A.; Schaefer, U. F.; Schneider, M.; Schall, C.; Wagner, C.; Lehr, C. M. *Proc. Natl. Acad. Sci. U. S. A.* **2012**, *109*, 18355−18360.

(19) Forier, K.; Messiaen, A. S.; Raemdonck, K.; Deschout, H.; Rejman, J.; De Baets, F.; Nelis, H.; De Smedt, S. C.; Demeester, J.; Coenye, T.; Braeckmans, K. *Nanomedicine (London, U. K.)* **2013**, *8*, 935−949.

(20) Mura, S.; Hillaireau, H.; Nicolas, J.; Kerdine-Romer, S.; Le Droumaguet, B.; Delomenie, C.; Nicolas, V.; Pallardy, M.; Tsapis, N.; Fattal, E. *Biomacromolecules* **2011**, *12*, 4136−4143.

(21) Groo, A. C.; Lagarce, F. *Drug Discovery Today* **2014**, *19*, 1097−1108.

(22) Patton, J. S. *Adv. Drug Delivery Rev.* **1996**, *19*, 3−36.

(23) Kowalczyk, A.; Oelschlaeger, C.; Willenbacher, N. *Meas. Sci. Technol.* **2015**, *26*, 15302−15316.

(24) Innes, A. L.; Carrington, S. D.; Thornton, D. J.; Kirkham, S.; Rousseau, K.; Dougherty, R. H.; Raymond, W. W.; Caughey, G. H.; Muller, S. J.; Fahy, J. V. *Am. J. Respir. Crit. Care Med.* **2009**, *180*, 203−210.

(25) Sanders, N. N.; De Smedt, S. C.; Van Rompaey, E.; Simoens, P.; De Baets, F.; Demeester, J. *Am. J. Respir. Crit. Care Med.* **2000**, *162*, 1905−1911.

DOI: 10.1021/acs.biomac.6b00164
Biomacromolecules 2016, 17, 1536−1542

(26) Axelrod, D.; Koppel, D. E.; Schlessinger, J.; Elson, E.; Webb, W. W. *Biophys. J.* **1976**, *16*, 1055−1069.
(27) Phair, R. D.; Misteli, T. *Nat. Rev. Mol. Cell Biol.* **2001**, *2*, 898−907.
(28) Lippincott-Schwartz, J.; Altan-Bonnet, N.; Patterson, G. H. *Nat. Cell Biol.* **2003**, *Suppl*, S7−14.

Size-limited penetration of nanoparticles into porcine respiratory mucus after aerosol deposition

Xabier Murgia, Paul Pawelzyk, Ulrich F. Schaefer, Christian Wagner, Norbert Willenbacher, and Claus-Michael Lehr

SUPPORTING INFORMAZION (SI)

SI 1. Serial dilutions of 100 nm, 200 nm and 500 nm COOH-modified green-fluorescent nanoparticles (Bang Laboratoriess, stock 1%) were prepared in triplicate, loaded into a 96-well plate, and their fluorescence intensity was measured with an automated plate reader (excitation 480 nm, emission 520 nm, gain 50; TECAN Infinite 200 PRO). A strong linear correlation was found between nanoparticle concentration (%) and fluorescence intensity (arbitrary units, a.u.). The orange arrows indicate the particle concentrations (w/v of mucus) used in *Fluorescence Recovery after Photobleaching* experiments.

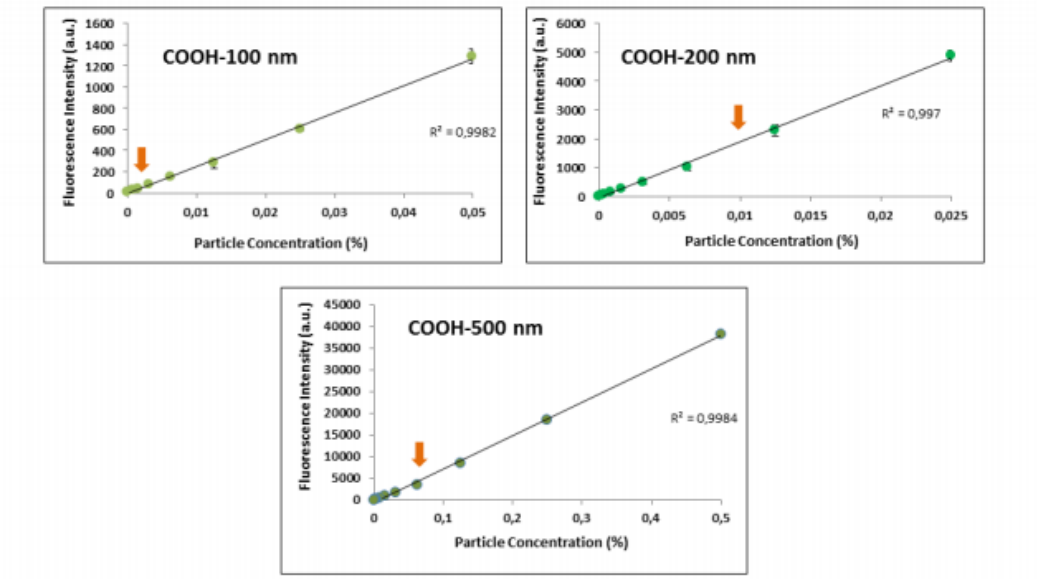

SI 2. Movie 1. Video-recording of 100 nm COOH-modified particles in native porcine pulmonary mucus. Pictures were taken with an inverted fluorescence microscope (AxioObserver D, Zeiss, Germany) with a Fluar 100x objective including an oil-immersion lens with a numerical aperture of 1.3. at a resolution of 0.062 µm per pixel and a frame rate of 50 frames per second. The field of view of the camera represents an area of 127 x 127 µm.

SI 3. Movie 2. Video-recording of 200 nm COOH-modified particles in native porcine pulmonary mucus. Pictures were taken with an inverted fluorescence microscope (AxioObserver D, Zeiss, Germany) with a Fluar 100x objective including an oil-immersion lens with a numerical aperture of 1.3. at a resolution of 0.062 µm per pixel and a frame rate of 50 frames per second. The field of view of the camera represents an area of 127 x 127 µm.

SI 4. Movie 3. Video-recording of 500 nm COOH-modified particles in native porcine pulmonary mucus. Pictures were taken with an inverted fluorescence microscope (AxioObserver D, Zeiss, Germany) with a Fluar 100x objective including an oil-immersion lens with a numerical aperture of 1.3. at a resolution of 0.062 µm per pixel and a frame rate of 50 frames per second. The field of view of the camera represents an area of 127 x 127 µm.

SI 5. Mean Squared Displacement (MSD, μm^2) of 100 nm, 200 nm and 500nm carboxylated nanoparticles in pulmonary pig mucus as a function of time scale (sec). The plots on the top describe the individual trajectories of particles in mucus samples that had been stored at -20°C (Frozen) and gradually thawed before analysis, whereas in the plots below the mucus sample were stored at 4 °C and experiments were conducted within 12-36 hours after mucus collection (Fresh). A comparable variability was found regarding the individual trajectories of the

differently-sized nanoparticles, irrespective of the storage method. The red line represents the mean MSD of all the trajectories.

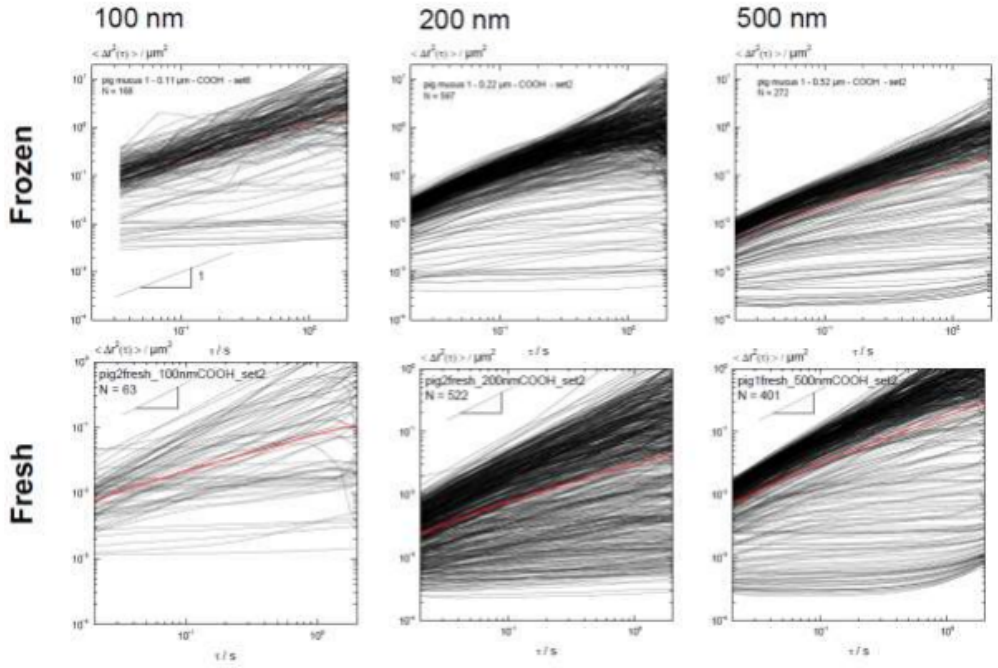

4.2 Tracing molecular and structural changes upon mucolysis with N-acetyl cysteine in human airway mucus

Xabier Murgia[a1], Branko Vukosavljevic[a1], Konrad Schwarzkopf[b], Ulrich F. Schaefer[c], Claus-Michael Lehr[a,c], Maike Windbergs[a,c,d]

[a]*Helmholtz Institute for Pharmaceutical Research Saarland (HIPS), Helmholtz Centre for Infection Research (HZI), Saarland University, 66123 Saarbruecken, Germany*

[b]*Department of Anesthesia and Intensive Care, Clinics Saarbruecken, 66119 Saarbruecken, Germany*

[c]*Biopharmaceutics and Pharmaceutical Technology, Department of Pharmacy, Saarland University, 66123 Saarbruecken, Germany*

[d]*Institute of Pharmaceutical Technology and Buchmann Institute for Molecular Life Sciences, Goethe University Frankfurt, 60438 Frankfurt am Main, Germany*

[1]*Equal contribution.*

Accepted 8 July 2017

International Journal of Pharmaceutics 2017, 533, 373–376

DOI: 10.1016/j.ijpharm.2017.07.022.

G Model
IJP 16837 No. of Pages 4

ARTICLE IN PRESS

International Journal of Pharmaceutics xxx (2017) xxx–xxx

Contents lists available at ScienceDirect

International Journal of Pharmaceutics

journal homepage: www.elsevier.com/locate/ijpharm

Tracing molecular and structural changes upon mucolysis with N-acetyl cysteine in human airway mucus

Branko Vukosavljevic[a,1], Xabier Murgia[a,1], Konrad Schwarzkopf[b], Ulrich F. Schaefer[c], Claus-Michael Lehr[a,c,*], Maike Windbergs[a,d,*]

[a] Helmholtz Institute for Pharmaceutical Research Saarland (HIPS), Helmholtz Centre for Infection Research (HZI), Saarland University, 66123 Saarbruecken, Germany
[b] Department of Anesthesia and Intensive Care, Clinics Saarbruecken, 66119 Saarbruecken, Germany
[c] Biopharmaceutics and Pharmaceutical Technology, Department of Pharmacy, Saarland University, 66123 Saarbruecken, Germany
[d] Institute of Pharmaceutical Technology and Buchmann Institute for Molecular Life Sciences, Goethe University Frankfurt, 60438 Frankfurt am Main, Germany

ARTICLE INFO

Article history:
Received 4 April 2017
Received in revised form 14 June 2017
Accepted 8 July 2017
Available online xxx

Keywords:
Human airway mucus
Freeze–drying
Confocal Raman microscopy
Scanning electron microscopy
Rheology

ABSTRACT

The conducting airways of the human lungs are lined by mucus, which lubricates the lung epithelium and provides a first-line protection against airborne threats. As a novel approach for visualization of the human mucus microstructure, we applied confocal Raman microscopy as a label-free and chemically selective technique. We were successfully able to chemically resolve the pulmonary surfactant from the mucus matrix and show its spatial distribution, as well as to visualize the structural changes within the freeze–dried mucus mesh upon chemical mucolysis. Subsequently, we performed rheological measurements before and after mucolysis and correlated morphology and chemical structure of the mucus with its rheological characteristics. These results do not only enrich the knowledge about the mucus microstructure, but can also, significantly contribute to rational development of future lung therapeutics.

1. Introduction

Among cellular and non-cellular biological barriers of the human lungs, mucus plays a prominent role in protecting the conducting airways and the underlying epithelial tissue against external airborne threats (Sigurdsson et al., 2013). As mucus lines the surface of the airways, its properties can affect pathophysiological processes as well as absorption of drugs administered via the pulmonary route, e.g. by particle trapping (Suk et al., 2014; Kim et al., 2015) and subsequent clearance by the mucociliary escalator (Knowles and Boucher, 2002). Therefore, insight into the biochemical mucus structure and understanding its composition and interactions is of high interest for elucidating the course of lung diseases as well as for rational development of effective therapeutics for lung application (Kumar et al., 2016; Sakuma et al., 2012; Yu et al., 2016; Nordg&rd et al., 2014).

Airway mucus forms a complex hydrogel (water content 95% w/w) incorporating glycoproteins (mucins, 2–5% w/w), non-mucin proteins, lipids, salts, DNA, enzymes, cellular debris, and pulmonary surfactant (Rubin, 2002; Schuster et al., 2013; Ruge et al., 2013).

The structural mesh for this hydrogel is constituted by mucins which consist of a polypeptide backbone with side glycans (O-glycosylated units) stabilized by intermolecular disulfide bonding (Sigurdsson et al., 2013). These bonds are formed between the thiol groups of cysteine residues in a reversible process called oxidative folding. This systematic overlapping of mucins leads to protein stabilization (Sevier and Kaiser, 2002) and to the formation of a tight mesh with a highly heterogeneous pore size (Murgia et al., 2016). However, chemical reduction leads to the reversion of this process by formation of free thiol groups (Fig. 1). This reaction is intentionally targeted when applying N-acetyl cysteine, which is currently the only approved thiol-based mucolytic agent for therapeutic purposes.

* Corresponding authors at: Institute of Pharmaceutical Technology and Buchmann Institute for Molecular Life Sciences, Goethe University Frankfurt, 60438 Frankfurt am Main, Germany and Helmholtz Institute for Pharmaceutical Research Saarland (HIPS), Helmholtz Centre for Infection Research (HZI), Saarland University, 66123 Saarbruecken, Germany.
E-mail addresses: windbergs@em.uni-frankfurt.de (C.-M. Lehr), claus-michael.lehr@helmholtz-hzi.de (M. Windbergs).
[1] These authors contributed equally to this work.

http://dx.doi.org/10.1016/j.ijpharm.2017.07.022
0378-5173/

G Model
IJP 16837 No. of Pages 4
ARTICLE IN PRESS

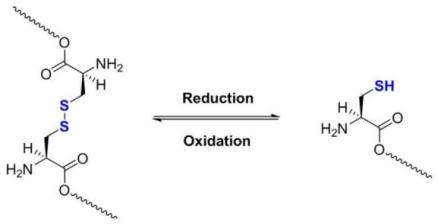

Fig. 1. Chemical reduction of a disulfide bond (-S-S-) in a cysteine dimer and oxidative folding of a thiol group (-SH) as reversible reaction.

Systematic analysis of the mucus microstructure in its native state is challenging, as it requires conserving the hydration state of the hydrogel to avoid collapsing of the gel mesh and thus dislocation of the compounds. Established techniques generally either require manipulation of the sample (e.g. staining, fixation) or can only visualize the morphological structure without the chemical information of the individual compounds.

In this study, we investigated human airway mucus with confocal Raman microscopy as a label-free and chemically selective technique to visualize its structure and composition. Mucus samples were analyzed in its native state as well as after freeze drying. We investigated structural changes within the mucus mesh upon chemical mucolysis with N-acetylcysteine as an established therapeutic mucolytic agent. Subsequently, we performed rheological measurements before and after mucolysis and correlated morphology and chemical structure of the mucus with its rheological characteristics.

2. Materials and methods

2.1. Materials

For acquisition of the reference spectrum, dipalmitoyl phosphatidylcholine (DPPC) was purchased from Avanti Polar lipids, Inc. (Alabaster, AL) and N-acetyl cysteine (NAC) from Sigma −Aldrich (Munich, Germany).

2.2. Mucus sample collection

Human airway mucus samples were collected by the endotracheal tube method (Nordgård et al., 2014) after informed consent from the patients and in compliance with a protocol approved by the Ethics Commission of the "Ärztkammer des Saarlandes" (file number 19/15). In brief, the tracheal tubes of patients undergoing elective surgery non-related to pulmonary conditions were collected after surgery. The distal portion of the tube (5–10 cm) was cut and placed in a 50 ml centrifuge tube. The mucus of each tracheal tube was pooled by centrifuging the samples at 1200 rpms for 30 s. Mucus samples were stored at −20 °C until use. This storage method does not have a significant influence neither on the viscoelasticity of mucus, nor in the diffusion coefficient of drugs (Sanders et al., 2000; Larhed et al., 1997). In total 10 mucus samples from independent patients were used in this study. Mean age of the patients was 58.3 ± 19 years, male: female ratio was 6:4, and mean surgery time 75 ± 34 min.

2.3. Freeze drying

Native mucus aliquots were gradually thawed and volumes of approximately 30–40 μl were spread over a Teflon surface and stored at −80 °C for 4 h. Thereafter, frozen mucus samples were immediately transferred to the freeze-drier (Alpha 2–4 LSC, Christ, Germany) and freeze-dried overnight at −80 °C. Freeze–dried mucus samples were stored in a dark and dry environment until analysis. For controlled mucolysis, mucus aliquots were incubated for two hours with NAC (100 mg/ml, 10% w/w) before starting the freeze-drying process(Yuan et al., 2015).

2.4. Scanning electron microscopy (SEM)

Fresh mucus samples were spread over the surface of a SEM imaging carbon disk and freeze-dried in situ following the aforementioned protocol. Freeze-dried mucus samples were gold-sputtered (QUORUM Q150R ES, Gala Instrument, Germany) and then transferred to the SEM (EVO HD15, Zeiss, Germany) for mucus-imaging.

2.5. Confocal Raman microscopy

Confocal Raman microscopy measurements of both, native and freeze-dried human tracheal mucus samples were performed using a WITec alpha 300R+ instrument (WITec GmbH, Ulm, Germany). The excitation source was a diode laser with a wavelength of 532 nm adjusted to a power of 30 mW. The setup was equipped with a Zeiss Epiplan Neofluar 50 x objective (NA = 0.8), with maximal lateral and axial resolution of around 0.34 μm and 1.47 μm, respectively, and a 100 x oil immersion objective (NA = 1.2), with maximal lateral and axial resolution of around 0.23 μm and 0.65 μm, respectively. Raman spectra were acquired with a spatial resolution of 0.5 μm; background subtracted and normalized to the most intense peak, and further converted into false color images using hierarchical cluster and basis analysis (WITec Project plus Software). In contrast to hierarchical cluster analysis as a binary approach, basis analysis is more sophisticated and involves Raman spectra of the pure compounds acquired from the sample as references. The false color image depicts the relative congruence of the spectra with the predefined reference spectra for each pixel. This approach is not binary and allows for a simultaneous weighted display of multiple components in one single pixel as visualized by color intensity differences.

2.6. Rheological measurements

Rheology experiments were conducted on an Anton-Paar MCR 102 rheometer (Graz, Austria) equipped with cone-plate geometry (diameter: 25 mm, cone angle: 2°) at controlled conditions (23.38 ± 0.5 °C). Frequency (ω) dependency of the storage modulus G' and the loss modulus G" was measured in the range between 0.1 and 40 rad/s at a strain amplitudes of 1%, within the linear viscoelastic region. The experiments were conducted with fresh mucus samples (no treatment) and also with fresh mucus samples that had been incubated with NAC (100 mg/ml, 10% w/w) for 2 h.

3. Results and discussion

Even though the microstructure of human mucus can be visualized by electron microscopy, the localization of its individual chemical compounds in the complex hydrogel matrix is still unknown. To overcome this challenge, we applied confocal Raman microscopy to elucidate the localization of the mucus compounds with a chemically selective and thus label-free approach. Raman microscopy is based on laser light scattering and different chemical bonds can be differentiated by their unique scattering patterns. Initial studies probing lung mucus with Raman spectroscopy identified a strong scattering signal generated by lipids, predominantly triolein (Koljenović et al., 2004).

Please cite this article in press as: B. Vukosavljevic, et al., Tracing molecular and structural changes upon mucolysis with N-acetyl cysteine in human airway mucus, Int J Pharmaceut (2017), http://dx.doi.org/10.1016/j.ijpharm.2017.07.022

G Model
IJP 16837 No. of Pages 4
ARTICLE IN PRESS
B. Vukosavljevic et al. / International Journal of Pharmaceutics xxx (2017) xxx–xxx

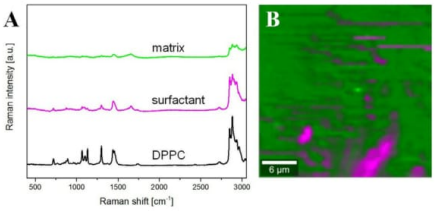

Fig. 2. Analysis of the native human airway mucus: (A) Single Raman spectra assigned to the mucus matrix, to pulmonary surfactant and to dipalmitoyl phosphatidylcholine (DPPC) as a reference, respectively; (B) False color Raman image representing the spatial distribution of the pulmonary surfactant in the mucus matrix (xy-scan). False colors depict the mucus matrix in green, and the pulmonary surfactant in pink, respectively. (For interpretation of the references to colour in this figure legend, the reader is referred to the web version of this article.)

As a first step in our study, we systematically investigated different mucus samples collected from human airways by Raman microscopy. After spectral assignment of the Raman peak patterns, we successfully differentiated individual signal contributions. Fig. 2 depicts a representative false color Raman image of human mucus with the mucus matrix (depicted in green, consisting of glycoproteins and lipids), as well as the pulmonary surfactant (depicted in pink). The surfactant spectrum is very distinctive and displays dipalmitoyl phosphatidylcholine (DPPC, Fig. 2A) as a major constituent of the pulmonary surfactant (Perez-Gil and Weaver, 2010). The most important spectral assignments of DPPC (reference spectrum presented in Fig. 2A) and surfactant-like spectra are: choline head group at 717 cm^{-1}, three distinct peaks at 1066 cm^{-1}, 1102 cm^{-1} and 1128 cm^{-1} representing the carbon backbone vibrations, and aliphatic ester at 1740 cm^{-1}.

As Raman imaging of the spatially resolved compound distribution within the mucus mesh was exacerbated by the samples' gel-like structure and the high water content, we freeze dried the mucus samples. Freeze-drying has already been reported as a valuable preparation technique for in vitro testing of the human skin and other tissues (Franzen et al., 2013) allowing for analysis of the mucus microstructure without chemical manipulation and fixation. However, we are aware that this and other fixation protocols may alter the pore size distribution of mucus (Schuster et al., 2013).

First, the ultrastructure of freeze-dried mucus was successfully visualized using SEM (Fig. 3A). It revealed the typical mesh-like structure with a highly heterogeneous pore size, ranging from pores in the nanoscale up to pores in the range of 1–10 µm. The structure is similar to native mucus which has previously been investigated by cryoSEM, thus suggesting that structural damage of the mucus mesh induced by the freeze drying process is most likely insignificant (Kirch et al., 2012). However, SEM images are limited to the morphological structure and cannot reveal the location of

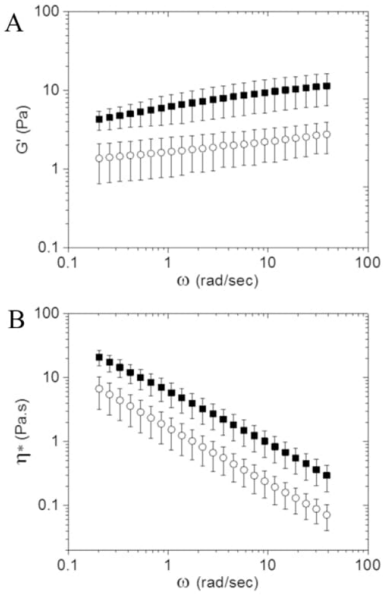

Fig. 4. Rheological properties of native tracheal mucus: (A) frequency (ω) sweep (0.2 to 40 rad/sec, strain 1%) showing the elastic modulus (G') of untreated (solid squares) and N-acetylcysteine-treated (NAC 10% w/w, empty circles) pulmonary mucus samples; (B) Complex viscosity (η*) as a function of frequency (ω) of untreated (solid squares) and NAC-treated (10% w/w, empty circles) pulmonary mucus samples. N = 3 from independent mucus samples.

the chemical mucus building blocks (mucins, proteins, lipids) and their chemical interactions. Consequently, we applied Raman imaging for further chemically selective and label-free visualization. Two Raman spectra, one consisting of all prominent glycoprotein and lipid related peaks, representing the mucus matrix, and the other one consisting of peaks corresponding to disulfide bonds (-S-S-) at 492 cm^{-1} and the surfactant related choline head group (-N+) at 717 cm^{-1} were successfully identified. Fig. 3B displays the mucus matrix spectrum in red and the cysteine-rich domains in blue. The coexistence of the disulfide bonds and the choline headgroup in the blue spectrum can be explained by local hydrophobic interaction between the cysteine-rich domains (disulfide bonds) and the surfactant itself (choline headgroups) which coexist in the airway mucus, as confirmed after analysis of native airway mucus (Fig. 2). After conversion of the Raman spectra into false-color images, areas in which mucins interact by disulfide binding could be visualized (Fig. 3C). These

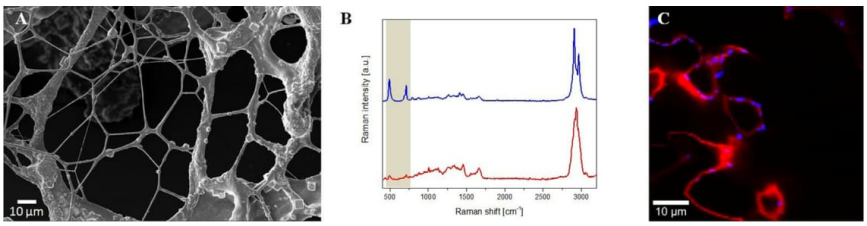

Fig. 3. Analysis of the freeze-dried mucus: (A) SEM image; (B) two individual single Raman spectra corresponding to the mucus matrix (red) and cysteine-rich domains (blue) with the spectral region of interest highlighted; (C) false color Raman image (same color coding like in 3B). (For interpretation of the references to colour in this figure legend, the reader is referred to the web version of this article.)

Please cite this article in press as: B. Vukosavljevic, et al., Tracing molecular and structural changes upon mucolysis with N-acetyl cysteine in human airway mucus, Int J Pharmaceut (2017), http://dx.doi.org/10.1016/j.ijpharm.2017.07.022

G Model
IJP 16837 No. of Pages 4
ARTICLE IN PRESS

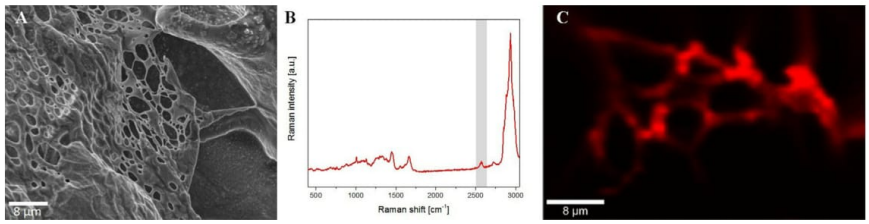

Fig. 5. Analysis of the freeze-dried mucus samples after treatment with N-acetylcysteine (NAC, 10% w/w): (A) SEM image; (B) Single Raman spectrum corresponding to the mucus matrix with the spectral region of interest highlighted; (C) false color Raman image (mucus matrix depicted in red). (For interpretation of the references to colour in this figure legend, the reader is referred to the web version of this article.)

areas, depicted in blue, were located in the edges of thin mucin fibers, thus most likely stabilizing the fragile macrostructure of human airway mucus.

Moreover, in order to investigate potential changes in the mucus microstructure upon mucolytic treatment, we incubated the human airway mucus with N-acetylcysteine (NAC, 10% w/w), as a therapeutic mucolytic agent (Yuan et al., 2015; Matera et al., 2016; Rubin, 2015). We performed rheological measurements with the mucus samples before and after treatment. The corresponding rheograms depict a significant decrease of the elastic modulus (G') arising from the chemical reduction of the inter-mucin disulfide bonds (Fig. 4A). In addition, the complex viscosity of mucus showed a marked decrease after NAC treatment in comparison to the untreated samples (Fig. 4B) (Yuan et al., 2015).

Additionally, SEM images of NAC-treated samples show a partially collapsed mesh structure (Fig. 5A) contrasting the structure of non-treated mucus (Fig. 3A).

Raman spectra of freeze dried mucus samples after mucolysis revealed the presence of free thiol (-SH) groups at 2560–2590 cm^{-1} (Fig. 5B, highlighted), thus proving the reduction of the disulfide bonds within the mucus matrix upon mucolytic treatment. In addition, no pure NAC signal can be detected after incubation of the mucus with NAC for two hours (data not shown). The false color Raman image presented in Fig. 5C reveals the presence of a mucus fiber-like structure even after chemical reduction with NAC, and similar pore size as shown with the corresponding SEM picture (Fig. 5A).

4. Conclusion

The airway mucus layer together with the alveolar pulmonary surfactant represents a major non-cellular pulmonary barrier to inhaled therapeutics. In this study, we investigated human airway mucus with confocal Raman microscopy to visualize and better understand its complex structure and composition. We successfully resolved the pulmonary surfactant from the mucus matrix in the native mucus hydrogel and revealed its spatial distribution. In the next step, we analyzed freeze-dried mucus discs before and after mucolytic treatment. Initially, we visualized cysteine rich domains (disulfide bonds), responsible for the structural stabilization of the mucus mesh. In contrast to this, upon mucolysis, we revealed the chemical reduction (thiol groups). Subsequently, we performed rheological measurements before and after mucolysis, proved the change of the viscoelastic properties, and correlated morphology and chemical structure of the mucus with its rheological characteristics. Our approach provides new insights into the airway mucus microstructure and brings Raman microscopy in focus as an upcoming tool for elucidation of the interaction mechanisms between the mucus and airborne threats, thus potentially contributing to more rational development of future lung therapeutics.

Author information

All authors have given approval to the final version of the manuscript. B.V. and X.M. contributed equally to this work.

Acknowledgments

X.M. was supported by the Marie Curie Initial Training Network PathChooser (PITNGA-2013-608373). The authors would like to thank Prof. Dr. Christian Wagner for assistance in the rheology measurements and Dr. Chiara De Rossi for her excellent technical assistance with the SEM.

References

Franzen, L., Vidlarova, L., Kostka, K.H., Schaefer, U.F., Windbergs, M., 2013. Exp. Dermatol. 22, 54.
Kim, M., Chen, W.G., Kang, J.W., Glassman, M.J., Ribbeck, K., Olsen, B.D., 2015. Adv. Mater. (Deerfield Beach, Fla.) 27, 4207.
Kirch, J., Schneider, A., Abou, B., Hopf, A., Schaefer, U.F., Schneider, M., Schall, C., Wagner, C., Lehr, C.M., 2012. Proc. Natl. Acad. Sci. U.S.A. 109, 18355.
Knowles, M.R., Boucher, R.C., 2002. J. Clin. Invest. 109, 571.
Koljenović, S., Bakker Schut, T.C., Van Meerbeeck, J.P., Maat, A.P.W.M., Burgers, S.A., Zondervan, P.E., Kros, J.M., Puppels, G.J., 2004. J. Biomed. Opt. 9, 1187.
Kumar, K., Castaño, E.J., Weidner, A.R., Yildirim, A., Goodwin, A.P., 2016. ACS Macro Lett. 5, 636.
Larhed, A.W., Artursson, P., Grasjo, J., Bjork, E., 1997. J. Pharm. Sci. 86, 660.
Matera, M.G., Calzetta, L., Cazzola, M., 2016. Expert Rev. Respir Med. 10, 89.
Murgia, X., Pawelzyk, P., Schaefer, U.F., Wagner, C., Willenbacher, N., Lehr, C.-M., 2016. Biomacromolecules 17, 1536.
Nordgård, C.T., Nonstad, U., Ø. Olderøy, M., Espevik, T., Draget, K.I., 2014. Biomacromolecules 15, 2294.
Perez-Gil, J., Weaver, T.E., 2010. Physiol. (Bethesda) 25, 132.
Rubin, B.K., 2002. Respir. Care 47, 761.
Rubin, B.K., 2015. Respir. Care 60, 825.
Ruge, C.A., Kirch, J., Lehr, C.-M., 2013. Lancet Respir. Med. 1, 402.
Sakuma, S., Suita, M., Inoue, S., Marui, Y., Nishida, K., Masaoka, Y., Kataoka, M., Yamashita, S., Nakajima, N., Shinkai, N., Yamauchi, H., Hiwatari, K.-i., Tachikawa, H., Kimura, R., Uto, T., Baba, M., 2012. Mol. Pharm. 9, 2933.
Sanders, N.N., De Smedt, S.C., Van Rompaey, E., Simoens, P., De Baets, F., Demeester, J., 2000. Am. J. Respir. Crit. Care Med. 162, 1905.
Schuster, B.S., Suk, J.S., Woodworth, G.F., Hanes, J., 2013. Biomaterials 34, 3439.
Sevier, C.S., Kaiser, C.A., 2002. Nat. Rev. Mol. Cell Biol. 3, 836.
Sigurdsson, H.H., Kirch, J., Lehr, C.M., 2013. Int. J. Pharm. 453, 56.
Suk, J.S., Kim, A.J., Trehan, K., Schneider, C.S., Cebotaru, L., Woodward, O.M., Boylan, N.J., Boyle, M.P., Lai, S.K., Guggino, W.B., Hanes, J., 2014. J. Controlled Release 178, 8.
Yu, M., Wang, J., Yang, Y., Zhu, C., Su, Q., Guo, S., Sun, J., Gan, Y., Shi, X., Gao, H., 2016. Nano Lett..
Yuan, S., Hollinger, M., Lachowicz-Scroggins, M.E., Kerr, S.C., Dunican, E.M., Daniel, B. M., Ghosh, S., Erzurum, S.C., Willard, B., Hazen, S.L., Huang, X., Carrington, S.D., Oscarson, S., Fahy, J.V., 2015. Sci. Transl. Med. 7 (276ra27).

Please cite this article in press as: B. Vukosavljevic, et al., Tracing molecular and structural changes upon mucolysis with N-acetyl cysteine in human airway mucus, Int J Pharmaceut (2017), http://dx.doi.org/10.1016/j.ijpharm.2017.07.022

4.3 Modelling the bronchial barrier in pulmonary drug delivery: a human bronchial epithelial cell line supplemented with human tracheal mucus

Xabi Murgia[a], Hanzey Yasar[a], Cristiane Carvalho-Wodarz[a], Brigitta Loretz[a], Sarah Gordon[a], Konrad Schwarzkopf[b], Ulrich Schaefer[c], and Claus-Michael Lehr[a,c]

[a]*Helmholtz Institute for Pharmaceutical Research Saarland (HIPS), Helmholtz Centre for Infection Research (HZI), Saarland University, 66123 Saarbruecken, Germany*

[b]*Department of Anesthesia and Intensive Care, Clinics Saarbruecken, 66119 Saarbruecken, Germany*

[c]*Biopharmaceutics and Pharmaceutical Technology, Department of Pharmacy, Saarland University, 66123 Saarbruecken, Germany*

Accepted 28 March 2017

European Journal of Pharmaceutics and Biopharmaceutics, 2017, 118, 79–88

DOI: 10.1016/j.ejpb.2017.03.020

European Journal of Pharmaceutics and Biopharmaceutics 118 (2017) 79–88

Contents lists available at ScienceDirect

European Journal of Pharmaceutics and Biopharmaceutics

journal homepage: www.elsevier.com/locate/ejpb

Modelling the bronchial barrier in pulmonary drug delivery: A human bronchial epithelial cell line supplemented with human tracheal mucus

Xabi Murgia [a], Hanzey Yasar [a], Cristiane Carvalho-Wodarz [a], Brigitta Loretz [a], Sarah Gordon [a], Konrad Schwarzkopf [b], Ulrich Schaefer [c], Claus-Michael Lehr [a,c,*]

[a] Helmholtz Institute for Pharmaceutical Research Saarland (HIPS), Helmholtz Centre for Infection Research (HZI), Saarland University, 66123 Saarbrücken, Germany
[b] Department of Anesthesia and Intensive Care, Klinikum Saarbrücken, 66119 Saarbrücken, Germany
[c] Biopharmaceutics and Pharmaceutical Technology, Department of Pharmacy, Saarland University, 66123 Saarbrücken, Germany

ARTICLE INFO

Article history:
Received 28 November 2016
Revised 16 March 2017
Accepted in revised form 28 March 2017
Available online 1 April 2017

Keywords:
Cystic fibrosis
Pulmonary mucus
Epithelial drug delivery
Nanoparticles

ABSTRACT

The airway epithelium together with the mucus layer coating it forms a protective system that efficiently filters and removes potentially harmful particles contained in inhaled air. The same mechanism, however, serves to entrap particulate drug carriers, precluding their interaction with their target. The mucus barrier is often neglected in *in vitro* testing setups employed for the assessment of pulmonary drug delivery strategies. Therefore, our aim was to more accurately model the bronchial barrier, by developing an *in vitro* system comprising a tight epithelial cell layer which may be optionally supplemented with a layer of human tracheal mucus. To form the epithelium *in vitro*, we used the cystic fibrosis cell line CFBE41o-, which can be grown as monolayers on Transwell® supports, expressing tight junctions as well as relevant transport proteins. In contrast to the cell line Calu-3, however, CFBE41o- does not produce mucus. Therefore, native human mucus, obtained from tracheal tubes of patients undergoing elective surgery, was used as a supplement. The compatibility of CFBE41o- cells with the human mucus was addressed with the MTT assay, and confirmed by fluorescein diacetate/propidium iodide live/dead staining. Moreover, the CFBE41o- cells retained their epithelial barrier properties after being supplemented with mucus, as evidenced by the high trans-epithelial electrical resistance values (~1000 Ω cm^2) together with a continued low level of paracellular transport of sodium fluorescein. Fluorescently-labeled chitosan-coated PLGA nanoparticles (NP, ~168 nm) were used as a model drug delivery system to evaluate the suitability of this *in vitro* model for studying mucus permeation and cell uptake. Comparing CFBE41o- cell monolayers with and without mucus, resp., showed that the NP uptake was dramatically reduced in the presence of mucus. This model may therefore be used as a tool to study potential mucus interactions of aerosolized drugs, and more specifically NP-based drug delivery systems designed to exert their effect in the bronchial region.

1. Introduction

The conducting airways of the lungs are coated with a viscoelastic secretion, the pulmonary mucus, which moisturizes the inhaled air and acts as a filter for inhaled particles. In the healthy state, mucus is composed of water (95% w/w), glycoproteins (mucins, 2–5%), salts, non-mucin proteins, lipids, DNA, enzymes, cells and bacteria [1–3]. The mucins are continuously secreted into the airway lumen by specialized secretory cells, and polymerize to form a mesh-like structure that is constantly being propelled out of the lungs by the ciliary beating of the airway epithelial cells – this creates a dynamic barrier termed as mucociliary clearance [4–6]. In disease states such as asthma, chronic obstructive pulmonary disease (COPD), and in particular cystic fibrosis (CF) considerable changes in the mucus can occur, leading to mucus oversecretion and mucus thickening [7–10]; this in turn can compromise the mucus clearance mechanism, providing optimal conditions for bacterial growth and chronic infection [11].

CF is a lethal genetic disease caused by a mutation of the CF transmembrane conductance regulator (CFTR). This results in numerous irregularities including an abnormal hydration of the airways, which leads to an impairment of the mucociliary machinery, recurrent infections, and eventually premature death [11]. The clinical management of CF focuses primarily on improving the mucociliary clearance and combating chronic infections rather

* Corresponding author at: Helmholtz Institute for Pharmaceutical Research Saarland (HIPS), Helmholtz Centre for Infection Research (HZI), Saarland University, 66123 Saarbrücken, Germany.
E-mail address: claus-michael.lehr@helmholtz-hzi.de (C.-M. Lehr).

http://dx.doi.org/10.1016/j.ejpb.2017.03.020
0939-6411/

than targeting the primary cause, namely correcting the genetic disease. The potential of nanomedicine to improve the efficiency of gene-therapy in such diseases by using nanoparticle (NP)-based drug delivery systems is considerable, as evidenced by efficient transfection of cell-based *in vitro* models including the CF cell line CFBE41o- [12–14]. This cell line was generated by transformation of CF airway cells with the SV40 virus and is homozygous for the most common CF mutation, the F508-CFTR mutation. Of particular interest to pharmaceutical research is the ability of this cell line to express tight-junction proteins such as claudin-1, ZO-1, and occludin [15], which confer on CFBE41o- monolayers significant epithelial barrier properties evidenced by high transepithelial electrical resistance (TEER) values [15–18]. This cell line also expresses a number of proteins relevant for pulmonary drug transport, including P-glycoprotein (P-gp), lung resistance-related P protein (LRP), and caveolin-1 [15]. Unfortunately, unlike other pulmonary cell lines such as Calu-3, which are able to secrete mucus [19–21], the CFBE41o- cell line lacks the capacity to synthesize and secret mucus onto the cell monolayer – a key feature that must be taken into account in the context of airway research. In particular, with regard to the use of NP-based drug delivery systems to treat bronchial diseases, our work and that of others has previously shown that particles with a diameter above 200 nm are almost exclusively trapped within the pulmonary mucus [3,22,23]. Moreover, with a net negative charge under physiological conditions [24,25], mucus represents a significant barrier to positively charged nanocarriers [21,26], which are often used in the context of nucleic acid delivery for transfection purposes [27–29].

Therefore, in the present study we explored the possibility to develop an *in vitro* model of the airways composed of a CFBE41o- cell layer coated with human tracheal mucus. Our aim was to take a step forward in accurately mimicking the scenario within the CF lung, by utilizing the positive features of the CFBE41o- cell line in the context of pharmaceutical research and further introducing mucus as a key non-cellular barrier of the airways. For this purpose we cultured CFBE41o- cells in Transwell® supports and added a layer of human tracheal mucus on top of the cell monolayer, creating an air-mucus interface. The biocompatibility of CFBE41o- cells with the human tracheal mucus was investigated by measurement of epithelial barrier properties upon incubation with the exogenous mucus. Ultimately, as a proof-of-concept validation of the implemented *in vitro* model, we produced chitosan-poly(D,L-lactide-co-glycolide; PLGA) nanoparticles and determined the effect of the mucus layer on the cellular uptake of such particles.

2. Methods

2.1. Human mucus sample collection

Undiluted human tracheal mucus samples were collected by the endotracheal tube method [3,30,31], after obtaining informed consent from patients and in compliance with a protocol approved by the Ethics Commission of The Chamber of Medicine Doctors of the Saarland (file number 19/15). The tracheal tube of patients undergoing elective surgery with general anesthesia, non-related to pulmonary conditions, was collected after surgery. The distal portion of the tracheal tube (5–10 cm), including the balloon, was cut and placed in a 50 ml centrifuge tube. The mucus of each tracheal tube was collected by centrifuging the samples at 190*g* for 30 s. Samples with visible blood contamination were excluded from the analysis. Mucus samples were stored at −20 °C until further use. In total 16 mucus samples from independent patients were used in this study. The mean age of the patients was 56.8 ± 4.8 years, the male: female ratio was 12:4, and 6 out of 16 patients were smokers.

2.2. Freeze-dried mucus disk preparation

Mucus samples frozen and stored at −20 °C were thawed gradually and allowed to reach room temperature. Thereafter, single mucus drops with an approximate weight of 30–40 mg (34.17 ± 1.82 mg, n = 45 mucus drops) were placed over a Teflon® surface and spread over delineated circular surfaces of 1.12 cm^2. The samples were then placed into an autoclavable sealing bag, stored at −80 °C for 4 h, and ultimately, freeze-dried overnight (Alpha 2-4 LSC, Christ, Germany). After completion of the preset freeze-drying program, the bag containing the mucus disks (1.7 ± 0.1 mg estimated solid content, for an estimated water content of 95%) was immediately sealed and stored in a dry atmosphere at room temperature until further use. Five different batches with 14–20 mucus disks per batch were used in this study.

2.3. Mucus characterization

2.3.1. Mucus bulk rheology

Experiments were conducted on an Anton-Paar MCR 102 rheometer (Graz, Austria) equipped with cone-plate geometry (diameter: 25 mm, cone angle: 2°) at room temperature. Strain amplitude (γ) sweeps were performed at a frequency of 1 Hz in the range of 0.1–10%. Frequency (ω) dependency of the storage modulus G' and the loss modulus G'' was measured in the range between 0.1 and 40 rad/s at a strain amplitude of 1%.

In the first set of experiments native undiluted tracheal mucus samples were gradually thawed and allowed to reach room temperature. Thereafter, an approximate volume of 150 µl of mucus was placed in the rheometer and the aforementioned protocol was conducted. In the second set of experiments previously freeze-dried and rehydrated mucus samples were analyzed. Mucus samples contained in 1.5 ml Eppendorf tubes were allowed to equilibrate to room temperature and weighed using a precision balance (CPA 224S, Sartorius, Göttingen, Germany). Afterwards, the samples were stored at −80 °C for 4 h followed by overnight freeze-drying (Alpha 2-4 LSC, Christ, Osterode am Harz, Germany). The freeze-dried (solid) content of the samples was weighed again to determine the water content of mucus. Mucus samples were then re-hydrated with exactly the same volume of sublimed water (Milli-Q water, Advantage A10, Merck Millipore, Billerica, MA), and were allowed to mix in a 360° multi-rotator (PTR-35, Grant instruments, UK) for at least two hours at room temperature. Thereafter, re-hydrated mucus samples were placed in the rheometer to perform the measurements as described above.

2.3.2. Scanning electron microscopy

The structure of pulmonary mucus was imaged by means of scanning electron microscopy (SEM). Human tracheal mucus samples were gradually thawed and spread over the surface of a SEM-imaging carbon disk. The mucus was freeze-dried *in situ* following the freeze-drying protocol as in Section 2.2. Freeze-dried mucus samples were gold-sputtered (QUORUM Q150R ES, Gala Instrumente, Germany) and then transferred to the SEM (EVO HD15, Zeiss, Germany) for imaging.

In order to image the CFBE41o- cell monolayer and the combined model comprising the cell monolayer and the overlying mucus, the cells were seeded onto Transwell® permeable supports and were cultured until a confluent monolayer was reached (see Section 2.4). The day before the SEM fixation the apical culture medium was removed and a mucus disk together with 100 µl of fresh medium were added to the apical compartment, creating an air mucus interface. The cells with the mucus disks in place were incubated for 24 h at 37 °C, 5% CO_2, in a horizontal shaker. After incubation the basolateral medium was aspirated and fixation was performed by adding 1 ml of glutaraldehyde 3% (Sigma)

in PBS to the basolateral compartment for 2 h. Subsequently, dehydration was carried out through a graded series of ethanol (30–100%, 10 min each). In the final step 150 µl of hexamethyldisilazane (Fluka) were added to the apical compartment. The filter of the Transwells® was then cut with a scalpel and mounted onto SEM-stacks. Samples were further sputtered with gold and transferred to the electron microscope.

2.4. Cell culture of CFBE41o-

CFBE41o- cells were a kind gift of Dr. Dieter C. Gruenert (University of California, San Francisco, CA, USA). Passages 78–90 were used in this study. Cells were passaged on a weekly basis (0.2×10^6 cells in a T75 flask) and grown in minimum essential medium (MEM, Gibco) supplemented with 10% fetal calf serum (FCS, Lonza), 5% non-essential amino acids (NEAA 100x, Gibco), 0.54 mg/ml of D-(+)-glucose (Sigma), and 100 µg/ml streptomycin and 100 U/ml penicillin, at 37 °C in a 5% CO_2 incubator. Unless otherwise stated, for experimental purposes cells were seeded onto Transwell® permeable supports (3640, Insert diameter 12 mm, growth area 1.12 cm^2, pore size 0.4 µm; Corning, Wiesbaden, Germany) at a density of 1.5×10^5 cells/cm^2 and grown under submerged conditions with apical/basolateral fluid volumes of 500 µl/1100 µl, respectively. The culture medium was replaced every 2–3 days.

2.5. Nanoparticle preparation and characterization

PLGA (50:50; Resomer RG 503H) was purchased from Evonik Industries AG (Darmstadt, Germany); ultrapure chitosan chloride salt (Protasan UP CL113) was obtained from FMC Biopolymer AS NovaMatrix (Sandvika, Norway). Polyvinyl alcohol (PVA) Mowiol®4-88 was purchased from Sigma-Aldrich (Germany); the lipophilic fluorescent dye 1,1′-dioctadecyl-3,3,3′,3′-tetramethylin dodicarbocyanine perchlorate (DiD) was obtained from Thermofisher Scientific (Oregon, USA). Ethyl acetate was purchased from Sigma-Aldrich (Germany), and purified water was produced freshly by a Milli-Q water purification system (Merck Millipore, Billerica, MA).

Drug free, DiD-labeled chitosan-PLGA NPs were used as a model drug delivery system to evaluate the uptake behavior on CFBE41o- cell monolayers with and without mucus. Such NPs were prepared by using a modified double-emulsion method according to Mittal et al. [32]. Briefly, a 0.2% w/v chitosan solution was first prepared by dissolving Protasan UP CL113 in a 2% w/v PVA solution. A 50 mg amount of PLGA was dissolved in 2 ml ethyl acetate and equilibrated with 15 µg/20 µl of DiD ethanolic solution under continuous stirring for 1 h at room temperature. A 400 µl volume of water was then added to the PLGA organic phase and sonicated with ultrasound (Branson Ultrasonic Corporation, USA) at 20% amplitude for 20 s to allow the primary emulsion to form. Immediately afterwards, the PVA chitosan solution was applied to the primary emulsion and sonicated using the same settings, leading to the formation of a w/o/w emulsion. Milli-Q water was added dropwise to the w/o/w emulsion to allow for the evaporation of the organic solvent. The resulting chitosan coated PLGA NPs were purified by centrifugation at 15,000*g* for 15 min and washed once with milli-Q water to remove any excess free dye. The size, polydispersity index (PDI) and ζ-potential of the DiD labeled chitosan-PLGA NPs were characterized using a Zetasizer Nano (Malvern Instruments, Malvern, UK). The morphological appearance of the carrier system was visualized using Transmission Electron Microscopy (TEM, JEM 2011, JEOL) and further with SEM (EVO HD15, Zeiss, Germany). Prior to the SEM measurements, NPs were put onto a carbon disk and gold-sputtered. In order to improve the contrast of the TEM images, NPs were further stained with 0.5% w/v phosphotungstic acid (Sigma).

2.6. Cytotoxicity assays

2.6.1. MTT assay

CFBE41o- cells were seeded in 96 well plates at a density of 20,000 cells per well and grown for 4 days. Cells were then washed twice with Hank's balanced salt solution (HBSS, Gibco) buffer, and 200 µl of fresh culture medium together with a freeze-dried mucus disk were added to the test wells. The cells were incubated for 24 h at 37 °C and 5% CO_2 in a horizontal shaker. Cells incubated with cell culture medium only served as positive controls (100% viability) and cells incubated with Triton-X 1% (Sigma) served as negative controls (0% viability). Following incubation, the mucus was removed by aspiration and the cells were washed twice with HBSS buffer. A 200 µl volume of the tetrazolium dye MTT (5 mg/ml) was added to each well, followed by 4 h incubation at 37 °C, 5% CO_2, in a horizontal shaker. Formed formazan crystals were then solubilized by adding 200 µl of dimethyl sulfoxide (DMSO, Sigma). The absorbance of each well at 560 nm was measured with a plate reader (Infinite M200 Pro, TECAN), and the percentage of viable cells in each well was calculated as previously described [33].

2.6.2. Live/dead staining with fluorescein diacetate (FDA) and propidium iodide (PI)

Cell monolayers were cultured for at least 10 days under submerged conditions. Live cells can take up and convert the non-fluorescent FDA into its fluorescent product fluorescein by means of cytosolic esterases, whereas PI cannot cross the membrane of viable cells but will stain the nuclei of non-viable cells by intercalating with the double helix DNA. Approximately 24 h before live/dead staining the apical medium was removed from each culture well and a mucus disk together with 100 µl of fresh culture medium were added to apical compartments. The cells with the mucus disks in place were incubated for 24 h at 37 °C and 5% CO_2 in a horizontal shaker. After 24 h, the mucus disks had dissolved creating an air-mucus interface in the apical compartment of each Transwell®. To proceed with the live/dead staining, medium was aspirated from mucus-containing apical compartments which were then washed twice with fresh medium. The cells were allowed to equilibrate for 30 min with 500 µl of freshly added cell culture medium, before this was replaced by 500 µl of the working solution of the FDA/PI live/dead stain (Sigma). The working solution itself was prepared in a 5 ml volume by adding 20 µl of FDA (5 mg/ml in acetone) and 100 µl of PI (2 mg/ml in PBS) to 4.88 ml of Phosphate-buffered saline (PBS, pH 7.4). The cells were incubated with the working solution for 5 min at room temperature, in the dark. The apical compartment of each well was then washed twice with cold PBS and the culture plate immediately transferred to a confocal laser scanning microscope (Leica TCS SP 8; Leica, Mannheim, Germany). Images of cell monolayers were acquired at 1024×1024 resolution, using either a 25x water immersion (Fluotar VISIR 25x/0.95) or a 63x water immersion objective (HC APO CS2 63x/1.20). Image analysis was performed using LAS X software (Leica Application Suite X; Leica, Mannheim, Germany). Non-stained cells were used to preset the initial confocal settings. Cells that were not exposed to mucus served as positive controls and cells incubated with Triton-X 1% served as negative controls.

2.7. Functional mucosal barrier property assays

2.7.1. Evolution of TEER values of CFBE41o- cells cultured under submerged conditions

TEER values were measured every 2–3 days for three weeks with an epithelial voltohmmeter equipped with STX2 chopstick

manual electrodes (EVOM, World Precision Instruments, USA). A sharp increase in TEER values is associated with a confluent cell monolayer and the development of tight-junctions between neighboring cells. The raw TEER values were corrected according to the background resistance value of the Transwell® filter itself, and the growth area of the filter (1.12 cm^2).

2.7.2. TEER measurements with and without mucus incubation

Cells were cultured for at least 10 days under submerged conditions. The apical medium was aspirated and a mucus disk together with 100 µl of fresh medium was added to the apical compartment. The cells with the mucus disks in place were incubated for 24 h at 37 °C and 5% CO_2, in a horizontal shaker. The next day, the mucus-containing apical compartment was aspirated, washed twice with fresh culture medium, and the cells were allowed to equilibrate for 30 min with 500 µl of freshly added cell culture medium in the apical compartment. Thereafter, TEER values were measured. Cells not exposed to mucus served as controls.

2.7.3. Permeability of sodium fluorescein

Cell monolayers were cultured under submerged conditions for 7 days (the time point at which CFBE41o- cells displayed the highest epithelial barrier properties, according to TEER measurements). Apical compartments were then washed with Krebs-Ringer buffer (KRB) (NaCl 142.03 mM, KCl 2.95 mM, $K_2HPO_4*3H_2O$ 1.49 mM, HEPES 10.07 mM, D-glucose 4.00 mM, $MgCl_2*6H_2O$ 1.18 mM, $CaCl_2*2H_2O$ 4.22 mM; pH 7.4) and a mucus disk together with 100 µl of KRB buffer were added, and incubated for 4 h. Control wells incubated with just 100 µl of KRB served as controls. After the incubation, the basolateral culture medium was aspirated and the cells were washed twice with KRB. A volume of 1.5 ml of fresh KRB was then added to the basolateral compartment. The transport study was initiated by adding 500 µl of sodium fluorescein (10 µg/ml) to the apical (donor) compartment. The paracellular transport of sodium fluorescein was determined by sampling 200 µl from the basolateral (acceptor) compartment at various time points (0, 5, 15, 30, 60, 90 and 120 min). The basolateral volume withdrawn at each sampling point was replaced by the same volume of fresh pre-warmed KRB buffer. Throughout the experiment the cells were incubated at 37 °C and 5% CO_2 on a horizontal shaker. The amount of sodium fluorescein in the acceptor compartment at each time-point was assessed by means of fluorescence intensity using a plate reader (Infinite M200PRO, Tecan, Germany) at excitation and emission wavelengths of 488 and 530 nm respectively. The apparent permeability coefficient (P_{app}) was then calculated by applying the formula:

$$P_{app} = (dQ/dt)\%(A * C_0) \quad (1)$$

where dQ/dt is the flux (µg/s of permeated sodium fluorescein, obtained from the slope of the linear region of each individual permeation profile), A the area of the filter insert (1.12 cm^2), and C_0 the initial donor concentration of sodium fluorescein. C_0 was assumed to be 8.33 µg/ml in all wells, considering that 500 µl of sodium fluorescein (10 µg/ml) were added to a pre-existing apical volume of 100 µl.

2.7.4. Permeability through mucus and cellular uptake of nanoparticles

CFBE41o- cells were cultured under submerged conditions for at least 10 days. The apical medium was then aspirated and a mucus disk with 100 µl of medium was added to the apical compartment followed by a 24 h incubation to allow for disk dissolution and creation of an air-mucus interface. Volumes of 400 µl of the DiD-labeled chitosan-PLGA NPs were then added to the apical compartment at a concentration of 40 µg/ml and were incubated for an additional 24 h. After incubation, the apical compartment, including the mucus, was aspirated and the cells were washed twice with PBS. In the following step 100 µl of wheat germ agglutinin (10 µg/ml, Vector Labs, CA, USA) were added to the apical compartment in order to stain the cell membrane. The cells were again washed twice with PBS and fixed with 3% paraformaldehyde (PFA, 15710-5, Electron Microscopy Science, USA) in PBS, for 30 min, at room temperature. After fixation cells were washed twice with PBS and then 200 µl of 4′,6-diamidino-2-phenylindole (0.1 µg/ml, DAPI, Life Technologies, Darmstadt, Germany) were added to the apical compartment (10–15 min), followed by two further washes with PBS. Cell monolayers underwent a total of 8 PBS washes, which removed almost all the mucus as well as extracellular NPs. Finally, the filter membrane of each Transwell® insert was cut out with a scalpel and mounted on a glass slide with mounting medium (DAKO, Product No 85 5302380-2, USA). Mounted samples were stored at 4 °C until analysis by confocal laser scanning microscopy (Leica TCS SP 8; Leica, Mannheim, Germany). Images were acquired at 1024 × 1024 resolution, using a 63x water immersion objective (HC APO CS2 63x/1.20). Image analysis was performed using LAS X software (Leica Application Suite X; Leica, Mannheim, Germany).

2.8. Statistical analysis

All values are given as mean ± standard error of the mean (SE). Statistical analysis was performed with the SPSS statistics software (IBM, Germany). The storage and loss moduli of the native versus the freeze-dried and re-suspended mucus were compared using one-way ANOVA. The TEER values before and after mucus addition, P_{app} values, and permeated amounts of sodium fluorescein were compared using an independent samples *t*-test with Levene's test for equality of variances. A $P < 0.05$ was accepted as significant.

3. Results and discussion

3.1. CFBE41o- monolayers display high TEER values already after 5 days in submerged culture

CFBE41o- cells grown under submerged conditions displayed high TEER values within just 5 days of being seeded on Transwell® supports (Fig. 1). The TEER values peaked between days 5–9 with values above 1500 Ω cm^2. TEER values stabilized after day 10 (with the exception of a slight decrease between days 10 and 15) at approximately 1000 Ω cm^2, indicating optimal epithelial barrier properties within this time period.

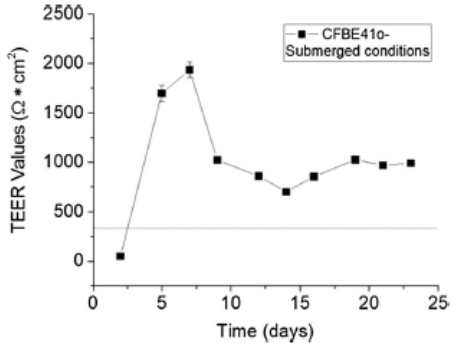

Fig. 1. Time-course of TEER values measured for the CFBE41o- cell line cultured under submerged conditions. The horizontal line at 300 Ω cm^2 indicates the threshold values deemed to indicate the presence of a tight barrier. The mean ± SE for n = 25, from 4 independent experiments are shown.

The noted TEER values are in line with previous studies and suggest the expression of functional tight junctions already within a few days of cell seeding on Transwell® membranes [15,16]. Equivalent bioelectric properties have been also described for other bronchial cell lines grown under submerged conditions such as 16HBE14o- cells, and the widely used Calu-3 cell line [34–36]. The Calu-3 cell line can secrete mucus, provided that cells are cultured at the air-liquid interface [20,21]. However, growing Calu-3 cells under this condition significantly decreases the TEER values [19,37] and significantly increases the culture time needed to achieve both a tight epithelial barrier ($\geq$300 Ω cm^2) and a confluent mucus layer on top of the cells [20,21]. The TEER values of CFBE41o- cells are similarly low when cultured at the air-liquid interface [15], bordering on the threshold values deemed to indicate the presence of a tight barrier. In order to develop a relevant model that mimics the CF airway for pharmaceutical testing purposes, we therefore sought to combine the optimal epithelial barrier properties displayed by the CFBE41o- cell line grown under submerged conditions with the option to either add, or not to add, a supplementary human mucus layer.

3.2. In vitro model concept

The concept of the novel *in vitro* model involves growing CFBE41o- cells in Transwell® supports under submerged conditions until the monolayer develops optimal barrier properties. At this time-point the overlying culture medium is removed and the apical compartment is supplemented with freeze-dried human mucus in combination with a minimal volume of medium, creating an air-mucus interface. The human tracheal mucus samples obtained for the present work were initially nonsterile and highly elastic. Mucus samples are difficult to manipulate, precluding the possibility of pipetting precise mucus volumes or efficiently distributing mucus over a cell monolayer without damaging it. To overcome this limitation, we developed a feasible alternative to freeze-dry small amounts of mucus in order to form thin disks, which could then be placed onto the cell monolayers and re-hydrated with a minimal amount of culture medium. Moreover, we speculate that the freeze-drying process may have accounted for a reduction in the microbial load of the exogenous human material.

3.3. Freeze-dried, re-suspended tracheal mucus show similar rheological properties to undiluted native mucus

The rheological properties of native undiluted mucus were compared to those of mucus samples that had undergone freeze-drying and subsequent re-hydration. With regard to the undiluted native tracheal mucus, in the tested strain range (0.1–10%) airway mucus was within the viscoelastic linear range (Fig. 2A, black symbols). Therefore a strain of 1% was chosen to determine the frequency dependence of the viscoelastic moduli. In the tested frequencies (0.1–40 rad/s) G′ dominated over G″ in all the three decades of frequencies tested (Fig. 2B, black symbols). These rheological properties are characteristic of cross-linked gels and are in line with previous studies reporting on the bulk rheological behavior of airway mucus [3,10,30]. The G″/G′ ratio of mucus determined at 1 rad/s represents a frequency value that is often used in mucus rheology to approximate the low velocities of mucociliary clearance [30,31,38]. Materials with a ratio ranging between $0 \leq G''/G' \leq 1$ are classified as viscoelastic solids. The G″/G′ ratio achieved here for the native tracheal mucus shows a mean value of 0.27 ± 0.01, in good agreement with the values reported by Schuster et al. and Rubin et al. in which a G″/G′ of 0.30 and 0.28 were respectively determined for airway mucus samples collected by the same method as employed in the current work [3,31].

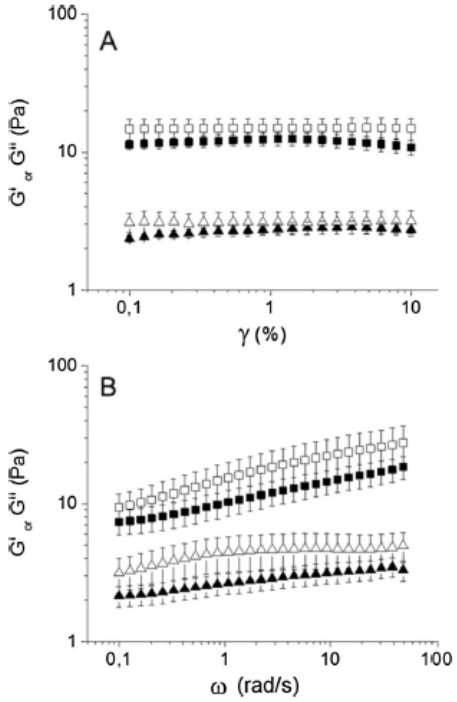

Fig. 2. Bulk rheology of native human tracheal mucus (solid symbols) compared to native airway mucus which was freeze-dried and re-suspended (open symbols). (A) Strain (γ)-dependent viscous (G′, triangles) and elastic (G′, squares) moduli from 0.1 to 10% strain at a frequency of 6.28 rad/s (1 Hz). (B) Frequency-dependent viscous (G″, triangles) and elastic (G′, squares) moduli from 0.1 to 50 rad/s at 1% strain. The mean ± SE for n = 5 independent mucus samples are shown.

Since our aim was to implement a mucus layer on top of the CFBE41o- cell monolayer using freeze-dried tracheal mucus, we investigated whether, upon re-hydration, the freeze-dried mucus would partially or completely recover the viscoelastic properties shown by the native material.

The water percentage of the mucus samples was 95.79 ± 0.62%, being the percentage of solid content of 4.20 ± 0.62. After re-hydration with exactly the same volume of sublimed water and 2 h of mixing in a 360° rotator, the freeze-dried mucus displayed very similar viscoelastic properties as the undiluted human mucus, with no statistical difference between the elastic or viscous moduli at any of the strains or frequencies tested. As with the native material, G′ exceeded G″ in both the amplitude and the frequency sweep test (Fig. 2, white symbols). The viscoelastic moduli were slightly, but not significantly, higher in the case of the freeze-dried and re-hydrated mucus in comparison to the native material. The mean G″/G′ ratio at 1 rad/s demonstrated a mean value of 0.29 ± 0.01, which confirms that intermolecular cross-linking and the characteristic mucus viscoelastic behavior were recovered after re-hydration.

3.4. CFBE41o- cells remain viable and retain their barrier properties after addition of external human freeze-dried mucus

The primary concern of adding an exogenous mucus to the CFBE41o- monolayers was a potential adverse effect that the human-derived tracheal mucus could exert on the cells. Previous studies attempting to implement exogenous mucus onto cell

monolayers, had shown a clear disruption of the epithelial barrier properties and even some cytotoxicity [39,40]. Boegh et al. found a significant barrier disruption after incubating Caco-2 cells with native porcine intestinal mucus, as evidenced by the dramatic decrease in TEER values [39], whereas Teubl et al. reported a reduced viability of the oral epithelial cell line TR146 after a 24 h incubation with mucins derived from bovine submaxillary glands [40]. We hypothesized that due to the common human origin of both the CFBE41o- cells and the tracheal mucus, the cells and the mucus would be better compatible. To assess any potential toxic effects that the exogenous freeze-dried mucus could exert on the cells, the MTT assay was performed on proliferating CFBE41o- cells. However, after 24 h of incubating the cells with mucus the viability was slightly higher than in untreated control cells, suggesting even a positive effect of human mucus on the human-derived CFBE41o- cells under such conditions (Fig. 3A).

In a subsequent step we sought to confirm the cell viability of CFBE41o- monolayers that were allowed to differentiate and to develop tight junctions in Transwell® using the so called live dead staining: in the case that cells are alive, the diffusion and subsequent esterase-mediated hydrolysis of the non-fluorescent dye FDA to the fluorescent product fluorescein will occur. In the case that cells are dead, PI will bind to DNA within the nuclei of cells in which the cell membrane is disrupted (Fig. 3B). After staining with the working solution of FDA/PI we observed tightly packed CFBE41o- cells in confluent monolayers emitting high fluorescence intensity in the fluorescein detection range (Fig. 3C–E), confirming the high cell viability previously observed in proliferating cells with the MTT assay.

Having confirmed with two different methods the compatibility of the CFBE41o- monolayers with exogenous mucus, the next step consisted of addressing whether CFBE41o- monolayers would retain their epithelial barrier properties after adding exogenous mucus. For that purpose we indirectly assessed the presence of tight junctions by comparing the TEER values of the cells before and 24 h after coating the monolayer with mucus (Fig. 4). Monolayers incubated without mucus but under the same experimental conditions were used as controls. Under both conditions the barrier properties of the CFBE41o- cell monolayers remained intact. Thus, unlike in the work of Boegh et al., where the TEER values dropped after adding external pig gastric mucus to Caco-2 cells [39], in the present constellation the barrier properties were maintained after mucus addition. The most plausible explanation for the compatibility between the CFBE41o- cells and the exogenous

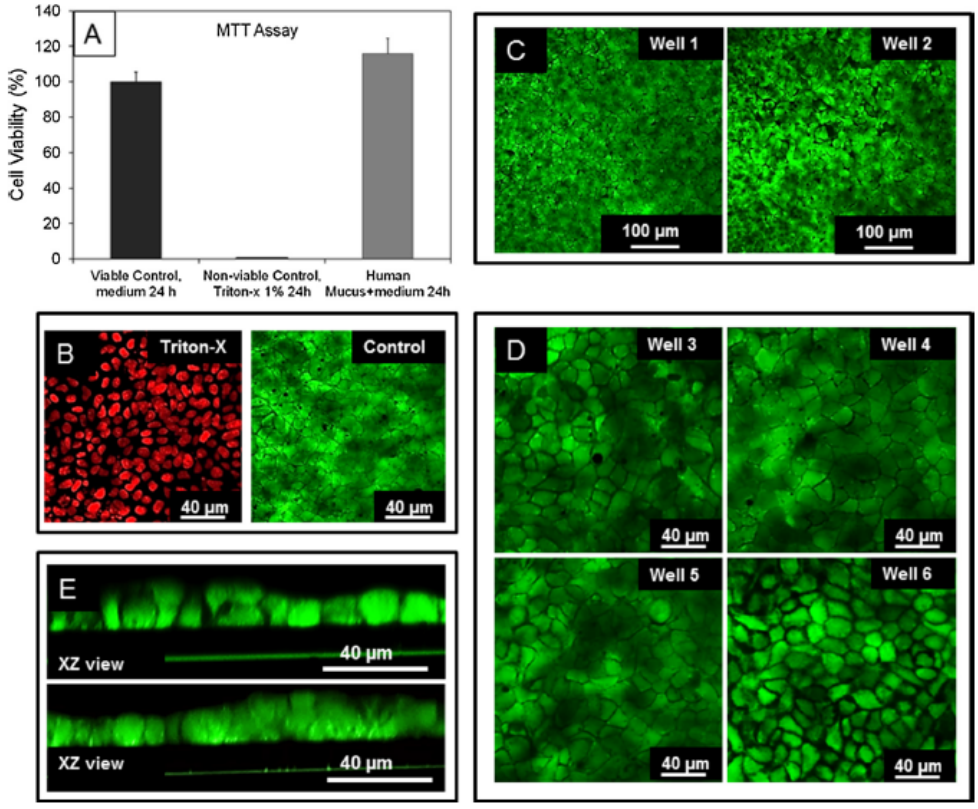

Fig. 3. The viability of CFBE41o- cells upon contact with exogenous human mucus was assessed with the MTT assay and by live/dead staining with fluorescein diacetate (FDA) and propidium iodide (PI). (A) CFBE41o- cells exposed to mucus for 24 h had a viability over 100% (grey bar), slightly greater than that of control cells incubated with the appropriate medium (black bar); CFBE41o- cells incubated with the detergent Triton-X served as a negative control with 0% viability. (B) Representative fluorescence microphotographs of the negative (left) and positive (right) controls for the live/dead staining; cells with their nuclei stained in red represent non-viable cells, whereas cells with a green cytoplasm represent viable cells. (C) and (D) Representative fluorescence microphotographs of independent experiments at different magnifications, showing different Transwells® (wells 1–6) supporting CFBE41o- monolayers that had been incubated for 24 h with human mucus in the apical compartment. (E) X-Z cross-sectional view of viable CFBE41o- monolayers that had been incubated for 24 h with human mucus.

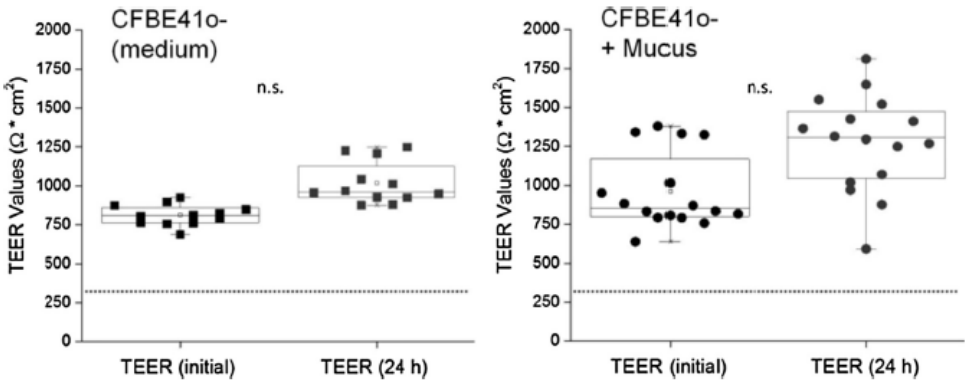

Fig. 4. The barrier properties of the CFBE41o- monolayers grown for at least 10 days under submerged conditions were monitored for 24 h. The TEER values were measured before (initial) and 24 h after addition of (CFBE41o- + Mucus, right). CFBE41o- cells not exposed to mucus but incubated under submerged conditions with regular medium served as controls (CFBE41o-, left). The horizontal line at 300 Ω cm^2 indicates the threshold values deemed to indicate the presence of a tight barrier. The mean ± SE of n = 12 (CFBE41o-) and n = 16 (CFBE41o- + mucus) from three independent experiments are shown. No significant (n.s.) differences were found.

pulmonary mucus may be the common human origin of both materials. In addition, the freeze-drying process may have contributed, in combination with the antibiotics in the cell culture medium, to keep the model sterile and to maintain high cell viability and intact barrier properties. No signs of bacterial contamination were observed with the use of freeze-dried mucus.

3.5. Sodium fluorescein transport

The pulmonary mucus is a selective barrier that allows the permeation of small molecules such as nutrients, growth factors, and antibodies, but significantly hinders the movement of particulates with a size greater than 100–200 nm [8,22,23]. The apical-to-basolateral transport of the small hydrophilic model drug sodium fluorescein (376.3 Da) is routinely used to assess the paracellular transport and the barrier properties of *in vitro* epithelial models [20,41,42]. We hypothesized that sodium fluorescein is small enough to permeate through the mucus pores and would not significantly interact with the mucus fibers due to its negative charge. Therefore, one could expect a similar transport rate of the molecule through the CFBE41o- monolayers, as well as equivalent P_{app} values, in either the presence or absence of mucus. CFBE41o- monolayers, with or without mucus, were indeed observed to act similarly as a barrier to paracellular transport (Fig. 5A), with both conditions resulting in P_{app} values below 1×10^{-6} cm/s. A slight although not significant lower extent of permeation of sodium fluorescein could however be observed in the CFBE41o- monolayers incubated with human mucus (Fig. 5B), most probably due to interactions between the compound and mucus elements in a setting of two unstirred layers of different viscosity within the first hour after sodium fluorescein addition.

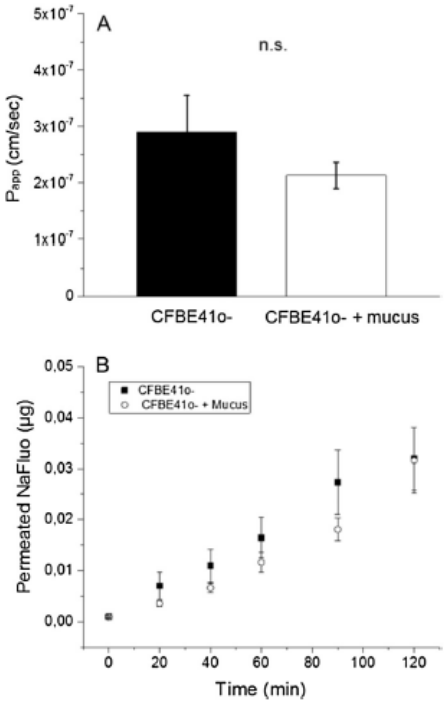

Fig. 5. The barrier properties of the CFBE41o- monolayers after their exposure to mucus were determined by measuring the permeability of sodium fluorescein (NaFluo) over time. (A) Apparent permeability (P_{app}) of sodium fluorescein through CFBE41o- monolayers compared to CFBE41o- monolayers supplemented with human mucus. (B) Permeated total amount of NaFluo over time through CFBE41o- monolayers (solid squares) compared to CFBE41o- monolayers supplemented with human mucus (empty circles). The mean ± SE for n = 20 from 3 independent experiments are shown. No significant (n.s.) differences were found.

3.6. Mucus is a barrier to polymeric nanoparticles

The mesh-like structure of pulmonary mucus is mainly given by a highly cross-linked mucin network (Fig. 6A). The size of the pores of the mucus mesh is highly heterogeneous and ranges from very small pores of just a few nanometers to larger pores on the micro-scale [22,23]. Therefore, mucus represents a steric barrier to the diffusion of NPs. In addition, mucus can also filter NPs by specific chemical interactions. For instance, the sialic acid-rich glycan side-chains of the mucins confer a negative charge on mucus [43]; mucins also possess non-glycosylated regions with a high capacity for hydrophobic interactions [44]. As a result, a large fraction of NPs with a size above 100 nm that theoretically can chemically interact with mucus will become immobilized within the mucus mesh [3,8,22,23]. These findings highlight the outstanding filtering properties of pulmonary mucus against NP-based drug

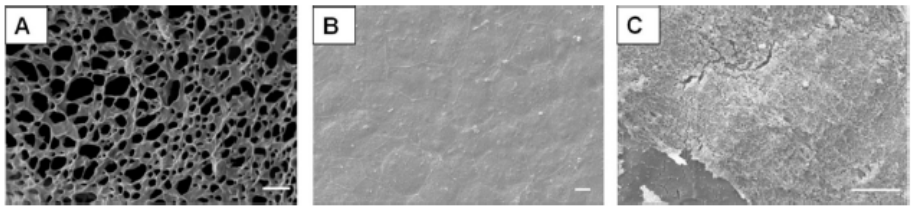

Fig. 6. (A) Scanning electron microscopy (SEM) image of freeze-dried human tracheal mucus. (B) Representative SEM image of a CFBE41o- monolayer; cell boundaries between neighboring cells are visible. (C) SEM image of human tracheal mucus on top of a CFBE41o- cell monolayer; the mucus mesh structure seen in (A) is lost due to the chemical fixation. Scale bar = 4 μm.

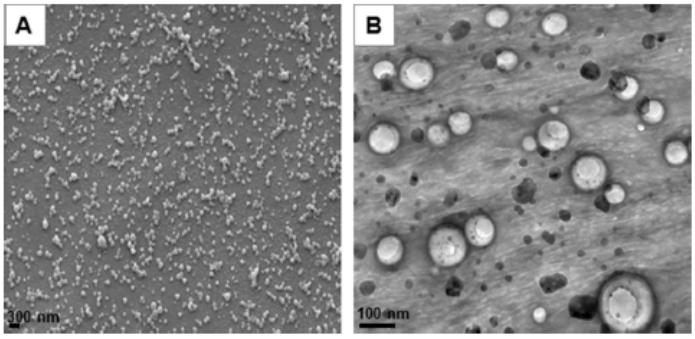

Fig. 7. (A) Scanning electron microscope (SEM) and (B) transmission electron microscope (TEM) images showing the morphology of DiD labeled chitosan-PLGA nanoparticles.

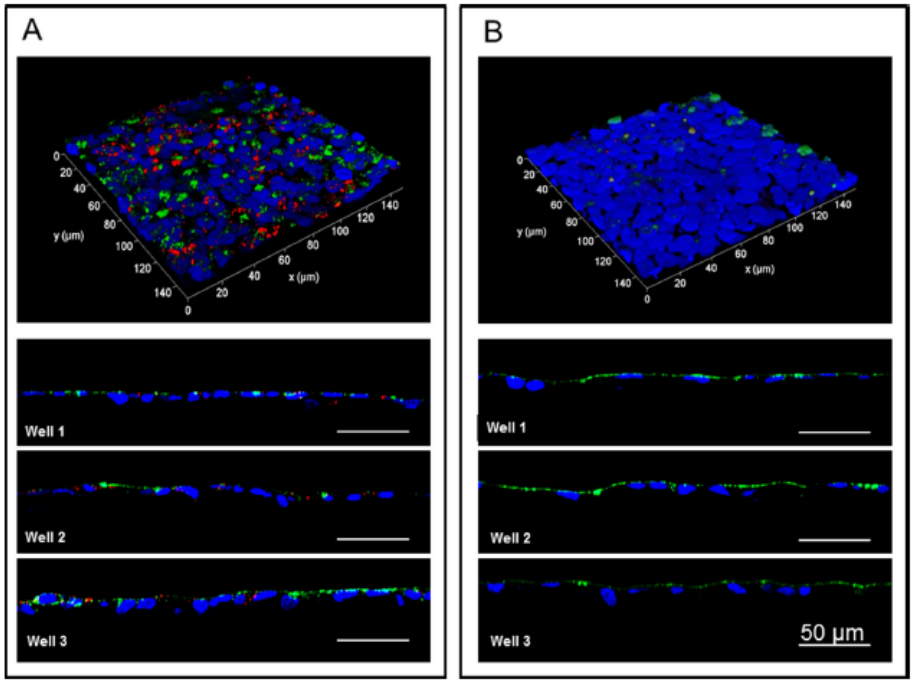

Fig. 8. Confocal laser scanning microscopy images of the cellular uptake study performed with DiD-labeled chitosan-PLGA nanoparticles (NP) on CFBE41o- cells with and without mucus. (A) CFBE41o- monolayers were incubated with 400 μl of the NP suspension (40 μg/ml) for 24 h; after incubation, although the apical surface was thoroughly washed with PBS, a widespread presence of NPs either in close contact with or internalized by cells was noted, as evidenced by the 3D rendering (top) and the X-Z cross-sections (wells 1–3). (B) CFBE41o- monolayers supplemented with human tracheal mucus were incubated with 400 μl of the NP suspension (40 μg/ml) for 24 h. After incubation, the apical surface was thoroughly washed with PBS, resulting in the removal of both mucus and entrapped NPs. The absence of NPs in contact with cells in this case indicates that a vast majority of the NPs were trapped within the mucus and washed away. Nuclei were stained with DAPI (blue), the cell membrane was stained with wheat germ agglutinin (green), and the DiD-labeled chitosan-PLGA NPs were labeled with DiD (red). (For interpretation of the references to color in this figure legend, the reader is referred to the web version of this article.)

delivery systems. As a proof of concept for the developed *in vitro* model, we incubated chitosan coated PLGA NPs for 24 h together with "naked" CFBE41o- cell monolayers (Fig. 6B), as well as with CFBE41o- cell monolayers supplemented with an additional mucus layer (Fig. 6C). Thereafter we qualitatively addressed NP uptake by means of confocal microscopy.

The produced chitosan-PLGA NPs had a size of 167.8 ± 3.6 nm (PDI 0.1 ± 0.01, Fig. 7) and were positively charged, as evidenced by a ζ-potential of 12.9 ± 1.9 mV.

This type of NPs was chosen because they have been already used for several applications of pulmonary nucleic acid delivery [45–47]. Additionally, chitosan coatings have been shown to induce efficient transfection in various cell lines [27,28], including CFBE41o- [12]. We hypothesized, however, that with a NP diameter close to 200 nm and due to the known mucoadhesive properties of chitosan [48], most of the NPs would be trapped within the mucus layer, precluding their cellular uptake. When NPs were incubated with the "naked" CFBE41o- cell monolayers, a significant uptake could be observed from the confocal images (Fig. 8A). On the other hand, when the chitosan-PLGA NPs were incubated with CFBE41o- monolayers that were supplemented with a layer of mucus, the number of NPs in close proximity to the cells was negligible, indicating that most of the NPs had been entrapped by the mucus layer (Fig. 8B) which was itself washed away during the staining/fixation procedure. This finding further confirmed our hypothesis, and indicates that the drug delivery efficiency of NP-based systems is dramatically reduced in mucosal tissues.

4. Conclusion

The aim of this work was to develop an *in vitro* model of the bronchial region comprising minimally an epithelial cell layer and a layer of pulmonary mucus. As a cellular element, we used the CF cell line CFBE41o-, which possesses a number of interesting features for pharmaceutical research such as the expression of tight junction proteins and proteins relevant for pulmonary drug transport. Nevertheless, this cell line is unable to secrete mucus, and therefore the cell monolayer alone as an *in vitro* model lacks a key protective element found in the airways *in vivo*. To complement the cell monolayer, small amounts of freeze-dried human tracheal mucus were placed on top of the CFBE41o- cells, creating an air-mucus interface. The rheological properties of the re-hydrated mucus were very similar to the native material. Moreover, the biocompatibility of the exogenous mucus with the cells could be demonstrated. The re-hydrated mucus behaved as a semi-permeable layer, allowing the small molecule sodium fluorescein to permeate but severely hindering the passage of positively-charged 168 nm diameter polymeric NPs, as evidenced by the low degree of particle uptake by CFBE41o- cells in the presence of mucus. Hence, this model combines the excellent epithelial barrier properties of CFBE41o- cells with the option to implement an additional mucus barrier. Moreover, the relatively short culture time needed to achieve a tight epithelial monolayer allows having a cell line-based mucus-containing *in vitro* model ready for experiments within a timeframe of less than a week. The model may therefore prove a useful tool to study inhalation pharmaceuticals targeted to the bronchial mucosa and in particular to address the role of mucus in this context.

Acknowledgements

The authors would like to acknowledge the excellent technical assistance of Dr Chiara de Rossi, Petra König, Peter Meiers, and Jana Westhues. This work was partly supported by the Marie Curie Initial Training Network PathChooser (PITNGA-2013-608373).

References

[1] B.K. Rubin, Physiology of airway mucus clearance, Respir. Care 47 (2002) 761–768.
[2] C.A. Ruge, J. Kirch, C.M. Lehr, Pulmonary drug delivery: from generating aerosols to overcoming biological barriers-therapeutic possibilities and technological challenges, Lancet Respir. Med. 1 (2013) 402–413.
[3] B.S. Schuster, J.S. Suk, G.F. Woodworth, J. Hanes, Nanoparticle diffusion in respiratory mucus from humans without lung disease, Biomaterials 34 (2013) 3439–3446.
[4] M.B. Antunes, N.A. Cohen, Mucociliary clearance – a critical upper airway host defense mechanism and methods of assessment, Curr. Opin. Allergy Clin. Immunol. 7 (2007) 5–10.
[5] B. Button, L.H. Cai, C. Ehre, M. Kesimer, D.B. Hill, J.K. Sheehan, R.C. Boucher, M. Rubinstein, A periciliary brush promotes the lung health by separating the mucus layer from airway epithelia, Science 337 (2012) 937–941.
[6] M.R. Knowles, R.C. Boucher, Mucus clearance as a primary innate defense mechanism for mammalian airways, J. Clin. Invest. 109 (2002) 571–577.
[7] F.L. Ramos, J.S. Krahnke, V. Kim, Clinical issues of mucus accumulation in COPD, Int. J. Chron. Obstruct. Pulmon. Dis. 9 (2014) 139–150.
[8] N.N. Sanders, S.C. De Smedt, E. Van Rompaey, P. Simoens, F. De Baets, J. Demeester, Cystic fibrosis sputum: a barrier to the transport of nanospheres, Am. J. Respir. Crit. Care Med. 162 (2000) 1905–1911.
[9] S. Yuan, M. Hollinger, M.E. Lachowicz-Scroggins, S.C. Kerr, E.M. Dunican, B.M. Daniel, S. Ghosh, S.C. Erzurum, B. Willard, S.L. Hazen, X. Huang, S.D. Carrington, S. Oscarson, J.V. Fahy, Oxidation increases mucin polymer cross-links to stiffen airway mucus gels, Sci. Transl. Med. 7 (2015) 276ra227.
[10] A.L. Innes, S.D. Carrington, D.J. Thornton, S. Kirkham, K. Rousseau, R.H. Dougherty, W.W. Raymond, G.H. Caughey, S.J. Muller, J.V. Fahy, Ex vivo sputum analysis reveals impairment of protease-dependent mucus degradation by plasma proteins in acute asthma, Am. J. Respir. Crit. Care Med. 180 (2009) 203–210.
[11] J.S. Elborn, Cystic fibrosis, Lancet 388 (2016) 2519–2531.
[12] E. Fernandez Fernandez, B. Santos-Carballal, W.M. Weber, F.M. Goycoolea, Chitosan as a non-viral co-transfection system in a cystic fibrosis cell line, Int. J. Pharm. 502 (2016) 1–9.
[13] R.J. Fields, C.J. Cheng, E. Quijano, C. Weller, N. Kristofik, N. Duong, C. Hoimes, M. E. Egan, W.M. Saltzman, Surface modified poly(beta amino ester)-containing nanoparticles for plasmid DNA delivery, J. Contr. Release 164 (2012) 41–48.
[14] N. Bangel-Ruland, K. Tomczak, E. Fernandez Fernandez, G. Leier, B. Leciejewski, C. Rudolph, J. Rosenecker, W.M. Weber, Cystic fibrosis transmembrane conductance regulator-mRNA delivery: a novel alternative for cystic fibrosis gene therapy, J. Gene Med. 15 (2013) 414–426.
[15] C. Ehrhardt, E.M. Collnot, C. Baldes, U. Becker, M. Laue, K.J. Kim, C.M. Lehr, Towards an in vitro model of cystic fibrosis small airway epithelium: characterisation of the human bronchial epithelial cell line CFBE41o, Cell Tissue Res. 323 (2006) 405–415.
[16] M. Kong, P. Maeng, J. Hong, R. Szczesniak, E. Sorscher, W. Sullender, J.P. Clancy, Respiratory syncytial virus infection disrupts monolayer integrity and function in cystic fibrosis airway cells, Viruses 5 (2013) 2260–2271.
[17] H.E. Nilsson, A. Dragomir, L. Lazorova, M. Johannesson, G.M. Roomans, CFTR and tight junctions in cultured bronchial epithelial cells, Exp. Mol. Pathol. 88 (2010) 118–127.
[18] N. Molenda, K. Urbanova, N. Weiser, K. Kusche-Vihrog, D. Gunzel, H. Schillers, Paracellular transport through healthy and cystic fibrosis bronchial epithelial cell lines – do we have a proper model?, PLoS ONE 9 (2014) e100621
[19] C.I. Grainger, L.L. Greenwell, D.J. Lockley, G.P. Martin, B. Forbes, Culture of Calu-3 cells at the air interface provides a representative model of the airway epithelial barrier, Pharm. Res. 23 (2006) 1482–1490.
[20] M. Haghi, P.M. Young, D. Traini, R. Jaiswal, J. Gong, M. Bebawy, Time- and passage-dependent characteristics of a Calu-3 respiratory epithelial cell model, Drug Dev. Ind. Pharm. 36 (2010) 1207–1214.
[21] S. Mura, H. Hillaireau, J. Nicolas, S. Kerdine-Romer, B. Le Droumaguet, C. Delomenie, V. Nicolas, M. Pallardy, N. Tsapis, E. Fattal, Biodegradable nanoparticles meet the bronchial airway barrier: how surface properties affect their interaction with mucus and epithelial cells, Biomacromolecules 12 (2011) 4136–4143.
[22] X. Murgia, P. Pawelzyk, U.F. Schaefer, C. Wagner, N. Willenbacher, C.M. Lehr, Size-limited penetration of nanoparticles into porcine respiratory mucus after aerosol deposition, Biomacromolecules 17 (2016) 1536–1542.
[23] J. Kirch, A. Schneider, B. Abou, A. Hopf, U.F. Schaefer, M. Schneider, C. Schall, C. Wagner, C.M. Lehr, Optical tweezers reveal relationship between microstructure and nanoparticle penetration of pulmonary mucus, Proc. Natl. Acad. Sci. USA 109 (2012) 18355–18360.
[24] J.S. Patton, J.D. Brain, L.A. Davies, J. Fiegel, M. Gumbleton, K.J. Kim, M. Sakagami, R. Vanbever, C. Ehrhardt, The particle has landed – characterizing the fate of inhaled pharmaceuticals, J. Aerosol. Med. Pulm. Drug Deliv. 23 (Suppl 2) (2010) S71–87.
[25] H.H. Sigurdsson, J. Kirch, C.M. Lehr, Mucus as a barrier to lipophilic drugs, Int. J. Pharm. 453 (2013) 56–64.
[26] X. Yang, K. Forier, L. Steukers, S. Van Vlierberghe, P. Dubruel, K. Braeckmans, S. Glorieux, H.J. Nauwynck, Immobilization of pseudorabies virus in porcine tracheal respiratory mucus revealed by single particle tracking, PLoS ONE 7 (2012) e51054.

[27] N. Csaba, M. Koping-Hoggard, M.J. Alonso, Ionically crosslinked chitosan/tripolyphosphate nanoparticles for oligonucleotide and plasmid DNA delivery, Int. J. Pharm. 382 (2009) 205–214.
[28] H.Q. Mao, K. Roy, V.L. Troung-Le, K.A. Janes, K.Y. Lin, Y. Wang, J.T. August, K.W. Leong, Chitosan-DNA nanoparticles as gene carriers: synthesis, characterization and transfection efficiency, J. Contr. Release 70 (2001) 399–421.
[29] M. Thomas, A.M. Klibanov, Non-viral gene therapy: polycation-mediated DNA delivery, Appl. Microbiol. Biotechnol. 62 (2003) 27–34.
[30] B.K. Rubin, B. Finegan, O. Ramirez, M. King, General anesthesia does not alter the viscoelastic or transport properties of human respiratory mucus, Chest 98 (1990) 101–104.
[31] B.K. Rubin, O. Ramirez, J.G. Zayas, B. Finegan, M. King, Collection and analysis of respiratory mucus from subjects without lung disease, Am. Rev. Respir. Dis. 141 (1990) 1040–1043.
[32] A. Mittal, K. Schulze, T. Ebensen, S. Weissmann, S. Hansen, C.M. Lehr, C.A. Guzman, Efficient nanoparticle-mediated needle-free transcutaneous vaccination via hair follicles requires adjuvantation, Nanomedicine 11 (2015) 147–154.
[33] N. Nafee, M. Schneider, U.F. Schaefer, C.M. Lehr, Relevance of the colloidal stability of chitosan/PLGA nanoparticles on their cytotoxicity profile, Int. J. Pharm. 381 (2009) 130–139.
[34] J.L. Sporty, L. Horalkova, C. Ehrhardt, In vitro cell culture models for the assessment of pulmonary drug disposition, Expert Opin. Drug Metab. Toxicol. 4 (2008) 333–345.
[35] M.E. Kreft, U.D. Jerman, E. Lasic, T. Lanisnik Rizner, N. Hevir-Kene, L. Peternel, K. Kristan, The characterization of the human nasal epithelial cell line RPMI 2650 under different culture conditions and their optimization for an appropriate in vitro nasal model, Pharm. Res. 32 (2015) 665–679.
[36] S. Loman, J. Radl, H.M. Jansen, T.A. Out, R. Lutter, Vectorial transcytosis of dimeric IgA by the Calu-3 human lung epithelial cell line: upregulation by IFN-gamma, Am. J. Physiol. 272 (1997) L951–958.
[37] C. Ehrhardt, J. Fiegel, S. Fuchs, R. Abu-Dahab, U.F. Schaefer, J. Hanes, C.M. Lehr, Drug absorption by the respiratory mucosa: cell culture models and particulate drug carriers, J. Aerosol. Med. 15 (2002) 131–139.
[38] J.G. Zayas, G.C. Man, M. King, Tracheal mucus rheology in patients undergoing diagnostic bronchoscopy. Interrelations with smoking and cancer, Am. Rev. Respir. Dis. 141 (1990) 1107–1113.
[39] M. Boegh, S.G. Baldursdottir, A. Mullertz, H.M. Nielsen, Property profiling of biosimilar mucus in a novel mucus-containing in vitro model for assessment of intestinal drug absorption, Eur. J. Pharm. Biopharm. 87 (2014) 227–235.
[40] B.J. Teubl, M. Absenger, E. Frohlich, G. Leitinger, A. Zimmer, E. Roblegg, The oral cavity as a biological barrier system: design of an advanced buccal in vitro permeability model, Eur. J. Pharm. Biopharm. 84 (2013) 386–393.
[41] A. Kuehn, S. Kletting, C. de Souza Carvalho-Wodarz, U. Repnik, G. Griffiths, U. Fischer, E. Meese, H. Huwer, D. Wirth, T. May, N. Schneider-Daum, C.M. Lehr, Human alveolar epithelial cells expressing tight junctions to model the air-blood barrier, Altex 33 (2016) 251–260.
[42] M.I. Hermanns, R.E. Unger, K. Kehe, K. Peters, C.J. Kirkpatrick, Lung epithelial cell lines in coculture with human pulmonary microvascular endothelial cells: development of an alveolo-capillary barrier in vitro, Lab. Invest. 84 (2004) 736–752.
[43] A. Ludwig, The use of mucoadhesive polymers in ocular drug delivery, Adv. Drug Deliv. Rev. 57 (2005) 1595–1639.
[44] S.K. Lai, Y.Y. Wang, J. Hanes, Mucus-penetrating nanoparticles for drug and gene delivery to mucosal tissues, Adv. Drug Deliv. Rev. 61 (2009) 158–171.
[45] A.J. Mahiny, A. Dewerth, L.E. Mays, M. Alkhaled, B. Mothes, E. Malaeksefat, B. Loretz, J. Rottenberger, D.M. Brosch, P. Reautschnig, P. Surapolchai, F. Zeyer, A. Schams, M. Carevic, M. Bakele, M. Griese, M. Schwab, B. Nurnberg, S. Beer-Hammer, R. Handgretinger, D. Hartl, C.M. Lehr, M.S. Kormann, In vivo genome editing using nuclease-encoding mRNA corrects SP-B deficiency, Nat. Biotechnol. 33 (2015) 584–586.
[46] M.N. Ravi Kumar, U. Bakowsky, C.M. Lehr, Preparation and characterization of cationic PLGA nanospheres as DNA carriers, Biomaterials 25 (2004) 1771–1777.
[47] J. Beisner, M. Dong, S. Taetz, N. Nafee, E.U. Griese, U. Schaefer, C.M. Lehr, U. Klotz, T.E. Murdter, Nanoparticle mediated delivery of 2'-O-methyl-RNA leads to efficient telomerase inhibition and telomere shortening in human lung cancer cells, Lung Cancer 68 (2010) 346–354.
[48] S. Dhawan, A.K. Singla, V.R. Sinha, Evaluation of mucoadhesive properties of chitosan microspheres prepared by different methods, AAPS PharmSciTech 5 (2004) e67.

4.4 Human airway mucus alters the susceptibility of P. aeruginosa biofilms to tobramycin but not colistin

Xabier Murgia[1,2*], Laura Müller[3*], Lorenz Siebenbürger[4], Carsten Boerger[4], Konrad Schwarzkopf[5], Katherina Sewald[3], Susanne Häussler[6], Armin Braun[3], Claus-Michael Lehr[1,4,7], Marius Hittinger[4], Sabine Wronski[3]

[1]Helmholtz Institute for Pharmaceutical Research (HIPS), Helmholtz Centre for Infection Research, Universitätscampus E8.1, 66123 Saarbrücken, Germany

[2]Korea Institute of Science and Technology, KIST Europe, Campus E7.1, 66123 Saarbrücken, Germany

[3]Fraunhofer Institute for Toxicology and Experimental Medicine ITEM, Biomedical Research in Endstage and Obstructive Lung Disease Hannover (BREATH), Member of the German Centre for Lung Research (DZL), Member of the REBIRTH Cluster of Excellence, Nikolai-Fuchs-Straße 1, 30625 Hannover, Germany

[4]PharmBioTec GmbH, Science Park 1, 66123 Saarbrücken, Germany

[5]Department of Anesthesia and Intensive Care, Klinikum Saarbrücken, Winterberg 1, 66119 Saarbrücken, Germany

[6]Helmholtz Institute for Infection Research, Inhoffenstraße 7, 38124 Braunschweig, Germany; TWINCORE, Centre for Experimental and Clinical Infection Research, Feodor-Lynen-Straße 7, 30625 Hannover, Germany

[7]Department of Pharmacy, Saarland University, Campus, 66123 Saarbrücken, Germany

**Equal contribution*

Accepted 5 July 2018

Journal of Antimicrobial Chemotherapy, 2018, available online

DOI: 10.1093/jac/dky241

J Antimicrob Chemother
doi:10.1093/jac/dky241

Journal of Antimicrobial Chemotherapy

Human airway mucus alters susceptibility of *Pseudomonas aeruginosa* biofilms to tobramycin, but not colistin

Laura Müller[1†], Xabier Murgia[2,3†], Lorenz Siebenbürger[4], Carsten Börger[4], Konrad Schwarzkopf[5], Katherina Sewald[1], Susanne Häussler[6,7], Armin Braun[1], Claus-Michael Lehr[2,4,8], Marius Hittinger[4] and Sabine Wronski[1*]

[1]*Fraunhofer Institute for Toxicology and Experimental Medicine (Fraunhofer ITEM), Biomedical Research in Endstage and Obstructive Lung Disease Hannover (BREATH), Member of the German Centre for Lung Research (DZL), Member of the REBIRTH Cluster of Excellence, Nikolai-Fuchs-Straße 1, 30625 Hannover, Germany;* [2]*Helmholtz Institute for Pharmaceutical Research (HIPS), Helmholtz Centre for Infection Research, Universitätscampus E8.1, 66123 Saarbrücken, Germany;* [3]*Korea Institute of Science and Technology, KIST Europe, Campus E7.1, 66123 Saarbrücken, Germany;* [4]*PharmBioTec GmbH, Science Park 1, 66123 Saarbrücken, Germany;* [5]*Department of Anaesthesia and Intensive Care, Klinikum Saarbrücken, Winterberg 1, 66119 Saarbrücken, Germany;* [6]*Helmholtz Institute for Infection Research, Inhoffenstraße 7, 38124 Braunschweig, Germany;* [7]*TWINCORE, Centre for Experimental and Clinical Infection Research, Feodor-Lynen-Straße 7, 30625 Hannover, Germany;* [8]*Department of Pharmacy, Saarland University, Campus, 66123 Saarbrücken, Germany*

*Corresponding author. Tel: +49-511-5350-444; Fax: +49-511-5350-155; E-mail: sabine.wronski@item.fraunhofer.de
†Contributed equally.

Received 23 February 2018; returned 27 March 2018; revised 9 May 2018; accepted 26 May 2018

Objectives: In the context of cystic fibrosis, *Pseudomonas aeruginosa* biofilms often develop in the vicinity of airway mucus, which acts as a protective physical barrier to inhaled matter. However, mucus can also adsorb small drug molecules administered as aerosols, including antibiotics, thereby reducing their bioavailability. The efficacy of antibiotics is typically assessed by determining the MIC using *in vitro* assays. This widespread technique, however, does not consider either bacterial biofilm formation or the influence of mucus, both of which may act as diffusion barriers, potentially limiting antibiotic efficacy.

Methods: We grew *P. aeruginosa* biofilms in the presence or absence of human tracheal mucus and tested their susceptibility to tobramycin and colistin.

Results: A significant reduction of tobramycin efficacy was observed when *P. aeruginosa* biofilms were grown in the presence of mucus compared with those grown in the absence of mucus. Diffusion of tobramycin through mucus was reduced; however, this reduction was more pronounced in biofilm/mucus mixtures, suggesting that biofilms in the presence of mucus respond differently to antibiotic treatment. In contrast, the influence of mucus on colistin efficacy was almost negligible and no differences in mucus permeability were observed.

Conclusions: These findings underline the important role of mucus in the efficacy of anti-infective drugs.

Introduction

Airway epithelium is covered by a thin mucus layer, enabling continuous clearance of inhaled pathogens, pollutants and other environmental particles. This process is achieved by constant mucus secretion into the airway lumen and the coordinated beating of epithelial cell cilia.[1,2] Unfortunately, in diseases such as COPD, asthma or cystic fibrosis (CF) the mucociliary machinery is significantly compromised,[3–5] reducing the mucus clearance rate and providing an optimal environment for bacterial infections.[6] In CF patients, a congenital mutation of the *CFTR* gene leads to abnormal expression of the CFTR chloride channel, resulting in an overall water imbalance of the airways that ultimately leads to increased mucus viscosity and recurrent infections.[7,8]

Pseudomonas aeruginosa is amongst the most prevalent pathogens found in chronically infected CF patients. The vast majority of CF patients are treated with antibiotics from early childhood. Inhaled tobramycin therapy in particular is relatively effective in early stages of *P. aeruginosa* infection and has increased the lifespan of CF patients.[7] Besides tobramycin, common inhaled antibiotics for the management of CF infections include colistin, levofloxacin and aztreonam.[9] Upon chronicity of the infection, eradication is difficult to achieve[10] due to the different mechanisms used by *P. aeruginosa* to evade both antibiotic

treatment and the host's defence. Therefore, the actual susceptibility of *P. aeruginosa* to antibiotic treatment in terms of antibiotic concentration can differ enormously from the MIC, as determined in routine *in vitro* tests. It is noteworthy that these assays are usually performed using planktonic bacteria, rather than bacterial biofilms, and do not consider the presence of mucus either.

In CF lungs, *P. aeruginosa* forms structured bacterial communities, referred to as biofilms.[11] These communities consist of bacterial cells surrounded by a self-produced extracellular matrix, known to protect bacteria from the host's immune system and from antibacterial treatment.[12] In their native airway environment, *P. aeruginosa* biofilms are often embedded in mucus, which represents an additional barrier to the diffusion of inhaled drugs.[13,14] Mucus is a hydrogel composed mainly of water and mucin glycoproteins. Mucins are continuously secreted into the airway lumen, where they form a cross-linked, mesh-like structure with a tight pore size that impedes penetration of inhaled coarse particles.[13] Moreover, the sugar side chains of these mucins are mostly negatively charged at physiological pH and can limit the diffusion of small molecules due to electrostatic interactions.[15] This might hold true in particular for tobramycin and colistin, which are polycationic antibiotics[9] and can thus undergo electrostatic interactions with these polyanionic hydrogel matrices. Therefore, the challenge for an effective antibiotic therapy is to overcome not only the extracellular matrix of the biofilms but also the mucus layer. These barriers are barely addressed in the currently available *in vitro* models used during pre-clinical development stages of anti-infective drug candidates.

The aim of our study was to investigate the impact of airway mucus on *P. aeruginosa* biofilm susceptibility to antibiotic treatment. For this purpose, *P. aeruginosa* biofilms were grown *in vitro* in the presence or absence of human tracheal mucus and the antibacterial efficacy of colistin and tobramycin under these more *in vivo*-like conditions was investigated.

Materials and methods

An expanded version of the Materials and methods section is available as Supplementary data at *JAC* Online.

Bacterial strains and antibiotics

PAO1 (ATCC 15692) and GFP-PAO1 (Thomas Bjarnsholt, Copenhagen) were used. Tobramycin sulphate salt and colistin sulphate salt were obtained from Sigma–Aldrich, Munich, Germany.

MIC assay

MIC assays were performed according to CLSI guidelines[15a] with antibiotic concentrations ranging from 0.125 to 512 mg/L.

Ethics

Collection and preparation of human mucus was approved by the Ethics Commission of The Chamber of Medicine Doctors of the Saarland (file number 19/15). Informed consent was obtained from all patients.

Extraction and preparation of human mucus

Undiluted human tracheal mucus samples were collected with the endotracheal tube method.[16–18] Mucus samples were collected by centrifugation and stored at −20°C until further use. Samples were freeze-dried and weighed before and after the process to determine the amount of sublimated water. Before its use, the freeze-dried mucus was exposed to UV radiation for 1 h and re-hydrated with PBS using the same volume that had previously been sublimated. With this re-suspension protocol, an elastic-dominant, bacteria-free mucus hydrogel was achieved.[19]

Biofilm cultivation and susceptibility testing

In short, 96-well plates were inoculated with 100 µL of bacterial suspension and 100 µL of mucus or PBS and samples were cultured under static conditions with 100% humidity, 37°C and 0% CO_2 for 24 h. Thereafter, samples were treated with 10 µL of tobramycin or colistin with a final concentration of 100, 300 or 900 mg/L representing 100×, 300× and 900× MIC, respectively. Efficacy was assessed according to the viable bacterial load determined by dilution plating and counting of cfu.

Tobramycin activity after pre-incubation in mucus

A volume of 100 µL of mucus was mixed with 10 µL of tobramycin suspension, resulting in a final concentration of 300 mg/L in the well. After 24 h of incubation, tobramycin-containing mucus was inoculated with 100 µL of PAO1 (2×10^7/mL), leading to a final tobramycin concentration of 150 mg/L. As positive treatment control 150 mg/L tobramycin with vehicle and a negative control without tobramycin were used. After further incubation for 24 h at 37°C, treatment efficacy was analysed visually for turbidity and by dilution plating and determination of cfu.

Laser scanning confocal microscopy

Briefly, GFP-tagged PAO1 biofilms were cultured in 96-well plates (µ-plate 96 well, ibidi, Martinsried, Germany) as described above. Imaging was performed using an LSM 510 Meta confocal microscope (Zeiss, Jena, Germany). The 488 nm argon laser line was used for excitation and the BP 505–530 filter for emission. Z-stacks were performed with intervals of 0.5 µm and a range of 30 µm using the Plan-Neofluar 40×/1.3 oil DIC objective. Images were processed using the imaging software Imaris version 7.6.5, including its associated surpass module (Bitplane Scientific Software, Zurich, Switzerland). The surface of all fluorescent signals above a determined threshold was computed as bacterial biomass. The obtained values were displayed as the surface area (in μm^2) covered with a GFP-positive signal.

Tobramycin and colistin diffusion studies

Briefly, experiments were performed using Transwell® membranes (Corning, Durham, NC, USA) with a surface of 0.33 cm^2 and a pore size of 4 µm. Biofilms in the presence or absence of mucus or sham-infected mucus samples with a total volume of 100 µL were cultured on the membrane of the Transwell® inserts overnight. Inserts were placed into the companion plates and 100 µL of 600 mg/L tobramycin or colistin solution in PBS was then added to the apical compartment. The basolateral compartment was filled with 600 µL of PBS. A volume of 50 µL was sampled from the basolateral compartment after 15, 30, 60, 90, 120 and 3600 min.

HPLC measurement

Briefly, HPLC and MS/MS methods similar to those described in the literature for tobramycin[20] and colistin[21] were applied with minor modifications.

Statistical analysis

Three independent runs were performed for each experiment with technical duplicates or technical triplicates (diffusion studies). All values are given as mean ± SD or mean ± SEM (diffusion studies). Statistical analysis

was performed with the GraphPad Prism software (GraphPad 7 Software, Inc., USA) using the Mann–Whitney *U*-test. Differences were considered statistically significant at the level of $P < 0.05$.

Results

Mucus characterization

Eighty-five independent mucus samples were used in this study. The mean age of the patients was 56.6±15.7 years; 54% were male and 46% female, and 24 out of 85 were smokers (28%). Individual samples were combined to produce 10 independent mucus batches. The water content of the mucus samples was 95%±1%. Mucus samples obtained with the method described above showed different mucin concentrations (8%–22% of the solid content), pH values between 7 and 8.5, and a DNA content of <1%.[19]

Biofilm susceptibility to antibiotic treatment in the presence of human mucus

P. aeruginosa biofilms exhibited an increased tolerance to both tobramycin and colistin (Figure 1) as compared with the MIC values for planktonic bacteria, which were 0.5–1 and 1 mg/L for tobramycin and colistin, respectively, in good agreement with the values previously reported in the literature.[22,23] For instance, full eradication of the biofilms grown in PBS required a concentration 900 times higher than the MIC, irrespective of the antibiotic used. In biofilms grown in a mucus environment, a concentration-dependent decrease in viable bacterial load could still be seen for both antibiotics; however, tobramycin efficacy was significantly impaired in the presence of mucus, leading to a shift of the IC_{50} value from 100 mg/L without mucus to >900 mg/L with mucus. Thus, killing of biofilm-grown bacteria was not achieved with tobramycin under normal culture conditions in the presence of mucus.

In contrast, colistin treatment efficacy was not affected by the mucus environment, with IC_{50} values of 170 and 190 mg/L for biofilms grown in PBS and in mucus, respectively. Complete bacterial killing by colistin could be observed with treatment concentrations of 300 and 900 mg/L, respectively.

Tobramycin activity in human mucus

In the biofilm susceptibility assay, treatment with tobramycin, but not colistin, was significantly less effective in the presence of mucus. To investigate whether this effect was due to inactivation of tobramycin by mucus, tobramycin efficacy was tested after pre-incubation in mucus. In these experiments, tobramycin pre-incubated in mucus exhibited bactericidal activity against planktonic bacteria similar to that of tobramycin alone, indicating maintained activity (Figure 2). In addition, reversibility of the antibiotic tolerance to tobramycin observed in the presence of mucus was investigated by performing an MIC assay subsequent to the biofilm susceptibility assays. For this purpose, we incubated PAO1 bacteria extracted from 48-h-old biofilms formed in mucus in order to determine whether the decreased susceptibility to antibiotic treatment was persistent. The MIC for PAO1 re-isolated from biofilms previously cultured in the presence of mucus was 0.5–2.5 mg/L and thus in the same range as the control MIC (0.5–1 mg/L), indicating that susceptibility was restored and the mucus environment did not induce genetic resistance of PAO1 to tobramycin.

Biofilm structure in human mucus environment

Confocal images of GFP-PAO1 were taken to visualize potential differences in terms of biofilm structure, bacterial density and total biomass induced by the mucus environment. An increased amount of bacterial GFP signal was observed in the presence of mucus (Figure 3a and d) compared with biofilms grown in the absence of mucus (Figure 3b and d), which was not due to unspecific autofluorescence of the mucus itself (Figure 3c). These observations also correlated with the cfu counts of these samples (Figure 3e). Both methods revealed a higher bacterial count for biofilms grown in the presence of human mucus.

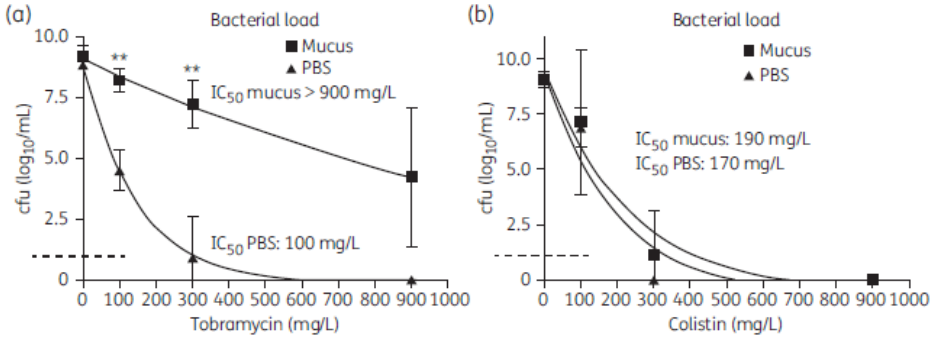

Figure 1. Biofilm susceptibility to antibiotic treatment. PAO1 biofilms grown in mucus or PBS for 24 h were treated with tobramycin (a) or colistin (b). After 24 h of incubation, efficacy was assessed by determination of cfu. The cfu counts are depicted logarithmically as regression curves showing the mean ± SD for $n = 3$ experiments, each with technical duplicates. A double asterisk indicates statistical significance at $P < 0.01$, according to the Mann–Whitney *U*-test, for comparison of mucus versus PBS at the individual concentrations. The broken line indicates the detection limit.

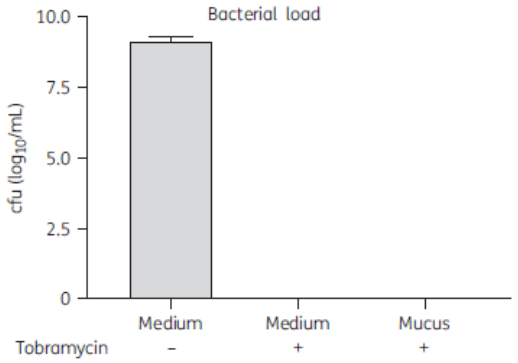

Figure 2. Tobramycin activity in human mucus. Mucus pre-incubated with tobramycin was inoculated with PAO1 and incubated for 24 h. Medium only and medium containing the same concentration of tobramycin were used as controls. Bar graphs show the mean + SD for $n = 2$ samples, each with technical duplicates.

Antibiotic diffusion through human mucus

Diffusion studies revealed significantly retarded and decreased diffusion of tobramycin through PAO1 biofilm formed within mucus (Figure 4a) compared with diffusion through pure mucus or biofilm formed in PBS. Diffusion through PBS only was used as control indicating 'free diffusion'. In all groups, fast diffusion was observed within the first 2 h, but diffusion through biofilm in mucus was significantly delayed. Equally in all groups, tobramycin diffusion decelerated over time until reaching saturation; however, the final cumulative masses varied, with mucus + PAO1 reaching the lowest value (Figure 4a), but they were near the theoretical maximal mass of 45 μg for both antibiotics. Table 1 shows the maximal cumulative mass (Y_{max}) of tobramycin, which was in a similar range for all experimental conditions. The half-life ($t_{1/2}$) of tobramycin was slightly increased for mucus only and markedly increased for biofilm in mucus (Table 1). Colistin diffusion was comparable for all groups (Figure 4b). No phase exponential association fit was performed for colistin, as standard deviations were too high. These findings are in agreement with the observed cfu reduction following antibiotic treatment.

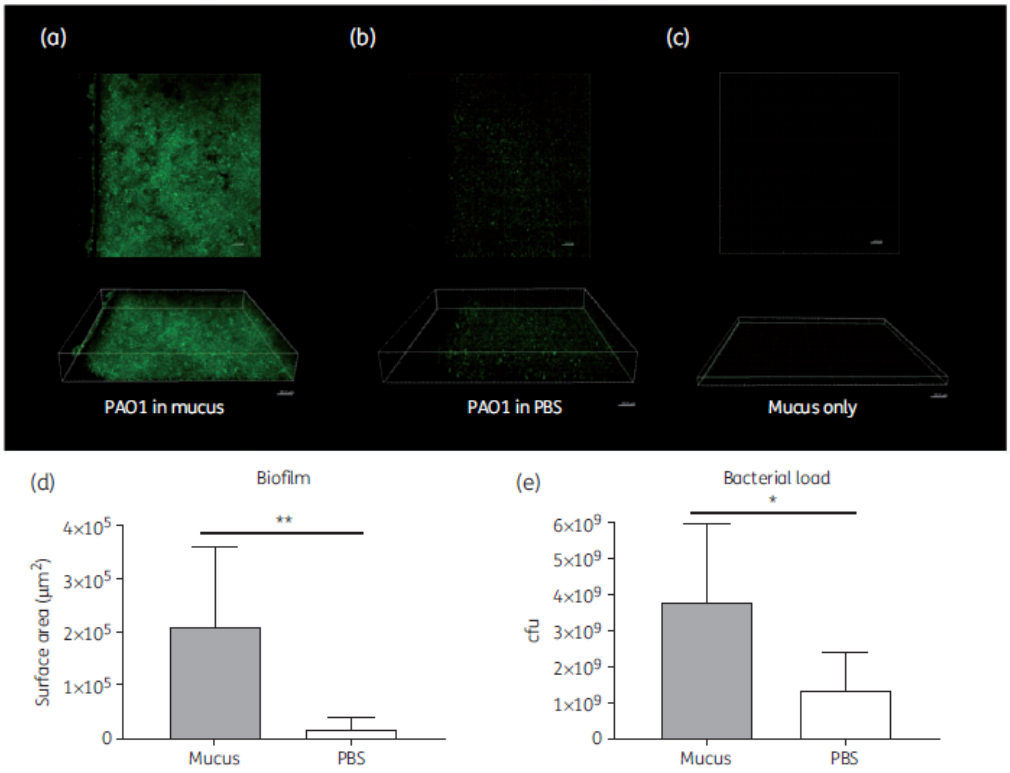

Figure 3. Biofilm structure and bacterial count in mucus. GFP-PAO1 biofilms were grown in mucus (a) or PBS (b) for 2 days and imaged by confocal microscopy. Uninfected mucus was imaged as a control (c). Fluorescence signals were quantified using Imaris software (d) and cfu were determined (e). Bar graphs show the mean + SD for $n = 3$ samples, each with technical duplicates. A non-parametric *t*-test (Mann–Whitney *U*-test) was performed for statistical analyses. *$P < 0.05$. **$P < 0.01$. Scale bars represent 20 μm.

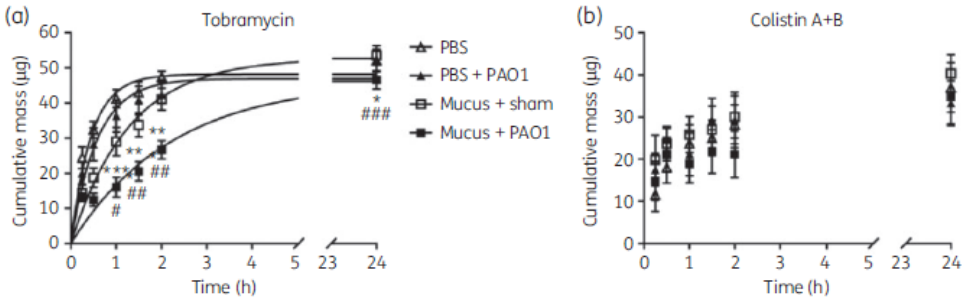

Figure 4. Tobramycin and colistin diffusion through biofilm formed in mucus. PAO1 biofilm cultured in mucus or PBS in the apical compartment of a Transwell® was treated with tobramycin or colistin. PBS only or sham-infected mucus was used as a control. Diffusion of the antibiotic was assessed by HPLC and is depicted as cumulative mass. Scatter plots show the mean ± SEM for $n = 3$ experiments, each with triplicates. A single asterisk, a double asterisk and a triple asterisk indicate statistical significance at $P < 0.05$, $P < 0.01$ and $P < 0.001$, respectively, according to the Mann–Whitney *U*-test, for comparison of biofilm in mucus with PBS. A single hash, a double hash and a triple hash indicate statistical significance at $P < 0.05$, $P < 0.01$ and $P < 0.001$, respectively, according to the Mann–Whitney *U*-test, for comparison of biofilm in mucus with mucus only. A one-phase exponential association fit was performed for tobramycin diffusion using GraphPad Prism 7, described by the equation $Y = Y_{max} \times (1 - e^{-k \times x})$.

Table 1. Y_{max} and $t_{1/2}$ of tobramycin following diffusion through biofilms in mucus

Tobramycin diffusion	PBS	PBS + PAO1	Mucus + sham	Mucus + PAO1
Y_{max} (µg)	44.75–52.13	41.11–54.28	46.65–58.94	41–51.48
$t_{1/2}$ (h)	0.22–0.43	0.24–0.66	0.65–1.16	1.19–1.98

A one-phase exponential association fit was performed using GraphPad Prism 7, described by the equation $Y = Y_{max} \times (1 - e^{-k \times x})$. Y_{max} (µg) and $t_{1/2}$ (h) of tobramycin were calculated for each group. The table shows the 95% CI for $n = 3$ transports, each with triplicates.

Discussion

Chronic airway infections with *P. aeruginosa* are a major cause of morbidity, especially among patients suffering from CF. Antibiotic treatment leads to improved lung function and life quality,[24] although permanent bacterial eradication is often not accomplished due to a variety of adaptation mechanisms of the pathogen. Biofilm formation is one of the most crucial resistance mechanisms used by many bacterial species. Different *in vitro* test systems, including pure bacterial cultures,[25] co-cultures of bacteria and epithelial cells,[26] and bacteria grown in artificial sputum medium,[27] have been used to investigate bacterial biofilm formation and the development of increased antibiotic tolerance. Bjarnsholt *et al.*[28] examined explanted CF lung and observed bacterial biofilm to be embedded in mucus with no direct contact with the airway epithelium, which was also found by Worlitzsch *et al.*[29] On the contrary, Crabbé *et al.*[30] co-cultured epithelial cells with *P. aeruginosa* and observed increased antibiotic efficacy in the presence of airway cells, suggesting that they might improve antibiotic efficacy. In the chronically infected CF lung, the viscous mucus of the airways is highly colonized with bacterial biofilms.[31] Biofilms as well as airway mucus are well known to act as a barrier to antibiotics.[13,14,32] For instance, the alginate found in the extracellular matrix of bacterial biofilms can adsorb antibiotic molecules,[32,33] and the negatively charged mucin glycoproteins offer multiple sites for electrostatic interactions,[15] in particular for polycationic antibiotics such as tobramycin and colistin.[34,35] So far, the ability to reduce the diffusion of antibiotic molecules has been shown separately for these individual elements. In CF airways, however, biofilms are formed within the respiratory mucus. Consequently, one could expect further reduction of antibiotic bioavailability due to the combined effect of the biofilm's extracellular matrix and mucus. In the present study, we investigated the susceptibility of *P. aeruginosa* biofilms to two polycationic antibiotics, tobramycin and colistin, in the presence or absence of human mucus.

Interestingly, biofilms grown in the presence of airway mucus led to a significant loss of efficacy for tobramycin, but not colistin, indicating that the mucus environment affects antibiotic tolerance of *P. aeruginosa* biofilms.

Even at tobramycin concentrations as high as 900 mg/L, full eradication of bacteria could not be achieved in our static *in vitro* model composed of *P. aeruginosa* biofilms and mucus. The tobramycin concentrations used in the present study correlate well with the maximum sputum concentrations found in CF patients, which have been reported to range from 486 to 695 mg/L.[9] The reported maximum sputum concentrations for colistin were around 40 mg/L, 2.5-fold lower than the lowest concentration used in this study, which was associated with a reduction of the cfu count, but was far from achieving full eradication of *P. aeruginosa* biofilms, either in the absence or in the presence of mucus.

The observed loss of efficacy could be due to a strong interaction between the polycationic antibiotics and the components of the biofilm and mucus,[34–36] which may have reduced bioavailability of the antibiotics. Hunt *et al.*[35] demonstrated that the diffusion of tobramycin through dialysate bags containing CF sputum was reduced due to tobramycin binding to sputum components. The reduced amount of unbound tobramycin might then lead to insufficient treatment. Similarly, Huang *et al.*[34] measured the diffusion of colistin through dialysate bags containing porcine mucins. They concluded that colistin binds to porcine mucins and thereby

loses its activity.[34] To address this issue, tobramycin was pre-incubated with human tracheal mucus for 24 h and its efficacy against planktonic *P. aeruginosa* was subsequently assessed. In this setting, tobramycin maintained its efficacy, implying that tobramycin was at least partly unbound and not inactivated by mucus. Moreover, *P. aeruginosa* re-isolated from 48-h-old biofilms was not associated with an increased MIC, indicating that no genetic resistance mechanisms were responsible for the decreased susceptibility to tobramycin. Instead, adaptive resistance mechanisms such as increased efflux pump activity, permeability changes due to alterations of lipopolysaccharides or porins, or expression of biofilm-specific genes might have resulted in increased bacterial tolerance.[9,37] Considering the mechanism of action of tobramycin (intracellular, binding to ribosomes, acting on metabolically active bacteria)[38] and colistin (extracellular, bacterial cell wall, acting independently of metabolism),[39] an increased efflux pump activity together with alterations in the outer membrane porins would impact the efficacy of tobramycin to a larger extent than that of colistin. Pamp *et al.*[40] found that the metabolic status of bacteria differs within a biofilm, leading to different antibiotic susceptibilities. Metabolically inactive bacteria might be less susceptible to tobramycin, but more susceptible to colistin.

The permeation kinetics studies of tobramycin and colistin through human tracheal mucus did not show a significant effect on the net permeation of the antibiotics. Compared with its permeation through the bare Transwell® membrane, tobramycin was just slightly, but not significantly, hindered by tracheal mucus alone, whereas no effect at all on colistin permeation through mucus was observed compared with the bare membrane. Although the experimental design applied in this study did not cover the kinetics of the first 15 min, the data suggest that tobramycin and colistin molecules are small enough to diffuse through the mucus pores and that the electrostatic interactions taking place between the polycationic antibiotics and mucins are transient and most probably are overcome fast enough not to be detected within the time span of our experiment. In contrast, the biofilm/mucus mixtures had a significant impact on the diffusion of tobramycin compared with its diffusion through mucus or biofilms alone. These results indicate that *P. aeruginosa* biofilms formed within human mucus might have a different structure that may further impact their susceptibility to tobramycin. Cattoir *et al.*[41] found that mucus controls the expression of virulence factors and influences several metabolic pathways after culturing *P. aeruginosa* strains originating from CF lungs in the presence or absence of mucus. *P. aeruginosa* has also been shown to adhere to human respiratory mucins. Vishwanath and Ramphal[42] assumed that this ability might facilitate mucus colonization. Landry *et al.*[43] suggested that human mucins influence both biofilm structure and antibiotic susceptibility. They detected that *P. aeruginosa* forms flat, homogeneous biofilms on a smooth surface like glass, but rather inhomogeneous biofilms in contact with mucins, as interactions with mucins lead to immobilization, resulting in enhanced biofilm formation and antibiotic resistance. In the present study, *P. aeruginosa* biofilms were grown in resuspended human tracheal mucus that previously had been freeze-dried. Upon resuspension, mucus keeps its native viscoelastic properties,[19] typical of cross-linked polymers. Thus, planktonic *P. aeruginosa* inoculated in human tracheal mucus could have been easily immobilized by the strict pore size of the mucin network, which has been reported to range from 100 to 400 nm in CF sputum.[5] The pores within the mucin network might act as *P. aeruginosa*-immobilizing scaffolds, while bacteria can degrade mucus components[44] and use them as nutrients[45] or even incorporate them into their extracellular matrix, leading to a compacted biomass. We observed significantly increased bacterial numbers in the presence of mucus; however, bacterial load did not further increase following 24 h of incubation, probably due to limitation of nutrients. Additionally, we compared bacterial growth in mucus, nutrient-rich LB medium and PBS and detected the highest bacterial numbers in the presence of mucus (Figure S1). Walker *et al.*[46] reported that *P. aeruginosa* uses biopolymers originating from necrotic neutrophils as a scaffold for formation of biofilms, which then display increased antibiotic tolerance.[47] Indeed, after growing *P. aeruginosa* biofilms for 48 h in the presence of mucus, we found a significantly higher amount of biomass compared with biofilms grown in the absence of mucus, which might also account for the reduced efficacy of tobramycin in our *in vitro* setting.

Biofilms are often associated with surfaces; however, it is now known that biofilms in CF lungs are not attached to surfaces, but are embedded in host material such as mucus.[28] Sønderholm *et al.*[48] inoculated agar beads with fluorescent *P. aeruginosa* to mimic the presence of a secondary matrix, suggesting that this affects biofilm physiology and consequent treatment susceptibility. Like Sønderholm *et al.*,[48] we believe that mucus could act as a secondary matrix in our system and probably also in the human lung. Palmer *et al.*[49] inoculated CF sputum with *P. aeruginosa* and observed strong bacterial growth and altered bacterial physiology. They concluded that CF sputum is a perfect bacterial growth medium for *P. aeruginosa* and influences bacterial communication and motility, which play important roles in biofilm formation. These results match well with our results. Based on the composition of CF sputum, Palmer *et al.*[50] developed a synthetic CF sputum medium. Like artificial sputum medium,[27] this preparation is mainly composed of amino acids, salts and some other components found in CF sputum, yielding a relatively low-viscosity fluid with approximately the same mean osmolality as CF sputum. Due to their composition, however, these artificial sputum media normally behave like Newtonian fluids, lacking the intermolecular interactions and covalent cross-links that give airway mucus its viscoelastic characteristic.

P. aeruginosa was found to form small aggregates with an average size ranging from 5 to 100 μm that were embedded in mucus.[28] Formation of aggregates could also be found in an agar bead model.[48] However, in the initial stages of biofilm formation that the timeframe of our experiments was able to cover—in contrast to chronic *P. aeruginosa* infection in severely diseased CF patients—bacteria were found to colonize the human mucus environment rather homogeneously instead of forming small aggregates. A more detailed confocal analysis with higher magnification would yield more information on biofilm structure.

In our system mucus is considered to be a very relevant environmental factor for biofilm formation in CF lungs; however, there are considerable differences between mucus from healthy humans and CF patients. In CF patients, hydration of secretion is impaired; consequently, respiratory mucus is dehydrated, resulting in increased viscosity. The predominant mucins MUC5AC and MUC5B are overproduced in CF lung secretion, triggered by *P. aeruginosa* LPS.[51] Chronic infection with *P. aeruginosa* leads to a

strong immune response with neutrophil granulocytes being the predominant immune cell. Vast amounts of necrotic neutrophils cause an increased DNA content in the mucus, which results in further thickening. These aspects have not been addressed in our system. An alternative method could be the use of CF sputum; however, sputum is an expectorated secretion, which is a mixture of mainly mucus and saliva in contrast to pure mucus directly originating from airway epithelium. Furthermore, we experienced mucus from explanted CF lungs to be highly colonized with different bacterial and fungal species, with high variation between patients. Therefore, we thought mucus from 'healthy' airways to be a valuable tool allowing performance of reproducible experiments.

Conclusions

In summary, a model considering mucus as the natural microenvironment for *P. aeruginosa* biofilms in human lungs has been successfully developed, suggesting that the mucus environment should be considered as a key factor in *in vivo* biofilm formation. Additionally, this might be of high relevance for anti-infective drug development. We noted significantly decreased efficacy of tobramycin, but not of colistin, against biofilms in the presence of human mucus. Biofilm formation in human mucus resulted in a more heterogeneous structure, a higher bacterial load and a significantly impaired transport rate for tobramycin, resulting in decreased tobramycin efficacy. More studies are needed, however, to further investigate the role of the mucus environment in *P. aeruginosa* biofilm formation and delineate the differential effects on antibiotic efficacy.

Acknowledgements

We would like to thank Professor Thomas Bjarnsholt (Department of Immunology and Microbiology, University of Copenhagen, Denmark) for providing us with the GFP-tagged PAO1 strain. We thank Karin Schlemminger [Department of Marketing and Public Relations, Fraunhofer Institute for Toxicology and Experimental Medicine (Fraunhofer ITEM)] for improving the grammar of our manuscript.

Funding

This work was supported by the Fraunhofer Institute for Toxicology and Experimental Medicine (Fraunhofer ITEM), the Helmholtz Institute for Pharmaceutical Research and PharmBioTec GmbH.

Transparency declarations

M. H., L. S., C. B. and C.-M. L. were employees of PharmBioTec GmbH at the time of publication. All other authors: none to declare.

Supplementary data

An expanded version of the Materials and methods section and Figure S1 are available as Supplementary data at *JAC* Online.

References

1 Bansil R, Turner BS. Mucin structure, aggregation, physiological functions and biomedical applications. *Curr Opin Colloid Interface Sci* 2006; **11**: 164–70.

2 Knowles MR, Boucher RC. Mucus clearance as a primary innate defense mechanism for mammalian airways. *J Clin Invest* 2002; **109**: 571–7.

3 Ramos FL, Krahnke JS, Kim V. Clinical issues of mucus accumulation in COPD. *Int J Chron Obstruct Pulmon Dis* 2014; **9**: 139–50.

4 Innes AL, Carrington SD, Thornton DJ *et al.* Ex vivo sputum analysis reveals impairment of protease-dependent mucus degradation by plasma proteins in acute asthma. *Am J Respir Crit Care Med* 2009; **180**: 203–10.

5 Sanders NN, De Smedt SC, Van Rompaey *et al.* Cystic fibrosis sputum: a barrier to the transport of nanospheres. *Am J Respir Crit Care Med* 2000; **162**: 1905–11.

6 Quon BS, Goss CH, Ramsey BW. Inhaled antibiotics for lower airway infections. *Ann Am Thorac Soc* 2014; **11**: 425–34.

7 Elborn JS. Cystic fibrosis. *Lancet* 2017; **388**: 2519–31.

8 Cowley AC, Thornton DJ, Denning DW *et al.* Aspergillosis and the role of mucins in cystic fibrosis. *Pediatr Pulmonol* 2017; **52**: 548–55.

9 Dalhoff A. Pharmacokinetics and pharmacodynamics of aerosolized antibacterial agents in chronically infected cystic fibrosis patients. *Clin Microbiol Rev* 2014; **27**: 753–82.

10 Tramper-Stranders GA, van der Ent CK, Molin S *et al.* Initial *Pseudomonas aeruginosa* infection in patients with cystic fibrosis: characteristics of eradicated and persistent isolates. *Clin Microbiol Infect* 2012; **18**: 567–74.

11 Matsui H, Wagner VE, Hill DB *et al.* A physical linkage between cystic fibrosis airway surface dehydration and *Pseudomonas aeruginosa* biofilms. *Proc Natl Acad Sci USA* 2006; **103**: 18131–6.

12 Bjarnsholt T. The role of bacterial biofilms in chronic infections. *APMIS Suppl* 2013; **121**: 1–51.

13 Murgia X, Loretz B, Hartwig O *et al.* The role of mucus on drug transport and its potential to affect therapeutic outcomes. *Adv Drug Deliv Rev* 2018; **124**: 82–97.

14 Deacon J, Abdelghany SM, Quinn DJ *et al.* Antimicrobial efficacy of tobramycin polymeric nanoparticles for *Pseudomonas aeruginosa* infections in cystic fibrosis: formulation, characterisation and functionalisation with dornase alfa (DNase). *J Control Release* 2015; **198**: 55–61.

15 Lillehoj EP, Kato K, Lu W *et al.* Cellular and molecular biology of airway mucins. *Int Rev Cell Mol Biol* 2013; **303**: 139–202.

15a National Committee for Clinical Laboratory Standards *Methods for Dilution Antimicrobial Susceptibility Tests for Bacteria That Grow Aerobically—Tenth Edition: Approved Standard M7-A10*. NCCLS, Wayne, PA, USA, 2015.

16 Rubin BK, Ramirez O, Zayas JG *et al.* Collection and analysis of respiratory mucus from subjects without lung disease. *Am Rev Respir Dis* 1990; **141**: 1040–3.

17 Vukosavljevic B, Murgia X, Schwarzkopf K *et al.* Tracing molecular and structural changes upon mucolysis with N-acetyl cysteine in human airway mucus. *Int J Pharm* 2017; **533**: 373–6.

18 Schuster BS, Suk JS, Woodworth GF *et al.* Nanoparticle diffusion in respiratory mucus from humans without lung disease. *Biomaterials* 2013; **34**: 3439–46.

19 Murgia X, Yasar H, Carvalho-Wodarz C *et al.* Modelling the bronchial barrier in pulmonary drug delivery: a human bronchial epithelial cell line supplemented with human tracheal mucus. *Eur J Pharm Biopharm* 2017; **118**: 79–88.

20 Shou D, Dong Y, Shen L *et al.* Rapid quantification of tobramycin and vancomycin by UPLC-TQD and application to osteomyelitis patient samples. *J Chromatogr Sci* 2014; **52**: 501–7.

21 Gobin P, Lemaître F, Marchand S *et al.* Assay of colistin and colistin methanesulfonate in plasma and urine by liquid chromatography-tandem mass spectrometry. *Antimicrob Agents Chemother* 2010; **54**: 1941–8.

22 Rees VE, Bulitta JB, Oliver A *et al.* Resistance suppression by high-intensity, short-duration aminoglycoside exposure against hypermutable and non-hypermutable *Pseudomonas aeruginosa*. *J Antimicrob Chemother* 2016; **71**: 3157–67.

23 Lin Y-W, Zhou QT, Cheah S-E *et al.* Pharmacokinetics/pharmacodynamics of pulmonary delivery of colistin against *Pseudomonas aeruginosa* in a mouse lung infection model. *Antimicrob Agents Chemother* 2017; **61**: e02025–16.

24 Waters V, Smyth A. Cystic fibrosis microbiology: advances in antimicrobial therapy. *J Cyst Fibros* 2015; **14**: 551–60.

25 Alipour M, Suntres ZE, Omri A. Importance of DNase and alginate lyase for enhancing free and liposome encapsulated aminoglycoside activity against *Pseudomonas aeruginosa*. *J Antimicrob Chemother* 2009; **64**: 317–25.

26 Hawdon NA, Aval PS, Barnes RJ *et al.* Cellular responses of A549 alveolar epithelial cells to serially collected *Pseudomonas aeruginosa* from cystic fibrosis patients at different stages of pulmonary infection. *FEMS Immunol Med Microbiol* 2010; **59**: 207–20.

27 Kirchner S, Fothergill JL, Wright EA *et al.* Use of artificial sputum medium to test antibiotic efficacy against *Pseudomonas aeruginosa* in conditions more relevant to the cystic fibrosis lung. *J Vis Exp* 2012; **5**: e3857.

28 Bjarnsholt T, Jensen PØ, Fiandaca MJ *et al.* *Pseudomonas aeruginosa* biofilms in the respiratory tract of cystic fibrosis patients. *Pediatr Pulmonol* 2009; **44**: 547–58.

29 Worlitzsch D, Tarran R, Ulrich M *et al.* Effects of reduced mucus oxygen concentration in airway *Pseudomonas* infections of cystic fibrosis patients. *J Clin Invest* 2002; **109**: 317–25.

30 Crabbé A, Liu Y, Matthijs N *et al.* Antimicrobial efficacy against *Pseudomonas aeruginosa* biofilm formation in a three-dimensional lung epithelial model and the influence of fetal bovine serum. *Sci Rep* 2017; **7**: 43321.

31 Sriramulu DD, Lunsdorf H, Lam JS *et al.* Microcolony formation: a novel biofilm model of *Pseudomonas aeruginosa* for the cystic fibrosis lung. *J Med Microbiol* 2005; **54**: 667–76.

32 Cao B, Christophersen L, Kolpen M *et al.* Diffusion retardation by binding of tobramycin in an alginate biofilm model. *PLoS One* 2016; **11**: e0153616.

33 Gordon CA, Hodges NA, Marriott C. Antibiotic interaction and diffusion through alginate and exopolysaccharide of cystic fibrosis-derived *Pseudomonas aeruginosa*. *J Antimicrob Chemother* 1988; **22**: 667–74.

34 Huang JX, Blaskovich MAT, Pelingon R *et al.* Mucin binding reduces colistin antimicrobial activity. *Antimicrob Agents Chemother* 2015; **59**: 5925–31.

35 Hunt BE, Weber A, Berger A *et al.* Macromolecular mechanisms of sputum inhibition of tobramycin activity. *Antimicrob Agents Chemother* 1995; **39**: 34–9.

36 Tseng BS, Zhang W, Harrison JJ *et al.* The extracellular matrix protects *Pseudomonas aeruginosa* biofilms by limiting the penetration of tobramycin. *Environ Microbiol* 2013; **15**: 2865–78.

37 Ciofu O, Rojo-Molinero E, Macià MD *et al.* Antibiotic treatment of biofilm infections. *APMIS* 2017; **125**: 304–19.

38 Le Goffic F, Capmau M-L *et al.* Mechanism of action of aminoglycoside antibiotics. *Eur J Biochem* 1979; **102**: 73–81.

39 Conly JM, Johnston BL. Colistin: the phoenix arises. *Can J Infect Dis Med Microbiol* 2006; **17**: 267–9.

40 Pamp SJ, Gjermansen M, Johansen HK *et al.* Tolerance to the antimicrobial peptide colistin in *Pseudomonas aeruginosa* biofilms is linked to metabolically active cells, and depends on the pmr and mexAB-oprM genes. *Mol Microbiol* 2008; **68**: 223–40.

41 Cattoir V, Narasimhan G, Skurnik D *et al.* Transcriptional response of mucoid *Pseudomonas aeruginosa* to human respiratory mucus. *MBio* 2013; **3**: e00410–12.

42 Vishwanath S, Ramphal R. Adherence of *Pseudomonas aeruginosa* to human tracheobronchial mucin. *Infect Immun* 1984; **45**: 197–202.

43 Landry RM, An D, Hupp JT *et al.* Mucin-*Pseudomonas aeruginosa* interactions promote biofilm formation and antibiotic resistance. *Mol Microbiol* 2006; **59**: 142–51.

44 Henke MO, John G, Rheineck C *et al.* Serine proteases degrade airway mucins in cystic fibrosis. *Infect Immun* 2011; **79**: 3438–44.

45 Johansson ME V, Ambort D, Pelaseyed T *et al.* Composition and functional role of the mucus layers in the intestine. *Cell Mol Life Sci* 2011; **68**: 3635–41.

46 Walker TS, Tomlin KL, Worthen GS *et al.* Enhanced *Pseudomonas aeruginosa* biofilm development mediated by human neutrophils. *Infect Immun* 2005; **73**: 3693–701.

47 Caceres SM, Malcolm KC, Taylor-Cousar JL *et al.* Enhanced in vitro formation and antibiotic resistance of nonattached *Pseudomonas aeruginosa* aggregates through incorporation of neutrophil products. *Antimicrob Agents Chemother* 2014; **58**: 6851–60.

48 Sønderholm M, Kragh KN, Koren K *et al.* *Pseudomonas aeruginosa* aggregate formation in an alginate bead model system exhibits in vivo-like characteristics. *Appl Environ Microbiol* 2017; **83**: e00113–17.

49 Palmer KL, Mashburn LM, Singh PK *et al.* Cystic fibrosis sputum supports growth and cues key aspects of *Pseudomonas aeruginosa* physiology. *J Bacteriol* 2005; **187**: 5267–77.

50 Palmer KL, Aye LM, Whiteley M. Nutritional cues control *Pseudomonas aeruginosa* multicellular behavior in cystic fibrosis sputum. *J Bacteriol* 2007; **189**: 8079–87.

51 Kreda SM, Davis CW, Rose MC. CFTR, mucins, and mucus obstruction in cystic fibrosis. *Cold Spring Harb Perspect Med* 2012; **2**: a009589.

Supplementary data

Bacterial strains and antibiotics

The *P. aeruginosa* wild-type strain PAO1 was obtained from DSMZ-German Collection of Microorganisms and Cell Cultures (DSMZ #19880, Braunschweig, Germany, ATCC 15692). Fluorescent GFP-tagged PAO1 carrying a GFP-tagged pMRP9 plasmid was kindly provided by Thomas Bjarnsholt (Department of Immunology and Microbiology, Copenhagen, Denmark). Two different antibiotics were used for susceptibility testing: tobramycin sulfate salt and colistin sulfate salt (both from Sigma Aldrich, Munich, Germany).

MIC assay

For determination of the MIC, 50 µl of PAO1 in cation-adjusted Mueller-Hinton broth (CAMHB, Becton Dickinson, Heidelberg, Germany) at a concentration of 2 x 10^6 cells/mL were transferred into the wells of a round-bottom 96-well plate (Nunc, Roskilde, Denmark). Two-fold dilutions of the respective antibiotics in CAMHB were added to bacterial suspensions, resulting in a final concentration range of 0.125-512 mg/L. A growth control was treated with CAMHB only. The plates were sealed with self-adhesive strips and incubated at 35 °C ± 2 °C for 24 h. Bacterial growth was visually assessed and the MIC was defined as lowest antibiotic concentration showing no visible growth of bacteria.[169]

Extraction and preparation of human mucus

Undiluted human tracheal mucus samples were collected with the endotracheal tube method.[63,121,128] The protocol was approved by the Ethics Commission of The Chamber of Medicine Doctors of the Saarland (file number 19/15). The tracheal tubes of patients undergoing elective surgery with general anesthesia, non-related to pulmonary conditions, were collected after surgery and placed in 50-mL centrifuge tubes. The mucus from each tracheal tube was collected by centrifuging the samples at 190 g for 30 s. Mucus samples were stored at -20 °C until further use.

Six to ten independent mucus samples were pooled to reach an approximate weight of 1 g. Mucus samples were then placed over a Teflon surface, inserted into an autoclavable sealing bag (Medipack, Christophorus CBC GmbH, Eppelheim, Germany), and stored at -80 °C for 4 h. The samples were then freeze-dried overnight (Alpha 2-4 LSC, Christ, Germany), sealed, and stored until use. The samples were weighed before and after the process to determine the amount of sublimated water.

Before its use for *P. aeruginosa* biofilm formation assays, the freeze-dried mucus was exposed to UV radiation for 1 h and re-hydrated with PBS using the same volume that had previously been sublimated. Mucus samples were allowed to re-hydrate on a shaker at 100 rpm at room temperature. As a control for every produced mucus batch, prior to any experiment, an aliquot of re-suspended mucus was incubated in agar plates for 24-h and inspected for bacterial growth.

Biofilm cultivation and susceptibility testing

PAO1 were cultivated in LB medium (Carl Roth, Karlsruhe, Germany) at 150 rpm and 37 °C for 17-20 h. The bacterial suspension was harvested and diluted in LB medium to an OD_{600} of 0.02, corresponding to a concentration of 2 x 10^7 bacteria/mL. Volumes of 100 µL of resuspended mucus or PBS (Lonza, Basel, Switzerland) was transferred to the wells of a 96-well plate (TPP, Trasadingen, Switzerland) and inoculated with 100 µL bacterial suspension. Bacteria-free LB medium was used as a sham infection control. The actual inoculum was confirmed by dilution plating and counting of colony-forming units (cfu). Pure mucus and PBS were tested for any bacterial contamination by dilution plating and cfu determination. For biofilm formation plates were incubated under static conditions with 100% humidity, 37 °C and 0% CO_2 for 24 h. Thereafter, samples were treated with 10 µL tobramycin or colistin with a final concentration of 0.1, 0.3 or 0.9 mg/mL each, representing 100x, 300x, and 900x MIC, respectively. LB medium was used as control. Efficacy was assessed according to viable bacterial load determined using 1:10 dilutions in PBS/0.05% Tween20 (Sigma Aldrich, Munich, Germany) and plating on Trypticase Soy Agar (TSA, Becton Dickinson, Heidelberg, Germany) to count cfu after overnight incubation at 37 °C. Biofilms including mucus or PBS were removed from well plates by using pipettes with extra wide pipette tips which allowed aspirating the viscoelastic biomass. Biofilms were aspirated several times to make sure that as much volume as possible was removed. Samples were transferred to glass vessels for dilutions and intensively vortexed for homogenous distribution. Samples were diluted in PBS containing 0.05% of tween to disrupt bacterial aggregates for a better counting on agar plates.

Tobramycin activity after pre-incubation in mucus

A volume of 100 µL of bacteria-free, resuspended mucus was mixed with 10 µL of tobramycin suspension, resulting in a final concentration of 0.3 mg/mL in the well. After 24 h of incubation, tobramycin-containing mucus was inoculated with 100 µL of PAO1 (2 x 10^7/mL), leading to a final tobramycin concentration of 0.15 mg/mL. As positive treatment control 0.15 mg/mL tobramycin with vehicle and a negative control without tobramycin were used. After further incubation for 24

h at 37 °C, treatment efficacy was analyzed visually for turbidity and by dilution plating and determination of cfu.

Laser scanning confocal microscopy

For confocal microscopy experiments *P. aeruginosa* biofilms were cultivated in 96-well plates suitable for fluorescence microscopy (µ-plate 96 well, ibidi, Martinsried, Germany) using a GFP-tagged strain as described above. Biofilms of GFP-PAO1 were grown in mucus or in PBS for 2 days. Uninfected mucus was used as control. Imaging was performed using an LSM 510 Meta inverse confocal microscope (Zeiss, Jena, Germany). The 488-nm argon laser line was used for excitation and the BP 505–530 filter for emission. Z-stacks were performed with intervals of 0.5 µm and a range of 30 µm using the plan-neofluar 40x/1.3 oil DIC objective. For biomass quantification images were processed with the imaging software IMARIS version 7.6.5, including its associated surpass module (Bitplane scientific software, Zurich, Switzerland). The surface of all fluorescent signals above a determined threshold was computed as bacterial biomass. The obtained values were displayed as surface area (in μm^2) covered with a GFP-positive signal.

Tobramycin and colistin diffusion studies

Experiments were performed using transwell® membranes (Corning, Durham, USA) with a surface of 0.33 cm^2 and a pore size of 4 µm. Biofilms in the presence or absence of mucus or sham-infected mucus samples with a total volume of 100 µL were cultivated on the membrane of the transwell® inserts overnight. During bacteria inoculation the transwell® inserts were placed on a sterile plastic surface to prevent loss of bacteria through the pores and allow proper biofilm formation. After 24 h, the inserts were placed into the companion plates and 100 µL of 0.6 mg/mL tobramycin or colistin solution in PBS were then added to the apical compartment. The basolateral compartment was filled with 600 µL of PBS. Volumes of 50 µL each were sampled from the basolateral compartment after 15, 30, 60, 90, 120 and 3600 min. After sample withdrawal the basolateral compartment was supplemented with 50 µL of fresh, pre-warmed PBS. The collected samples were diluted in PBS and sterile filtered with 0.2 µm pore-size polyethersulfone (PES) filters (VWR, Radnor, USA) prior to analysis. Previous experiments had confirmed that this filtration step had no impact on antibiotic concentrations (data not shown). Tobramycin and colistin concentrations at each time point were determined by HPLC measurements.

HPLC measurement

HPLC and MS/MS methods similar to those described in literature for tobramycin[170] and colistin[171] were applied with minor modifications. A Dionex Ultimate 3000 HPLC system with a Machery-

Nagel Nucleodur C18 Gravity-SB ec 100 x 2 (3 µm) with guard column coupled to a TSQ Quantum Access Max tandem mass spectrometer was used for the measurements. Samples were analyzed by single measurements. Concentrations were determined using the obtained areas of the analytes.

Statistical analysis

Three independent runs were performed for each experiment with technical duplicates or technical triplicates (diffusion studies). All values are given as mean ± standard deviation (SD) or mean ± standard error of the mean (SE) (diffusion studies). Statistical analysis was performed with the GraphPad Prism software (GraphPad 7 Software, Inc, USA) using the Mann-Whitney test. Differences were considered statistically significant at the level of $p < 0.05$.

Figure S1. Bacterial count in mucus, LB medium and PBS. Biofilms were grown in mucus, LB medium or PBS for 48 h. Bacterial load was assessed by determination of cfu. Bar graphs show the mean + SD for n = 3 samples with technical duplicates each. * indicates statistical significance with $P < 0.05$, according to the Mann-Whitney test.

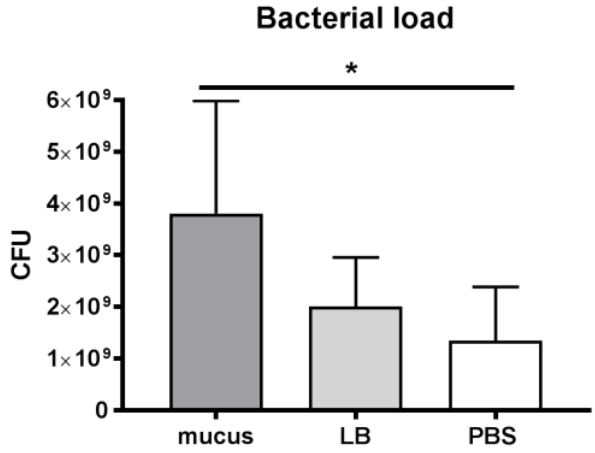

5. References

1. Leff Paul T, A. R. and S. *Respiratory physiology: Basics and applications*. (W.B. Saunders Co, 1993).

2. Murgia, X., de Souza Carvalho, C. & Lehr, C.-M. Overcoming the pulmonary barrier: new insights to improve the efficiency of inhaled therapeutics. *Eur. J. Nanomedicine* **6,** 157–169 (2014).

3. Bur, M. & Lehr, C.-M. Pulmonary cell culture models to study the safety and efficacy of innovative aerosol medicines. *Expert Opin. Drug Deliv.* **5,** 641–652 (2008).

4. Inayama, Y. *et al.* The differentiation potential of tracheal basal cells. *Lab. Invest.* **58,** 706–717 (1988).

5. Widdicombe, J. H. & Wine, J. J. Airway Gland Structure and Function. *Physiol. Rev.* **95,** 1241 LP-1319 (2015).

6. Rubin, B. K. Secretion properties, clearance, and therapy in airway disease. *Transl. Respir. Med.* **2,** 6 (2014).

7. Widdicombe, J. G. & Pack, R. J. The Clara cell. *Eur. J. Respir. Dis.* **63,** 202–20 (1982).

8. Steimer, A., Haltner, E. & Lehr, C.-M. Cell culture models of the respiratory tract relevant to pulmonary drug delivery. *J. Aerosol Med.* **18,** 137–82 (2005).

9. Wanner, A., Salathé, M. & O'Riordan, T. G. Mucociliary clearance in the airways. *Am. J. Respir. Crit. Care Med.* **154,** 1868–1902 (1996).

10. Ross, M. H. & Pawlina, W. *Histology - A Text and Atlas*. (Lippincot Williams and Wilkins, 2005).

11. Ochs, M. *et al.* The Number of Alveoli in the Human Lung. *Am. J. Respir. Crit. Care Med.* **169,** 120–124 (2004).

12. Crapo, J. D., Barry, B. E., Gehr, P., Bachofen, M. & Weibel, E. R. Cell number and cell characteristics of the normal human lung. *Am. Rev. Respir. Dis.* **125,** 740–5 (1982).

13. Frank, J. A. Claudins and alveolar epithelial barrier function in the lung. *Annals of the New York Academy of Sciences* **1257,** 175–183 (2012).

14. Hittinger, M. *et al.* Autologous co-culture of primary human alveolar macrophages and epithelial cells for investigating aerosol medicines. Part I: Model Characterisation. *ATLA Altern. to Lab. Anim.* **44,** 337–347 (2016).

15. Müller, L. *et al.* Oxidative stress and inflammation response after nanoparticle exposure: differences between human lung cell monocultures and an advanced three-dimensional model of the human epithelial airways. *J. R. Soc. Interface* **7,** S27 LP-S40 (2010).

16. Perez-Gil, J. & Weaver, T. E. Pulmonary surfactant pathophysiology: current models and open questions. *Physiology (Bethesda).* **25,** 132–141 (2010).

17. Bernhard, W. Lung surfactant: Function and composition in the context of development and respiratory physiology. *Ann. Anat.* **208,** 146–150 (2016).

18. Jeffery, P. K. & Li, D. Airway mucosa: Secretory cells, mucus and mucin genes. *Eur. Respir. J.* (1997). doi:10.1183/09031936.97.10071655

19. Mühlfeld, C. *et al.* Pre-ischaemic exogenous surfactant reduces pulmonary injury in rat ischaemia/reperfusion. *Eur. Respir. J.* **33,** 625 LP-633 (2009).

20. Nicod, L. P. Lung defences: an overview. *Eur. Respir. Rev.* **14,** 45 LP-50 (2005).

21. Alonso, M. J. & Csaba, N. S. *Nanostructured Biomaterials for Overcoming Biological Barriers*. (The Royal Society of Chemistry, 2012). doi:10.1039/9781849735292

22. Ruge, C. a. *et al.* Uptake of nanoparticles by alveolar macrophages is triggered by surfactant protein A. *Nanomedicine Nanotechnology, Biol. Med.* **7,** 690–693 (2011).

23. Ruge, C. A. *et al.* The Interplay of Lung Surfactant Proteins and Lipids Assimilates the Macrophage Clearance of Nanoparticles. *PLoS One* **7,** e40775 (2012).

24. Miyata, R. & van Eeden, S. F. The innate and adaptive immune response induced by alveolar macrophages exposed to ambient particulate matter. *Toxicol. Appl. Pharmacol.* **257,** 209–226 (2011).

25. Byrne, A. J., Mathie, S. A., Gregory, L. G. & Lloyd, C. M. Pulmonary macrophages: key players in the innate defence of the airways. *Thorax* (2015).

26. Patton, J. S. & Byron, P. R. Inhaling medicines: delivering drugs to the body through the lungs. *Nat Rev Drug Discov* **6,** 67–74 (2007).

27. Mathias, N. R. & Hussain, M. A. Non-invasive Systemic Drug Delivery: Developability Considerations for Alternate Routes of Administration. *J. Pharm. Sci.* **99,** 1–20 (2017).

28. Dolovich, M. B. & Dhand, R. Aerosol drug delivery: developments in device design and clinical use. *Lancet* **377,** 1032–1045 (2011).

29. Patton, J. S., Bukar, J. G. & Eldon, M. A. Clinical Pharmacokinetics and Pharmacodynamics of Inhaled Insulin. *Clin. Pharmacokinet.* **43,** 781–801 (2004).

30. Tepper, S. J. Orally Inhaled Dihydroergotamine: A Review. *Headache J. Head Face Pain* **53,** 43–53 (2013).

31. d'Angelo, I. *et al.* Improving the efficacy of inhaled drugs in cystic fibrosis: Challenges and emerging drug delivery strategies. *Adv. Drug Deliv. Rev.* **75,** 92–111 (2014).

32. Allen, T. M. & Cullis, P. R. Drug Delivery Systems: Entering the Mainstream. *Science (80-.).* **303,** 1818 LP-1822 (2004).

33. Ho, D.-K. *et al.* Farnesylated Glycol Chitosan as a Platform for Drug Delivery: Synthesis, Characterization, and Investigation of Mucus–Particle Interactions. *Biomacromolecules* **19,** 3489–3501 (2018).

34. Sykes, E. A. *et al.* Tailoring nanoparticle designs to target cancer based on tumor pathophysiology. *Proc. Natl. Acad. Sci.* **113,** E1142 LP-E1151 (2016).

35. Ho, D. K. *et al.* Polysaccharide Submicrocarrier for Improved Pulmonary Delivery of Poorly Soluble Anti-infective Ciprofloxacin: Preparation, Characterization, and Influence of Size on Cellular Uptake. *Mol. Pharm.* (2018). doi:10.1021/acs.molpharmaceut.7b00967

36. Herd, H. *et al.* Nanoparticle Geometry and Surface Orientation Influence Mode of Cellular Uptake. *ACS Nano* **7,** 1961–1973 (2013).

37. Pelaz, B. *et al.* Diverse Applications of Nanomedicine. *ACS Nano* **11,** 2313–2381 (2017).

38. Huckaby, J. T. & Lai, S. K. PEGylation for enhancing nanoparticle diffusion in mucus. *Adv. Drug Deliv. Rev.* (2017). doi:https://doi.org/10.1016/j.addr.2017.08.010

39. Schipper, N. G. M. *et al.* Chitosans as absorption enhancers of poorly absorbable drugs. *Eur. J. Pharm. Sci.* **8,** 335–343 (1999).

40. Menina, S. *et al.* Invasin-functionalized liposome nanocarriers improve the intracellular delivery of anti-infective drugs. *RSC Adv.* **6,** 41622–41629 (2016).

41. Farkhani, S. M. *et al.* Cell penetrating peptides: Efficient vectors for delivery of nanoparticles, nanocarriers, therapeutic and diagnostic molecules. *Peptides* **57,** 78–94 (2014).

42. Barthold, S. *et al.* Overview of inhaled nanopharmaceuticals. *ISAM Textb. Aerosol Med. (eds B. Rothen-Rutishauser R. Dhand), Int. Soc. Aerosols Med.* 330–351 (2015).

43. Wright, B. M. A NEW NEBULISER. *Lancet* **272,** 24–25 (1958).

44. Son, Y. J. & McConville, J. T. Advancements in dry powder delivery to the lung. *Drug Development and Industrial Pharmacy* **34,** 948–959 (2008).

45. Newman, S. P. Can lung deposition data act as a surrogate for the clinical response to inhaled asthma drugs? *Br. J. Clin. Pharmacol.* **49,** 529–537 (2000).

46. Heyder, J. Deposition of Inhaled Particles in the Human Respiratory Tract and Consequences for Regional Targeting in Respiratory Drug Delivery. *Proc. Am. Thorac. Soc.* **1,** 315–320 (2004).

47. Mitchell, J. P., Nagel, M. W., Wiersema, K. J. & Doyle, C. C. Aerodynamic particle size analysis of aerosols from pressurized metered-dose inhalers: Comparison of andersen 8-stage cascade impactor, next generation pharmaceutical impactor, and model 3321 aerodynamic particle sizer aerosol spectrometer. *AAPS PharmSciTech* **4,** 425–433 (2003).

48. Laube, B. L. *et al.* What the pulmonary specialist should know about the new inhalation therapies. *European Respiratory Journal* (2011). doi:10.1183/09031936.00166410

49. O'Callaghan, C. & Barry, P. W. The science of nebulised drug delivery. *Thorax* (1997). doi:10.1136/thx.52.2008.S31

50. Murgia, X., Loretz, B., Hartwig, O., Hittinger, M. & Lehr, C.-M. The role of mucus on drug transport and its potential to affect therapeutic outcomes. *Adv. Drug Deliv. Rev.* (2017). doi:https://doi.org/10.1016/j.addr.2017.10.009

51. Antunes, M. B. & Cohen, N. A. Mucociliary clearance – a critical upper airway host defense mechanism and methods of assessment. *Curr. Opin. Allergy Clin. Immunol.* **7,** (2007).

52. Bansil, R. & Turner, B. S. Mucin structure, aggregation, physiological functions and biomedical applications. *Curr. Opin. Colloid Interface Sci.* **11,** 164–170 (2006).

53. Boegh, M. & Nielsen, H. M. Mucus as a Barrier to Drug Delivery - Understanding and Mimicking the Barrier Properties. *Basic Clin. Pharmacol. Toxicol.* **116,** 179–186 (2015).

54. Thornton, D. J. & Sheehan, J. K. From Mucins to Mucus. *Proc. Am. Thorac. Soc.* **1,** 54–61 (2004).

55. Rose, M. C. Mucins: structure, function, and role in pulmonary diseases. *Am. J. Physiol. - Lung Cell. Mol. Physiol.* **263,** L413 LP-L429 (1992).

56. Murgia, Xabi; de Souza Carvalho, Cristiane; Lehr, C.-M. Overcoming the pulmonary barrier: new insights to improve the efficiency of inhaled therapeutics. *European Journal of Nanomedicine* **6,** 157–169 (2014).

57. Gwozdzinski K , Slomiany A, Nishikawa H, Okazaki Z, S. B. Gastric Mucin Hydrophobicity: Effects of Associated and Covalently Bound Lipids, Proteolysis, and Reduction. *Biochem Int* **17,** 907–917 (1988).

58. Lillehoj, E. P., Kato, K., Lu, W. & Kim, K. C. Cellular and Molecular Biology of Airway Mucins. *Int. Rev. Cell Mol. Biol.* **303,** 139–202 (2013).

59. Johansson, M. E. V, Sjövall, H. & Hansson, G. C. The gastrointestinal mucus system in health and disease. *Nat. Rev. Gastroenterol. Hepatol.* **10,** 352–361 (2013).

60. Turner, B. S., Bhaskar, K. R., Hadzopoulou-Cladaras, M. & LaMont, J. T. Cysteine-rich regions of pig gastric mucin contain von Willebrand factor and cystine knot domains at the carboxyl terminal1The sequences described in this paper have been submitted to the GenBank Nucleotide Sequence Database, and have been assigned the Ge. *Biochim. Biophys. Acta - Gene Struct. Expr.* **1447,** 77–92 (1999).

61. Perez-Vilar, J. & Hill, R. L. The Structure and Assembly of Secreted Mucins. *J. Biol. Chem.* **274,** 31751–31754 (1999).

62. SANDERS, N. N. *et al.* Cystic Fibrosis Sputum. *Am. J. Respir. Crit. Care Med.* **162,** 1905–1911 (2000).

63. Schuster, B. S., Suk, J. S., Woodworth, G. F. & Hanes, J. Nanoparticle diffusion in respiratory mucus from humans without lung disease. *Biomaterials* **34,** 3439–3446 (2013).

64. Suk, J. S. *et al.* The penetration of fresh undiluted sputum expectorated by cystic fibrosis patients by non-adhesive polymer nanoparticles. *Biomaterials* **30,** 2591–2597 (2009).

65. Lieleg, O. & Ribbeck, K. Biological Hydrogels as Selective Diffusion Barriers. *Trends Cell Biol.* **21,** 543–551 (2011).

66. Huang, J. X. *et al.* Mucin binding reduces colistin antimicrobial activity. *Antimicrob. Agents Chemother.* **59,** 5925–5931 (2015).

67. Murgia, X. *et al.* Modelling the bronchial barrier in pulmonary drug delivery: A human bronchial epithelial cell line supplemented with human tracheal mucus. *Eur. J. Pharm. Biopharm.* **118,** 79–88 (2017).

68. Bhattacharjee, S. *et al.* Nanoparticle passage through porcine jejunal mucus: Microfluidics and rheology. *Nanomedicine Nanotechnology, Biol. Med.* **13,** 863–873 (2017).

69. Mura, S. *et al.* Biodegradable Nanoparticles Meet the Bronchial Airway Barrier: How Surface Properties Affect Their Interaction with Mucus and Epithelial Cells. *Biomacromolecules* **12,** 4136–4143 (2011).

70. Foster, W. M., Langenback, E. & Bergofsky, E. H. Measurement of tracheal and bronchial mucus velocities in man: relation to lung clearance. *J. Appl. Physiol.* **48,** 965 LP-971 (1980).

71. Friedman, M. *et al.* Acute Effects of an Aerosol Hair Spray on Tracheal Mucociliary Transport. *Am. Rev. Respir. Dis.* **116,** 281–286 (1977).

72. Henning, A. *et al.* Embryonic Chicken Trachea as a New In Vitro Model for the Investigation of Mucociliary Particle Clearance in the Airways. *AAPS PharmSciTech* **9,** 521–527 (2008).

73. Cooper, J. L., Quinton, P. M. & Ballard, S. T. Mucociliary transport in porcine trachea: differential effects of inhibiting chloride and bicarbonate secretion. *Am. J. Physiol. - Lung Cell. Mol. Physiol.* **304,** L184–L190 (2013).

74. Möller, W. *et al.* Mucociliary and long-term particle clearance in the airways of healthy nonsmoker subjects. *J. Appl. Physiol.* **97,** 2200 LP-2206 (2004).

75. Ramos, F. L., Krahnke, J. S. & Kim, V. Clinical issues of mucus accumulation in COPD. *International Journal of COPD* **9,** 139–150 (2014).

76. Innes, A. L. *et al.* Ex vivo sputum analysis reveals impairment of protease-dependent mucus degradation by plasma proteins in acute asthma. *Am. J. Respir. Crit. Care Med.* **180,** 203–210 (2009).

77. Kreda, S. M., Davis, C. W. & Rose, M. C. CFTR, Mucins, and Mucus Obstruction in Cystic Fibrosis. *Cold Spring Harb. Perspect. Med.* **2,** a009589 (2012).

78. Elborn, J. S. Cystic fibrosis. *Lancet* **388,** 2519–2531 (2017).

79. Stigliani, M. *et al.* Rheological Properties of Cystic Fibrosis Bronchial Secretion and in Vitro Drug Permeation Study: The Effect of Sodium Bicarbonate. *J. Aerosol Med. Pulm. Drug Deliv.* **29,** 337–345 (2016).

80. Matsui, H. *et al.* Evidence for Periciliary Liquid Layer Depletion, Not Abnormal Ion Composition, in the Pathogenesis of Cystic Fibrosis Airways Disease. *Cell* **95,** 1005–1015 (1998).

81. PERKS, B. & SHUTE, J. K. DNA and Actin Bind and Inhibit Interleukin-8 Function in Cystic Fibrosis Sputa. *Am. J. Respir. Crit. Care Med.* **162,** 1767–1772 (2000).

82. Yuan, S. *et al.* Oxidation increases mucin polymer cross-links to stiffen airway mucus gels. *Sci. Transl. Med.* **7,** 276ra27-276ra27 (2015).

83. Bjarnsholt, T. The role of bacterial biofilms in chronic infections. *APMIS* **121,** 1–51 (2013).

84. Coutinho, H. D. M., Falcão-Silva, V. S. & Gonçalves, G. F. Pulmonary bacterial pathogens in cystic fibrosis patients and antibiotic therapy: a tool for the health workers. *Int. Arch. Med.* **1,** 24 (2008).

85. Mulcahy, L. R., Isabella, V. M. & Lewis, K. Pseudomonas aeruginosa biofilms in disease.

Microb. Ecol. **68,** 1–12 (2014).

86. Høiby, N., Ciofu, O. & Bjarnsholt, T. Pseudomonas aeruginosa biofilms in cystic fibrosis. *Future Microbiology* **5,** 1663–1674 (2010).

87. Müller, L. *et al.* Human airway mucus alters susceptibility of Pseudomonas aeruginosa biofilms to tobramycin, but not colistin. *J. Antimicrob. Chemother.* **73,** 2762–2769 (2018).

88. Winstanley, C., O'Brien, S. & Brockhurst, M. A. Pseudomonas aeruginosa Evolutionary Adaptation and Diversification in Cystic Fibrosis Chronic Lung Infections. *Trends Microbiol.* **24,** 327–337 (2016).

89. Dalhoff, A. Pharmacokinetics and pharmacodynamics of aerosolized antibacterial agents in chronically infected cystic fibrosis patients. *Clin. Microbiol. Rev.* **27,** 753–782 (2014).

90. Haworth, C. *et al.* Inhaled Liposomal Ciprofloxacin in Patients with Bronchiectasis and Chronic Pseudomonas Aeruginosa Infection: Results from Two Parallel Phase III Trials (ORBIT-3 and -4). in *B14. CLINICAL TRIALS ACROSS PULMONARY DISEASE* A7604–A7604 (American Thoracic Society, 2017). doi:doi:10.1164/ajrccm-conference.2017.195.1_MeetingAbstracts.A7604

91. Hunt, B. E., Weber, A., Berger, A., Ramsey, B. & Smith, A. L. Macromolecular mechanisms of sputum inhibition of tobramycin activity. *Antimicrob. Agents Chemother.* **39,** 34–39 (1995).

92. Cone, R. A. Barrier properties of mucus. *Adv. Drug Deliv. Rev.* **61,** 75–85 (2009).

93. Lai, S. K., Wang, Y.-Y. & Hanes, J. Mucus-penetrating nanoparticles for drug and gene delivery to mucosal tissues. *Adv. Drug Deliv. Rev.* **61,** 158–171 (2009).

94. Bhat, P. G., Flanagan, D. R. & Donovan, M. D. The limiting role of mucus in drug absorption: Drug permeation through mucus solution. *Int. J. Pharm.* **126,** 179–187 (1995).

95. Larhed, A. W., Artursson, P. & Björk, E. The Influence of Intestinal Mucus Components on the Diffusion of Drugs. *Pharm. Res.* **15,** 66–71 (1998).

96. Larhed, A. W., Artursson, P., Gråsjö, J. & Björk, E. Diffusion of Drugs in Native and Purified Gastrointestinal Mucus. *J. Pharm. Sci.* **86,** 660–665 (2017).

97. Desai, M. A., Mutlu, M. & Vadgama, P. A study of macromolecular diffusion through native porcine mucus. *Experientia* **48,** 22–26 (1992).

98. Desai, M. A. & Vadgama, P. Estimation of effective diffusion coefficients of model solutes through gastric mucus: assessment of a diffusion chamber technique based on spectrophotometric analysis. *Analyst* **116,** 1113–1116 (1991).

99. Murgia, X. *et al.* Size-limited penetration of nanoparticles into porcine respiratory mucus after aerosol deposition. *Biomacromolecules* **17,** 1536–1542 (2016).

100. Kirch, J. *et al.* Optical tweezers reveal relationship between microstructure and nanoparticle penetration of pulmonary mucus. *Proc. Natl. Acad. Sci. U. S. A.* **109,** 18355–18360 (2012).

101. Shaikh, R., Raj Singh, T. R., Garland, M. J., Woolfson, A. D. & Donnelly, R. F. Mucoadhesive drug delivery systems. *J. Pharm. Bioallied Sci.* **3,** 89–100 (2011).

102. Bernkop-Schnürch, A. & Dünnhaupt, S. Chitosan-based drug delivery systems. *European Journal of Pharmaceutics and Biopharmaceutics* **81,** 463–469 (2012).

103. Lehr, C.-M., Bouwstra, J. A., Schacht, E. H. & Junginger, H. E. In vitro evaluation of mucoadhesive properties of chitosan and some other natural polymers. *Int. J. Pharm.* **78,** 43–48 (1992).

104. Iqbal, J. *et al.* Preactivated thiomers as mucoadhesive polymers for drug delivery. *Biomaterials* **33,** 1528–1535 (2012).

105. Dünnhaupt, S. *et al.* Distribution of thiolated mucoadhesive nanoparticles on intestinal mucosa. *Int. J. Pharm.* **408,** 191–199 (2011).

106. Cui, F., Qian, F. & Yin, C. Preparation and characterization of mucoadhesive polymer-coated nanoparticles. *Int. J. Pharm.* **316,** 154–161 (2006).

107. Lai, S. K., Wang, Y.-Y., Hida, K., Cone, R. & Hanes, J. Nanoparticles reveal that human cervicovaginal mucus is riddled with pores larger than viruses. *Proc. Natl. Acad. Sci. U. S. A.* **107,** 598–603 (2010).

108. Wang, Y.-Y. *et al.* Mucoadhesive Nanoparticles May Disrupt the Protective Human Mucus Barrier by Altering Its Microstructure. *PLoS One* **6,** e21547 (2011).

109. Duncan, G. A., Jung, J., Hanes, J. & Suk, J. S. The Mucus Barrier to Inhaled Gene Therapy. *Mol. Ther.* **24,** 2043–2053 (2016).

110. Suk, J. S., Xu, Q., Kim, N., Hanes, J. & Ensign, L. M. PEGylation as a strategy for improving nanoparticle-based drug and gene delivery. *Adv. Drug Deliv. Rev.* **99,** 28–51 (2016).

111. Lai, S. K. *et al.* Drug carrier nanoparticles that penetrate human chronic rhinosinusitis mucus. *Biomaterials* **32,** 6285–6290 (2011).

112. Schneider, C. S. *et al.* Nanoparticles that do not adhere to mucus provide uniform and long-lasting drug delivery to airways following inhalation. *Sci. Adv.* **3,** (2017).

113. Yu, T. *et al.* Liposome-based mucus-penetrating particles (MPP) for mucosal theranostics: Demonstration of diamagnetic chemical exchange saturation transfer (diaCEST) magnetic resonance imaging (MRI). *Nanomedicine* **11,** 401–405 (2015).

114. Ensign, L. M. *et al.* Ex vivo characterization of particle transport in mucus secretions coating freshly excised mucosal tissues. *Mol. Pharm.* **10,** 2176–2182 (2013).

115. Kim, A. J. *et al.* Use of Single-Site Functionalized PEG-Dendrons to Prepare Gene Vectors that Penetrate Human Mucus Barriers. *Angew. Chem. Int. Ed. Engl.* **52,** 3985–3988 (2013).

116. García, K. P. *et al.* Zwitterionic-Coated 'Stealth' Nanoparticles for Biomedical Applications: Recent Advances in Countering Biomolecular Corona Formation and Uptake by the Mononuclear Phagocyte System. *Small* **10,** 2516–2529 (2014).

117. Shan, W. *et al.* Enhanced Oral Delivery of Protein Drugs Using Zwitterion-Functionalized Nanoparticles to Overcome both the Diffusion and Absorption Barriers. *ACS Appl. Mater. Interfaces* **8,** 25444–25453 (2016).

118. Nordgård, C. T. & Draget, K. I. Co association of mucus modulating agents and nanoparticles for mucosal drug delivery. *Adv. Drug Deliv. Rev.* **124,** 175–183 (2018).

119. Nordgård, C. T., Nonstad, U., Olderøy, M. Ø., Espevik, T. & Draget, K. I. Alterations in Mucus Barrier Function and Matrix Structure Induced by Guluronate Oligomers. *Biomacromolecules* **15,** 2294–2300 (2014).

120. Balsamo, R., Lanata, L. & Egan, C. G. Mucoactive drugs. *Eur. Respir. Rev.* **19,** 127 LP-133 (2010).

121. Vukosavljevic, B. *et al.* Tracing molecular and structural changes upon mucolysis with N-acetyl cysteine in human airway mucus. *Int. J. Pharm.* **553,** 373–376 (2017).

122. Suk, J. S. *et al.* N-acetylcysteine Enhances Cystic Fibrosis Sputum Penetration and Airway Gene Transfer by Highly Compacted DNA Nanoparticles. *Mol. Ther.* **19,** 1981–1989 (2011).

123. Deacon, J. *et al.* Antimicrobial efficacy of tobramycin polymeric nanoparticles for Pseudomonas aeruginosa infections in cystic fibrosis: Formulation, characterisation and functionalisation with dornase alfa (DNase). *J. Control. Release* **198,** 55–61 (2015).

124. Müller, C. *et al.* Preparation and characterization of mucus-penetrating papain/poly(acrylic acid) nanoparticles for oral drug delivery applications. *J. Nanoparticle Res.* **15,** 1353 (2012).

125. Dünnhaupt, S., Kammona, O., Waldner, C., Kiparissides, C. & Bernkop-Schnürch, A. Nano-carrier systems: Strategies to overcome the mucus gel barrier. *Eur. J. Pharm. Biopharm.* **96,** 447–453 (2015).

126. Dawson, M., Wirtz, D. & Hanes, J. Enhanced Viscoelasticity of Human Cystic Fibrotic Sputum Correlates with Increasing Microheterogeneity in Particle Transport. *J. Biol. Chem.* **278,** 50393–50401 (2003).

127. Xing, L. *et al.* Sputum microRNA biomarkers for identifying lung cancer in indeterminate solitary pulmonary nodules. *Clin. Cancer Res.* **21,** 484–489 (2015).

128. Rubin, B. K., Ramirez, O., Zayas, J. G., Finegan, B. & King, M. Collection and Analysis of Respiratory Mucus from Subjects without Lung Disease. *Am. Rev. Respir. Dis.* **141,** 1040–1043 (1990).

129. Boegh, M., Baldursdóttir, S. G., Müllertz, A. & Nielsen, H. M. Property profiling of biosimilar mucus in a novel mucus-containing in vitro model for assessment of intestinal drug absorption. *Eur. J. Pharm. Biopharm.* **87,** 227–235 (2014).

130. Boegh, M., Baldursdottir, S. G., Nielsen, M. H., Müllertz, A. & Nielsen, H. M. Development and Rheological Profiling of Biosimilar Mucus. *Annu. Trans. Nord. Rheol. Soc.* **21,** 233–240 (2013).

131. Hamed, R. & Fiegel, J. Synthetic tracheal mucus with native rheological and surface tension properties. *J. Biomed. Mater. Res. Part A* **102,** 1788–1798 (2014).

132. Ernst, J. *et al.* Polyester-based particles to overcome the obstacles of mucus and biofilms in the lung for tobramycin application under static and dynamic fluidic conditions. *Eur. J. Pharm. Biopharm.* **131,** 120–129 (2018).

133. Nafee, N., Forier, K., Braeckmans, K. & Schneider, M. Mucus-penetrating solid lipid nanoparticles for the treatment of cystic fibrosis: Proof of concept, challenges and pitfalls. *Eur. J. Pharm. Biopharm.* **124,** 125–137 (2018).

134. Nafee, N. *et al.* Antibiotic-free nanotherapeutics: Ultra-small, mucus-penetrating solid lipid nanoparticles enhance the pulmonary delivery and anti-virulence efficacy of novel quorum sensing inhibitors. *J. Control. Release* **192,** 131–140 (2014).

135. Groo, A.-C. & Lagarce, F. Mucus models to evaluate nanomedicines for diffusion. *Drug Discov. Today* **19,** 1097–1108 (2014).

136. Grießinger, J. *et al.* Methods to determine the interactions of micro- and nanoparticles with mucus. *Eur. J. Pharm. Biopharm.* **96,** 464–476 (2015).

137. Li, X. *et al.* Novel mucus-penetrating liposomes as a potential oral drug delivery system: preparation, in vitro characterization, and enhanced cellular uptake. *Int. J. Nanomedicine* **6,** 3151–3162 (2011).

138. Zabaleta, V. *et al.* Oral administration of paclitaxel with pegylated poly(anhydride) nanoparticles: Permeability and pharmacokinetic study. *Eur. J. Pharm. Biopharm.* **81,** 514–523 (2012).

139. Torge, A. *et al.* Ciprofloxacin-loaded lipid-core nanocapsules as mucus penetrating drug delivery system intended for the treatment of bacterial infections in cystic fibrosis. *Int. J. Pharm.* **527,** 92–102 (2017).

140. Saltzman, W. M., Radomsky, M. L., Whaley, K. J. & Cone, R. A. Antibody diffusion in human cervical mucus. *Biophys. J.* **66,** 508–515 (1994).

141. Santos, R. S. *et al.* Effect of Native Gastric Mucus on in vivo Hybridization Therapies Directed at Helicobacter pylori. *Mol. Ther. Nucleic Acids* **4,** e269 (2015).

142. Axelrod, D., Koppel, D. E., Schlessinger, J., Elson, E. L. & Webb, W. W. Mobility measurement by analysis of fluorescence recovery kinetics. *Biophys J* **16,** 1055–1069 (1976).

143. Phair, R. D. & Misteli, T. Kinetic modelling approaches to in vivo imaging. *Nat. Rev. Mol. Cell Biol.* **2,** 898 (2001).

144. Schuster, B. S., Ensign, L. M., Allan, D. B., Suk, J. S. & Hanes, J. Particle tracking in drug and gene delivery research: state-of-the-art applications and methods. *Adv. Drug Deliv. Rev.* **91,** 70–91 (2015).

145. Oelschlaeger, C., Willenbacher, N. & Neser, S. Multiple-Particle Tracking (MPT) Measurements of Heterogeneities in Acrylic ThickenerSolutions BT - Surface and Interfacial Forces – From Fundamentals to Applications. in (eds. Auernhammer, G. K., Butt, H.-J. & Vollmer, D.) 74–79 (Springer Berlin Heidelberg, 2008).

146. Hittinger, M. *et al.* Preclinical safety and efficacy models for pulmonary drug delivery of antimicrobials with focus on in vitro models. *Adv. Drug Deliv. Rev.* **85,** 44–56 (2015).

147. Button, B. *et al.* A Periciliary Brush Promotes the Lung Health by Separating the Mucus Layer from Airway Epithelia. *Science (80-.).* **337,** 937–941 (2012).

148. Haghi, M. *et al.* Mono- and Cocultures of Bronchial and Alveolar Epithelial Cells Respond

Differently to Proinflammatory Stimuli and Their Modulation by Salbutamol and Budesonide. *Mol. Pharm.* **12,** 2625–2632 (2015).

149. Sears, P. R., Davis, C. W., Chua, M. & Sheehan, J. K. Mucociliary interactions and mucus dynamics in ciliated human bronchial epithelial cell cultures. *Am. J. Physiol. - Lung Cell. Mol. Physiol.* **301,** L181–L186 (2011).

150. Salomon, J. J. *et al.* The Cell Line NCI-H441 Is a Useful in Vitro Model for Transport Studies of Human Distal Lung Epithelial Barrier. *Mol. Pharm.* **11,** 995–1006 (2014).

151. Salomon, J. J. *et al.* Organic cation transporter function in different in vitro models of human lung epithelium. *Eur. J. Pharm. Sci.* **80,** 82–88 (2015).

152. Ehrhardt, C. *et al.* 16HBE14o- Human Bronchial Epithelial Cell Layers Express P-Glycoprotein, Lung Resistance-Related Protein, and Caveolin-1. *Pharm. Res.* **20,** 545–551 (2003).

153. Haghi, M. *et al.* Time- and passage-dependent characteristics of a Calu-3 respiratory epithelial cell model. *Drug Dev. Ind. Pharm.* **36,** 1207–1214 (2010).

154. Grainger, C. I., Greenwell, L. L., Lockley, D. J., Martin, G. P. & Forbes, B. Culture of Calu-3 Cells at the Air Interface Provides a Representative Model of the Airway Epithelial Barrier. *Pharm. Res.* **23,** 1482–1490 (2006).

155. Ehrhardt, C. *et al.* Towards an in vitro model of cystic fibrosis small airway epithelium: characterisation of the human bronchial epithelial cell line CFBE41o-. *Cell Tissue Res.* **323,** 405–415 (2006).

156. Mangal, S., Gao, W., Li, T. & Zhou, Q. (Tony). Pulmonary delivery of nanoparticle chemotherapy for the treatment of lung cancers: challenges and opportunities. *Acta Pharmacol. Sin.* **38,** 782–797 (2017).

157. Alton, E. *et al.* Cationic lipid-mediated CFTR gene transfer to the lungs and nose of patients with cystic fibrosis: a double-blind placebo-controlled trial. *Lancet* **353,** 947–954 (2017).

158. Dubosky, M. N., Chen, Y.-F., Henriksen, M. E. & Vines, D. L. Vibrating Mesh Nebulizer Compared With Metered-Dose Inhaler in Mechanically Ventilated Subjects. *Respir. Care* **62,** 391–395 (2017).

159. Franzen, L., Vidlářová, L., Kostka, K.-H., Schaefer, U. F. & Windbergs, M. Freeze-drying as a preserving preparation technique for in vitro testing of human skin. *Exp. Dermatol.* **22,** 54–56 (2012).

160. Kuehn, A. *et al.* Human alveolar epithelial cells expressing tight junctions to model the air-blood barrier. *ALTEX* **33,** 251–260 (2016).

161. Stigliani, M., Haghi, M., Russo, P., Young, P. M. & Traini, D. Antibiotic transport across bronchial epithelial cells: Effects of molecular weight, LogP and apparent permeability. *Eur. J. Pharm. Sci.* **83,** 45–51 (2016).

162. Lepeltier, E. *et al.* Squalenoylation of chitosan: A platform for drug delivery? *Biomacromolecules* **16,** 2930–2939 (2015).

163. Kong, M. *et al.* Respiratory syncytial virus infection disrupts monolayer integrity and

function in cystic fibrosis airway cells. *Viruses* **5,** 2260–2271 (2013).

164. Nilsson, H. E., Dragomir, A., Lazorova, L., Johannesson, M. & Roomans, G. M. CFTR and tight junctions in cultured bronchial epithelial cells. *Exp. Mol. Pathol.* **88,** 118–127 (2010).

165. Moreau-Marquis, S., Redelman, C. V., Stanton, B. A. & Anderson, G. G. Co-culture Models of Pseudomonas aeruginosa Biofilms Grown on Live Human Airway Cells. *J. Vis. Exp.* (2010). doi:10.3791/2186

166. Anderson, G. G., Moreau-Marquis, S., Stanton, B. A. & O'Toole, G. A. In vitro analysis of tobramycin-treated Pseudomonas aeruginosa biofilms on cystic fibrosis-derived airway epithelial cells. *Infect. Immun.* **76,** 1423–1433 (2008).

167. Tseng, B. S. *et al.* The extracellular matrix protects Pseudomonas aeruginosa biofilms by limiting the penetration of tobramycin. *Environ. Microbiol.* **15,** 2865–2878 (2013).

168. Ciofu, O., Rojo-Molinero, E., Macià, M. D. & Oliver, A. Antibiotic treatment of biofilm infections. *APMIS* **125,** 304–319 (2017).

169. CLSI. *Methods for Dilution Antimicrobial Susceptibility Tests for Bacteria That Grow Aerobically*. *Approved Standard-Tenth Edition. CLSI document M07-A10.* (2015). doi:10.4103/0976-237X.91790

170. Shou, D. *et al.* Rapid quantification of tobramycin and vancomycin by UPLC-TQD and application to osteomyelitis patient samples. *J. Chromatogr. Sci.* **52,** 501–507 (2014).

171. Gobin, P., Lemaître, F., Marchand, S., Couet, W. & Olivier, J. C. Assay of colistin and colistin methanesulfonate in plasma and urine by liquid chromatography-tandem mass spectrometry. *Antimicrob. Agents Chemother.* **54,** 1941–1948 (2010).

6. List of Scientific Publications

Original Research Articles

1. Murgia X, Pawelzyk P, Schaefer UF, Wagner C, Willenbacher N, Lehr C-M. *Size-limited penetration of nanoparticles into porcine respiratory mucus after aerosol deposition*. Biomacromolecules **2016**;17:1536–42.

2. Murgia X, Yasar H, Carvalho-Wodarz C, Loretz B, Sarah G, Schwarzkopf K, Schaefer U, Lehr, C-M. *Modelling the bronchial barrier in pulmonary drug delivery: A human bronchial epithelial cell line supplemented with human tracheal mucus*. Eur J Pharm Biopharm **2017**;118:79–88.

3. Vukosavljevic B, Murgia X, Schwarzkopf K, Schaefer UF, Lehr C-M, Windbergs M. *Tracing molecular and structural changes upon mucolysis with N-acetyl cysteine in human airway mucus*. Int J Pharm **2017**;553:373–6.

4. Müller L, Murgia X, Siebenbürger L, Börger C, Schwarzkopf K, Sewald K, Häussler S, Braun A, Lehr C-M, Hittinger M, Wronski S. *Human airway mucus alters susceptibility of Pseudomonas aeruginosa biofilms to tobramycin, but not colistin*. J Antimicrob Chemother **2018**;73:2762–9.

5. Graef F, Richter R, Fetz V, Murgia X, De Rossi C, Schneider-Daum N, Allegretta G, Elgaher W, Haupenthal J, Empting M, Beckmann F, Brönstrup M, Hartmann R, Gordon S, Lehr, Claus-Michael. *In Vitro Model of the Gram-Negative Bacterial Cell Envelope for Investigation of Anti-Infective Permeation Kinetics*. ACS Infect Dis **2018**;

6. Ho D-K, Frisch S, Biehl A, Terriac E, De Rossi C, Schwarzkopf J, Lautenschläger F, Loretz B, Murgia X, Lehr, Claus-Michael. *Farnesylated Glycol Chitosan as a Platform for Drug Delivery: Synthesis, Characterization, and Investigation of Mucus–Particle Interactions*. Biomacromolecules **2018**;

7. Yasar H, Biehl A, De Rossi C, Yasar H, Biehl A, De Rossi C, Koch M, Murgia X, Loretz B, Lehr, C-M. *Kinetics of mRNA delivery and protein translation in dendritic cells using lipid-coated PLGA nanoparticles*. J Nanobiotechnology **2018**;16:72.

8. Vukosavljevic B, Hittinger M, Hachmeister H, Pilger C, Murgia X, Gepp M, Gentile L, Huwer H, Schneider-Daum N, Huser T, Lehr C-M, Windbergs M. *Vibrational spectroscopic imaging and live cell video microscopy for studying differentiation of primary human alveolar epithelial cells*, Submitted to Journal of Biophotonics. In Reply.

Review Articles

9. Murgia X, Loretz B, Hartwig O, Hittinger M, Lehr C-M. *The role of mucus on drug transport and its potential to affect therapeutic outcomes*. Adv Drug Deliv Rev **2018**;124:82–97.

10. Murgia X, de Souza Carvalho C, Lehr C-M. *Overcoming the pulmonary barrier: new insights to improve the efficiency of inhaled therapeutics*. Eur J Nanomedicine **2014**;6:157–69.

Book Chapters

11. Murgia X, Barthold S, Kunschke N, Loretz B, Carvalho C, Lehr C-M. *Chapter 8: Overview of Inhaled Nanopharmaceuticals*. In book: ISAM Textbook of Aerosol Medicine. Publisher: International Society for Aerosols in Medicine; Editors: Barbara Rothen- Rutishauser and Rajiv Dhand (**2014**)

12. Schneider-Daum N, Hittinger M, Murgia X, Lehr C-M. *Chapter 3: Cellular and non- cellular barriers to particle transport across the air-liquid interface of the lungs*. In book: Bio-Nano-Responses. Publisher: Springer; Editors: Peter Gehr and Reinhard Zellner. In Reply.

Patent

13. *Development of a thiol group-based mucolytic to increase the diffusion of nanoparticles through mucus*. Murgia X, Ho DK, Lehr C-M. In preparation

7. Acknowledgments

In the first place, I would like to thank my *Doktorvater* Prof. Dr. Claus—Michael Lehr for giving me the opportunity to be part of his research group and for providing guidance and wise advice during this scientific journey.

I am grateful to apl. Prof. Ulrich Schäffer, who provided key scientific advice at the beginning of this thesis project. | extend this acknowledgment to Dr. Brigitta Loretz and Dr. Cristiane da Souza Cravalho-Wodarz, who performed very well in the role of supervisors.

Scientific collaboration has been key to achieve the results of this work. Therefore, | am indebted with all the co-authors of the original research papers included in this thesis. A special word goes to Dr. Marius Hittinger, Laura Müller, and Dr. Paul Pawelzyk for their hard work in the lab and during the writing/publishing process.

A sincere acknowledgement goes to the technicians of our Institute. Your efforts go unnoticed for many but the tremendous work you do keeps our labs running smoothly. Thank you, Dr. Chiara de Rossi, Petra König, Jana Westhues, Peter Meiers and Marijas Jurisic.

In such a large research group, I had the chance to meet many colleagues from all over the world. Just to name a few Flo, Ariana, Hanzey, Jing, Stephanie, Emad, Jenny, Sara, Sarah, the other Sarah, Elise, Simon, Salem, Alejandro, Ankit, Robert, Carlos... and many-many more. Thanks to all of you for your help and the good times shared together.

My fellow colleagues, co-authors and, principally, friends Dr. Branko Vukosavljevic and Dr. Duy-Khiet Ho deserve a special mention. Branko, thank you for your good *spectroscopic vibrations*. Khiet, thank you for the *good chemistry* between us. True friends can be counted with one hand and I was lucky enough to find two. Then, this time has been well worthwhile.

I am thankful to my parents. They say they are proud of their son. Now that I am a father myself, I can say that I am very proud of you as well. My brother Aitor and my sister Zuri are always in my thoughts (and in our *WhatsApp* group ;). I would also like to thank my *in-laws* Beate and Felix for their support.

The last paragraph is dedicated to my main priority: my dear wife Kathrin and my children June and Matti. Kathrin, we started the Saarland adventure together some years ago. I can only thank

you for your love and your wholehearted (multidisciplinary) support. June and Matti, your vital energy and your joy bring happiness to our lives. Without the three of you I could have had finished this thesis in half of the time ;-D, however, my life would not have been as thrilling as it is: I love you!